

CATALYSTS FOR ELECTRO-OXIDATION OF
METHANOL

A THESIS
SUBMITTED TO

GOA UNIVERSITY
FOR THE DEGREE OF
DOCTOR OF PHILOSOPHY
(IN CHEMISTRY)

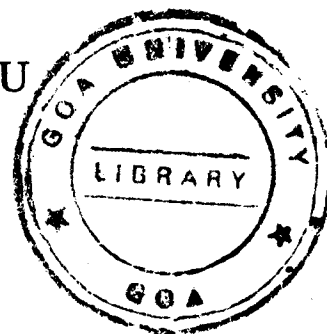
BY

PURNAKALA V. SAMANT

DEPARTMENT OF CHEMISTRY
GOA UNIVERSITY
TALEIGAO PLATEAU
GOA-403 206
DEC 1999.

547
SAM/CAT

T-164



DEDICATED TO MY
MOTHER
Mrs. INDIRABAI V. SAMANT
AND FATHER
LATE VASANT SAMANT

STATEMENT

I hereby state that this thesis for the Ph.D degree on "Catalysts for Electro-oxidation of methanol" is my original work and that it has not previously formed the basis for the award of any degree, diploma, associateship and fellowship or any other similar title to the best of my knowledge and information.


Dr. Julio B. Fernandes.

30.12.1999.
(Research Guide)


Ms. Purnakala V. Samant

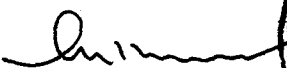
(Candidate)

IV. STATUS OF CORRECTIONS:

Both the external examiners and the Internal Examiner has recommended acceptance of the thesis in the as submitted form.

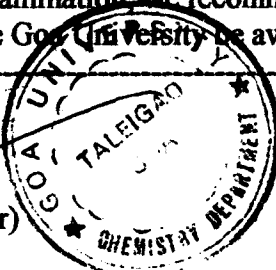
V RECOMMENDATION OF THE ORAL BOARD

On the basis of evaluation of the thesis and the performance of the candidate at the viva-voce examination, we recommend that the degree of Doctor of Philosophy in Chemistry of the Goa University be awarded to the candidate.


Prof. A.K. Shukla
(External Examiner)


Dr. J. B. Fernandes
(Internal Examiner)

Date: March 30, 2000



CERTIFICATE

As required under the University ordinance, I certify that the thesis entitled "Catalyst for Electro-oxidation of Methanol" submitted by Ms Purnakala V. Samant for the award of Doctor of Philosophy in Chemistry is a record of research done by the candidate during the period of study under my guidance and that it has not previously formed the basis for the award to the candidate of any degree, diploma, associateship, fellowship or other similar titles.



**Dr. Julio B. Fernandes,
Research Guide,
Department of Chemistry,
Goa University.**

ACKNOWLEDGEMENTS

With deep sense of gratitude I wish to express my sincere thanks to Dr. Julio B. Fernandes for valuable guidance, whole hearted support, encouragement, helpful and inspiring discussions he rendered to me, throughout the course of this investigation. I am very much grateful to him, for being so sensitive and caring, wise and understanding and shaping my mind towards scientific temperament. Its my pleasure to have been associated with him; he has been a constant source of inspiration; being considerate and warmth he had shown me throughout the course of this work. I owe him a lot in my life.

My thanks are also due to Dr. J.S. Budkuley, Prof. and Head, Department of Chemistry for providing the necessary facilities during various stages of my work. I thank Dr. B. A. Gomes, Principal, Govt. college of Arts, Sci. & Comm., Sanquelim for all the help received from him.

My sincere thanks are due to Dr. A. K. Shukla, S. S. C. U, IISc, Bangalore, for allowing to carry out experimental studies and helping me in constructing my experimental set up. I am indebted to Dr. N. M. Gupta, Head, Applied Chemistry Division, BARC, Mumbai, for helping me to carry out part of my experimental studies in BARC. My sincere thanks are also due to Dr Nanda Haram, Scientist, TIFR, Mumbai, for timely help and providing me facility of cyclic voltammetry. I am grateful to Dr. R. Rangrajan Scientist, Naval Academy Mumbai, for his kind courtesy in providing teflon emulsion required for my work. I am thankful to Dr. K. Vijayamohanan Scientist, NCL-Pune, for helping and showing keen interest during initial stages in this work.

I am extremely grateful to Dr. A. S. Arico, Institute C.N.R./ T.A.E Messina Italy, for helping me in providing carbon paper and Nafion 117 for my work. My special thanks are due to Prof. Neil J Coville, Conference Chairman, CATSA'99, from University of Witwatersrand, Johannesburg, South Africa, for waving me conference fee, and providing nice hospitality during my stay in South Africa.

My thanks are also due to Dr P. C. Rao Scientist, GOD, NIO, Dona- Paula, Goa for scanning SEM micrographs of my samples. I am very much thankful to Mr. Ravi Chawhan, Tracer, for patiently helping me in drawing figures required for the thesis.

My thanks are also due to Prof. J.P.P Pacheco, Head, Dept of Chemistry, for his cooperation, Dr. Joydeep Bhattacharjee for his encouragement and all colleagues from Govt. College Sanquelim-Goa for their support.

I extend heartfelt thanks to my all research friends, for creating warm, healthy and happy environment. My special thanks to Ms. Yadnyaseni, Ms Mukta for their help. I also thank all the laboratory, and the library staff for their cooperation.

Finally but not least, I am grateful and thankful to my mother Mrs Indirabai, my brothers Dr. Pandharinath, Santosh, and Sanjay, my sisters and all brother in laws for their encouragement and support in all my endeavors. I am really indebted to my brother in law Adv. Somanath V. Patil for sponsoring me air fare for my trip to South Africa.

CONTENTS...

	Page No
SUMMARY AND CONCLUSIONS	ix-xii
CHAPTER -1	
INTRODUCTION TO DIRECT METHANOL FUEL CELL.	
1.1 Fuel cell and its Principle	2
1.2 Direct methanol fuel cell	12
1.3 Electrocatalysts in DMFC	14
1.4 Reaction Mechanism involved in DMFC	23
1.5 Conclusions.	33
References	37
CHAPTER 2	
EXPERIMENTAL(Synthesis and Characterization of Catalysts)	
2.1 Catalyst synthesis.	
2.1.1 Synthesis of Ni ²⁺ and Fe ³⁺ doped manganese oxides.	44
2.1.2 Synthesis of Cu ₂ O, CuO and Cu ₂ O / NaY.	44

2.1.3	Synthesis of Platinum and Platinum bimetallic catalysts.	44
2.1.4	Synthesis of Pt / C.	47
2.1.5	Synthesis of Pt-Ru/C.	48
2.2	Characterization by instrumental techniques.	
2.2.1	Xray diffraction.	48
2.2.2	SEM	48
2.2.3	Cyclic Voltammetry.	48
2.2.4	<i>In situ</i> FTIR spectroscopy.	49
2.3	Hydrogen peroxide decomposition studies.	50

CHAPTER -3

ELECTROCATALYSIS.

3.1	General method for Fabrication of porous Carbon Electrode.	52
3.2	Electrochemical measurements towards methanol oxidation.	56
3.3	Results and Discussions	
3.3.1	Nickel modified manganese oxide as an active electrocatalyst.	57
3.3.2	Electrocatalytic activity of Copper Y based zeolite catalyst.	68
3.3.3	Enhanced electrocatalytic activity of Pt(HY) and Pt-Ru(HY).	74
3.3.4	Pt-M (M=Ru, Ni, Sn & Pd) as active electrocatalyst.	86

3.4 Cyclic Voltammetric studies.	92
3.4.1 HY catalyst.	97
3.4.2 Pt(HY) catalyst	100
3.4.3 Pt-Ru (HY) ^b catalyst.	106
3.4.4 Pt-Ru (HY) ^h catalyst.	108
3.5 <i>In situ</i> FTIR studies.	
3.5.1 CO adsorption studies.	110
3.5.2 Effect of CH ₃ OH / O ₂ on Pt(HY)	115
3.5.3 Effect of CH ₃ OH / O ₂ on Pt-Ru(HY)	123
3.5.4 Conclusion.	126
References	127

CHAPTER-4

VAPOUR PHASE METHANOL OXIDATION FUEL CELL.

4.1 Introduction	128
4.2 Cell Design and Construction.	134
4.3 Fabrication of Electrode.	138
4.4 Results and Discussions.	142
References	154

List of Figures and tables

Figures:

- 1.1 Fuel cell powered bus.
- 1.2 Fuel cell powered zero-emission buses.
- 1.3 A typical H₂- O₂ PEM cell.
- 1.4 Schematic diagram of H₂ -O₂ PEM fuel cell.
- 1.5 (A) Typical sketch of CH₃OH / H₂SO₄ / O₂ fuel cell.
- 1.5(B) A solid - polymer direct methanol fuel cell.
- 1.6 Polarization curves obtained for Pt and Pt-Cr catalyst on carbon (XC-72) in 2.5 M CH₃OH and 1 M CH₃OH at 60 ° C.
- 1.7 Polarisation curves obtained for Pt and Pt-Fe catalyst.
- 1.8 Effect of reduction procedure on the activity of platinum particulate catalyst for CH₃OH oxidation at 60 ° C 2.5 M CH₃OH and 1 M CH₃OH.
- 1.9 Polarization data for Pt / Ru electrode in 2.5 M CH₃OH and 1 M CH₃OH at 60 ° C with increased catalyst loading made by sulphito group.
- 1.10 Polarization data for Pt / M [M= Pd, Au, Os, Ir, Ru] in 2.5 M CH₃OH and 1 M CH₃OH at 60 ° C
- 1.11 Comparative polarization data for Pt- Ru, Pt-Ru-Ga, Pt-Ru-Cr electrode.
- 1.12 Comparison of steady state V-I data for Pt / Ru / Os / Ir and Pt / Ru / Ir
- 1.13 Polarization data for Pt / TiO₂ and Pt / ZrO₂ in 2.5 M CH₃OH and 1 M CH₃OH at 60 ° C.
- 1.14 Idem for Pt: Pt / HFO₂, Pt /Nb₂O₅ and Pt / Ta₂O₅.

- 1.15 Basic model for methanol oxidation through an electrocatalytic surface generated by passivating the surface with an oxide film.
- 3.1 Conventional three electrode assembly set up.
- 3.2 Schematic diagram of die for pressing electrode powder into pellet.
- 3.3 Polarization curves (2.5 M H₂SO₄ / 1M CH₃OH) for electrooxidation of methanol on modified manganese dioxide electrode at 25 ° C and 60 ° C
- 3.4 Polarization curves (2.5 M H₂SO₄ / 1M CH₃OH) for electrooxidation of methanol on modified manganese oxide electrode at 25 ° C and 60 ° C as a function of heat treatment.
- 3.5 Polarization curves (2.5 M H₂SO₄ / 1M CH₃OH) for electrooxidation of methanol on modified manganese oxide electrode at 25 ° C and 60 ° C as a function of molar composition of Ni²⁺
- 3.6 Tafel plots (2.5 M H₂SO₄ / 1M CH₃OH) of Fe³⁺ doped and Ni²⁺ doped manganese dioxide.
- 3.7 Tafel plots (2.5 M H₂SO₄ / 1M CH₃OH) of manganese dioxide containing varying amounts of Ni²⁺
- 3.8 Tafel plots (2.5 M H₂SO₄ / 1M CH₃OH) of different catalyst materials.
- 3.9 Tafel plots (2.5 M H₂SO₄ / 1M CH₃OH) for electrooxidation of methanol as a function catalyst composition (W / W) with respect to Cu₂O / NaY.
- 3.10 Possible rate determining steps in electrochemical reduction.
- 3.11 Possible intrazeolite mechanism for reduction of Cu₂O during electrooxidation of methanol.
- 3.12 Polarization curves (2.5 M H₂SO₄ / 1M CH₃OH) for methanol oxidation on various catalyst at 60 ° C.

- 3.13 Tafel plots (2.5 M H₂SO₄ / 1M CH₃OH) for methanol oxidation on various electrocatalyst at 60 ° C.
- 3.14 Peroxide decomposition profiles with different catalyst at the initial concentration of 0.13 M H₂O₂ in 0.1 M H₂SO₄ recorded as a function of time.
- 3.15 Arrhenius plots for catalytic decomposition of H₂O₂.
- 3.16 Correlation between rate of methanol oxidation interms of current density and energy of activation.
- 3.17 Tafel plots for various catalyst in (2.5 M H₂SO₄ / 1M CH₃OH) for methanol oxidation at 60 ° C.
- 3.18 XRD pattern of HY, Pt/ HY, Pt-M /Y [M= Ru, Pd, Sn, Ni].
- 3.18(A) X.R.D pattern of HY, Pt (HY) and Pt-Ru (HY) catalyst
- 3.18 (B) S.E. M. micrographs of HY, Pt (HY) and Pt-Ru (HY)catalyst.
- 3.19 SEM photographs of Pt-M /Y catalysts.
- 3.20 Cyclic voltammograms of HY catalyst
- 3.21 Cyclic voltammogram of Pt(HY) catalyst at 60°C
- 3.22 Cyclic voltammogram of Pt-Ru(HY)^b catalyst at 60°C
- 3.23 Cyclic voltammogram of Pt-Ru(HY)^h catalyst at 60°C
- 3.24 Cyclic voltammogram of Pt-Ru(HY)^h catalyst at ambient temperature
- 3.25 Relation between I_p v/s v^{1/2}
- 3.26 CO adsorption spectra on HY Pt(HY), Pt-Ru(HY)
- 3.27 Deconvolution spectrum of CO and CO₂

- 3.28 *ir* spectra of adsorbed methanol / O₂ on Pt(HY) catalyst at various temperature after evacuation
- 3.29 *ir* spectra of pure methanol.
- 3.30 Subtraction spectra of CH₃OH / O₂ absorption on Pt(HY) after 30 minutes.
- 3.31 Subtraction spectra of Methanol adsorption on Pt(HY) after 30 minutes.
- 3.32 Methanol / O₂ adsorption on Pt-Ru(HY) at various temperatures after evacuation.
- 3.33 *ir* spectra of CH₃OH / O₂ on Pt-Ru(HY) at different temperatures after 30 minutes.
- 4.1 Schematic diagram of DMFC.
- 4.2 Typical polarization curve of a PEM cell.
- 4.3 Gas transport inside a MEA using a conventional flow field design.
- 4.4 Design specification of the cell used for vapor phase direct methanol fuel cell.
- 4.5 Flow pattern of channels on cathode and anode
- 4.6 Comparison between composite electrode and standard electrode.
- 4.7 Schematic diagram illustrating a conventional MEA and thin film MEA.
- 4.8 V-I plots of PEM fuel cell as function of methanol concentration.
- 4.9 V-I plots of PEM fuel cell as function of oxygen pressure.
- 4.10 V-I plots of PEM fuel cell as function of oxygen pressure.
- 4.11 V-I plots of PEM fuel cell as function of temperature.
- 4.12 V-I plots of PEM fuel cell with humidified oxygen as a function of flow rate.
- 4.13 Model structure of methanol fuel cell.

List of Tables:

- 3.1. Variation of overpotential at different temperature as a function of modified manganese dioxide at a current density of 100 mA / cm^2
- 3.2. Variation of overpotential as a function of heat treatment on Mn-Ni catalyst at a current density of 100 mA / cm^2 .
- 3.3. Variation of overpotential as a function of molar concentration of Ni in Mn at a current density of 100 mA / cm^2 at 60° C .
- 3.4. Variation of current density for various catalyst at an overpotential of 250 mV at 60° C .
- 3.5. Peak current and peak potential at 50 mV/s for various catalysts.
- 3.6. Assignments for IR absorption of HY and Pt-Ru (HY)
- 3.7. Comparison of particle size by XRD and SEM measurements.
- 3.8. Relative catalytic activity in terms of current density various catalyst at an overpotential of 250 mV at 60° C .
- 4.1 Permeation rates corresponding to various methanol concentration.
- 4.2 Variation of conductivity of nafion with temperature.

SUMMARY AND CONCLUSIONS

Direct methanol fuel cells are considered as attractive energy source in transportation for future. Most of the automobiles at present, use oil as fuel. It causes air pollution and thus not environmentally friendly. The only alternative to gasoline is fuel cell, which converts chemical energy of a fuel directly into chemical energy without burning it. Current research efforts are directed towards search for more efficient electrocatalysts. The aim of the present investigation was

1. To discover newer / alternative catalytic materials.
2. To improve upon the currently used noble metal catalyst viz. Pt-Ru by
 - i) Changing synthesis strategy.
 - ii) using more active catalyst supports.
3. To provide deeper insight in reaction mechanism.

The work of this thesis is described through following Chapters.

Chapter 1:

Introduction to direct methanol fuel cell.

In this chapter various aspects of fuel cell including principle and construction of H₂-O₂ fuel cell are reviewed. The need for direct methanol fuel cell is brought out by the fact that there are multiple problems associated with H₂ as fuel.

- i) Difficulty in water management.
- ii) Pt anode is extremely CO intolerant
- iii) Problems associated with hydrogen storage.

In contrast methanol is

- i) Inexpensive.
- ii) Easy to handle
- iii) Easily available.

This chapter further discusses the principle and construction of direct methanol fuel cell and various types of electrocatalysts. The mechanisms for electrooxidation of methanol are also discussed

- i) Pt, ii) Pt-Ru, iii) Pt-Sn, iv) M- WO_{3-x} v) base metal oxides catalyst.

CHAPTER 2:

Experimental (Synthesis and Characterization of Catalysts).

This chapter describes various methods of preparation of catalysts and their subsequent characterization. The catalysts are classified into following groups;

Group A: Nickel-modified manganese oxide.

Group B: Copper oxides with and without Y zeolite.

Group C: Pt and Pt - Ru supported on active carbon and Y zeolite.

Group D: Pt-M (HY) catalysts where [M= Ru, Ni, Sn, Pd].

All the above catalysts were synthesized by the use of appropriate precursors. The catalysts were characterized by instrumental techniques such as X.R.D, S.E.M and *in situ* FTIR with adsorption of CO and methanol.

Some of the catalysts are further characterized by cyclic voltammetry. This chapter also describes evaluation ^{of} catalytic activity by decomposition of hydrogen peroxide.

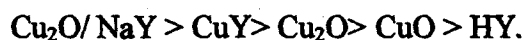
CHAPTER -3:

Electrocatalysis.

In this chapter half cell polarization studies were performed on all the catalysts thus synthesized, by fabricating porous carbon electrode, and three electrode assembly. The working electrode was mounted on a specially designed teflon holder and polarization tests were carried out using standard calomel electrode as reference and platinum as counter electrode. Electrocatalytic activity was evaluated from resulting tafel plots (η v/s $\log i$). The following conclusions could be drawn;

A) Among Ni modified manganese oxide electrodes, ~~the activity~~ the activity of the electrode was found to dependent on i) temperature of thermal treatment ii) amount and nature of the dopant. An optimum composition of 4:1.3 is desirable for better catalytic activity.

B) Among copper oxides with / without Y zeolite catalysts, Cuprous oxide containing ~25 % NaY showed highest catalytic activity. In general catalytic activity followed the order



C) In group C type of catalysts Pt-Ru (HY) showed highest electrocatalytic activity. The activity followed the order



D) Within group D type of catalysts, Pt-Ru (HY) showed highest catalytic activity, also Pt-Ni (HY) catalyst was found to possess high catalytic activity almost comparable to Pt-Ru (HY).

CHAPTER -4 :

Vapour Phase Direct Methanol Fuel Cell (DMFC)

A prototype direct methanol fuel cell is designed and fabricated with nafion membrane polymer electrolyte encapsulated between porous gas diffusion catalyst layers. The cell performance is studied by changing various parameters such as

1. Concentration of methanol.
2. Methanol flow rate.
3. Pressure of oxygen at cathode.
4. Level of humidification of reactants.

The results are discussed in terms of methanol flux ,extent of methanol crossover through electrolyte membrane and level of membrane humidification.

It is observed that the voltage output is highly stable over a long period of time; suggesting high stability of the electrocatalysts.

CHAPTER 1

INTRODUCTION TO DIRECT METHANOL FUEL CELL

CHAPTER 1
INTRODUCTION TO DIRECT METHANOL
FUEL CELL

This chapter is divided into following sections:

1.1 Fuel cell and its principle:

1.2 Direct methanol fuel cell:

1.3 Electrocatalysts in DMFC:

1.4 Reaction mechanism involved in DMFC:

1.5 Conclusion:

Millions of people today depend on automobiles as their main source of transportation, being most efficient and convenient. Unfortunately, most of the automobiles use fuels such as oil. After the combustion engine consumes gasoline, it releases carbon monoxide, nitrogen oxides and hydrocarbons. These chemicals cause air pollution, acid rain and the build up of greenhouse gases in the atmosphere, which result in destruction of our precious ozone layer. In addition to these disastrous effects on the environment, gasoline is a finite energy source [1]. Therefore, another efficient and cheap energy source needs to be found quickly. Ideally, this energy source should be limited in its supply and friendly to the environment.

Many alternatives have been considered like batteries and solar power. Batteries are very large and it consumes over 17 times as much space and 45 times as much weight as gasoline tank; also solar powered cars are limited to its use on sunny days.

Only alternative to gasoline is the fuel cell, which produce no polluting emissions and they contain no moving parts and run relatively cool-- below the boiling point of water and is highly efficient. Fuel cells are tested on a large scale by utilities around the world [2-3]. Fuel cells are looked upon as a new generation of vehicles [4-9]. It is expected that initially sale of zero emission vehicle will take place in the countries like U.S, Germany, and Japan by 2003. Fuel cell Powered Zero -Emission Buses are shown in figure 1.1 and 1.2 .

☛ 1.1 Fuel cell and its principle:

Fuel cell constitutes an important method of converting chemical energy into electrical energy directly, without the necessity for combustion in a heat engine [10-16]. The development has been slow over a long period, and most research has been devoted to the *hydrogen* -fuelled cell.

☛ Principles :

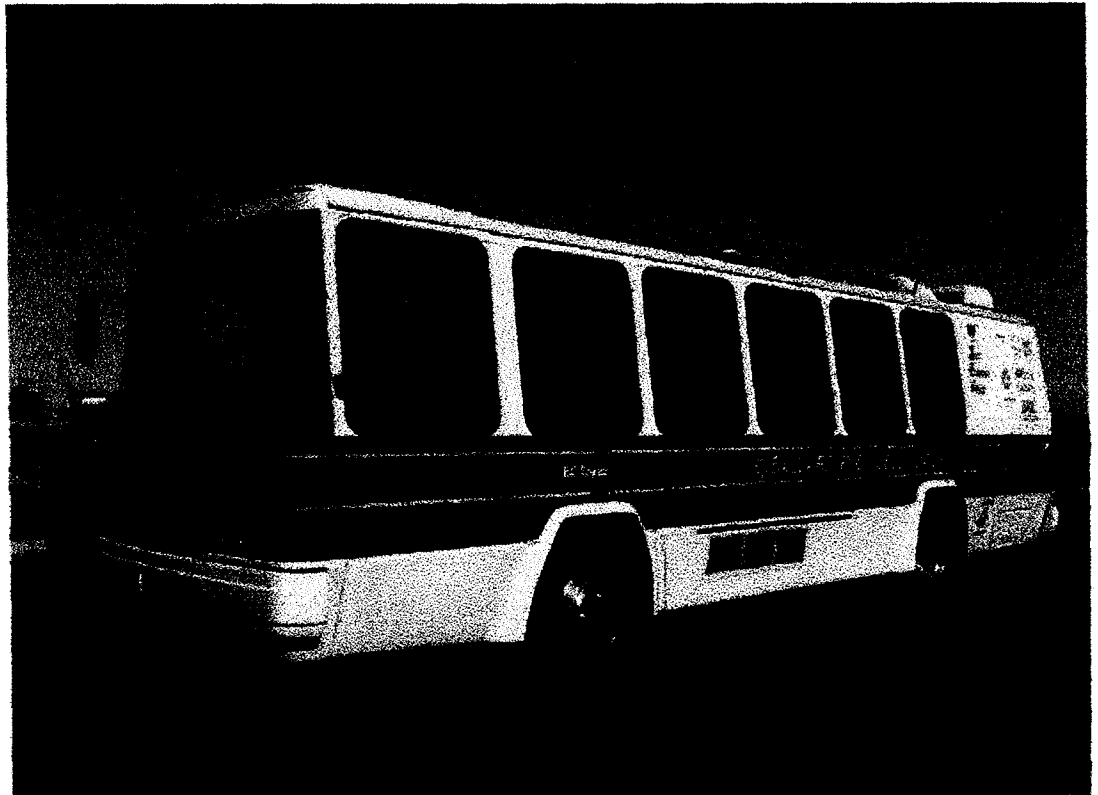
☛ What makes a fuel cell?

- Hydrogen.
- A thin & flat cell made up of two electrodes separated by a plastic sheet called a membrane. The Cathode and Anode are formed by electrochemically active catalyst layers, typically Platinum.
- Oxygen or air
- External circuit.

The full H_2-O_2 fuel cell assembly is shown in fig 1.3

☛ So how does fuel cell work ?

Hydrogen gas is at first exposed to the anode. The anode then draws the electron from the resulting hydrogen leaving a proton (H^+). On the opposite side of cell, the cathode adsorbs oxygen from the air. This produces a potential and causes the electron to move through an external circuit. This creates a current through the circuit which powers the motors



Dryden Flight Research Center EC95-42937-1 Photographed 1995
Fuel Cell Powered Bus

Fig 1.1 Fuel cell powered bus



Fig 1.2 Fuel cell Powered zero-emission buses

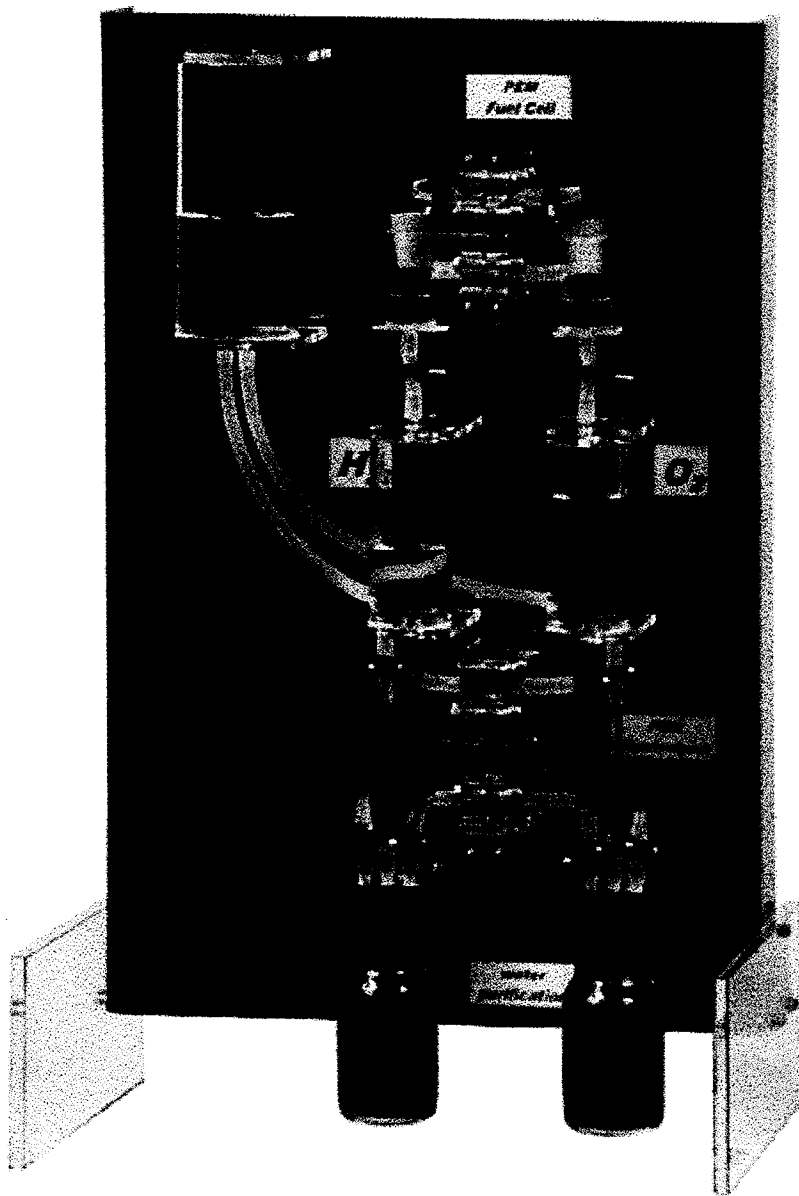


Fig 1.3 Typical H₂-O₂ Fuel cell

☛ What makes up a fuel cell engine?

To make a fuel cell system, several single cells must be assembled in series or parallel to form a stack of desired current, voltage and power. These stacks are constructed with humidifiers, pumps and gas fitters to form a fuel cell engine. An air compressor is needed to compress the air while the humidifier is used to keep PEM membrane moist since it conducts the protons in the electrolyte only through an aqueous environment. By keeping the membrane hydrated, allows the fuel cell to operate properly.

☛ What are the problems associated with H_2-O_2 fuel cell ?

Despite high energy efficiency of fuel cells, some of the energy is lost due to overpotentials of the anodic and cathodic reactions. This is simply the voltage needed to overcome the potential barrier of the oxygen and hydrogen electrode reactions. As electrons flow through the circuit the voltage drops and the efficiency of the cell decreases. Thus more efficient materials are need to be used to prevent the dramatic voltage drop.

Efficiency is also lost by internal cell resistance because of inadequate mass transfer of the reacting species at the electrodes. Thus, the current density needs to be improved in order to make the hydrogen fuel cell more practical for use in automobiles.

Other problem is that the water management in the cell is difficult to control. The PEM fuel cell requires an aqueous membrane to operate efficiently. The fuel cell cannot operate on a hot or sunny day, as this will cause the water inside to evaporate, resulting in the drying of the

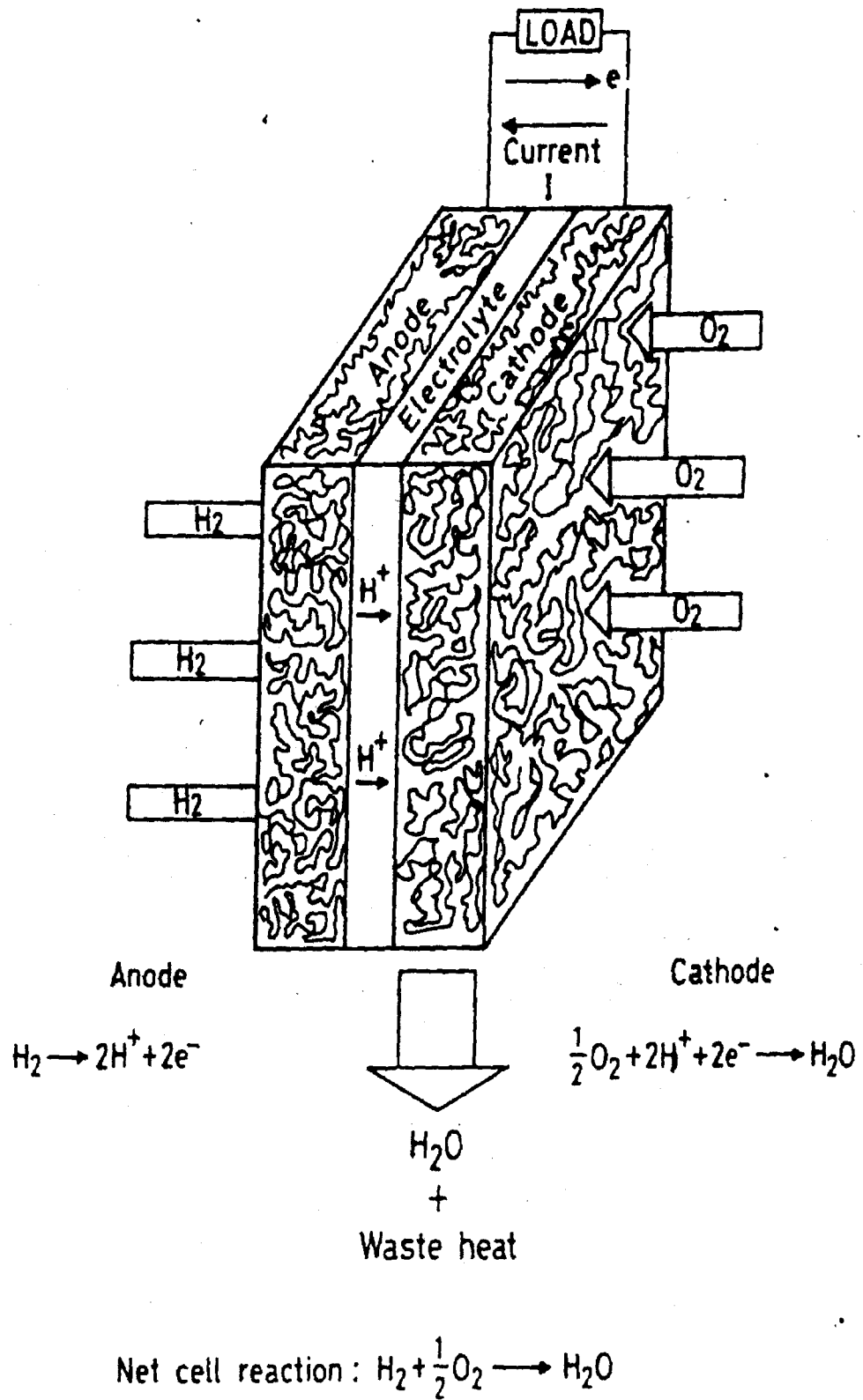


Fig. 1.4 An acidic electrolyte hydrogen-oxygen fuel cell.

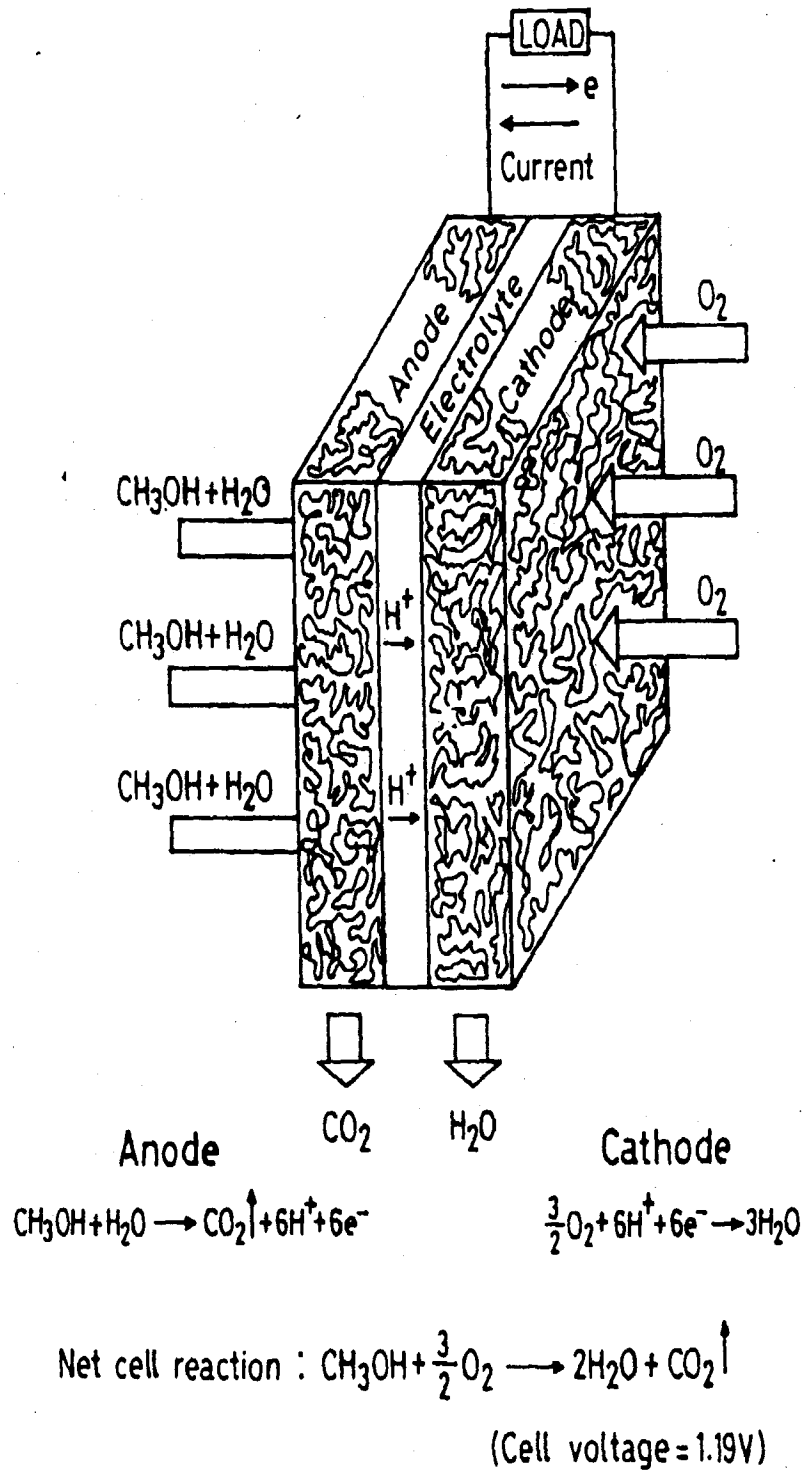


Fig.1.5BA solid-polymer electrolyte direct methanol fuel cell.

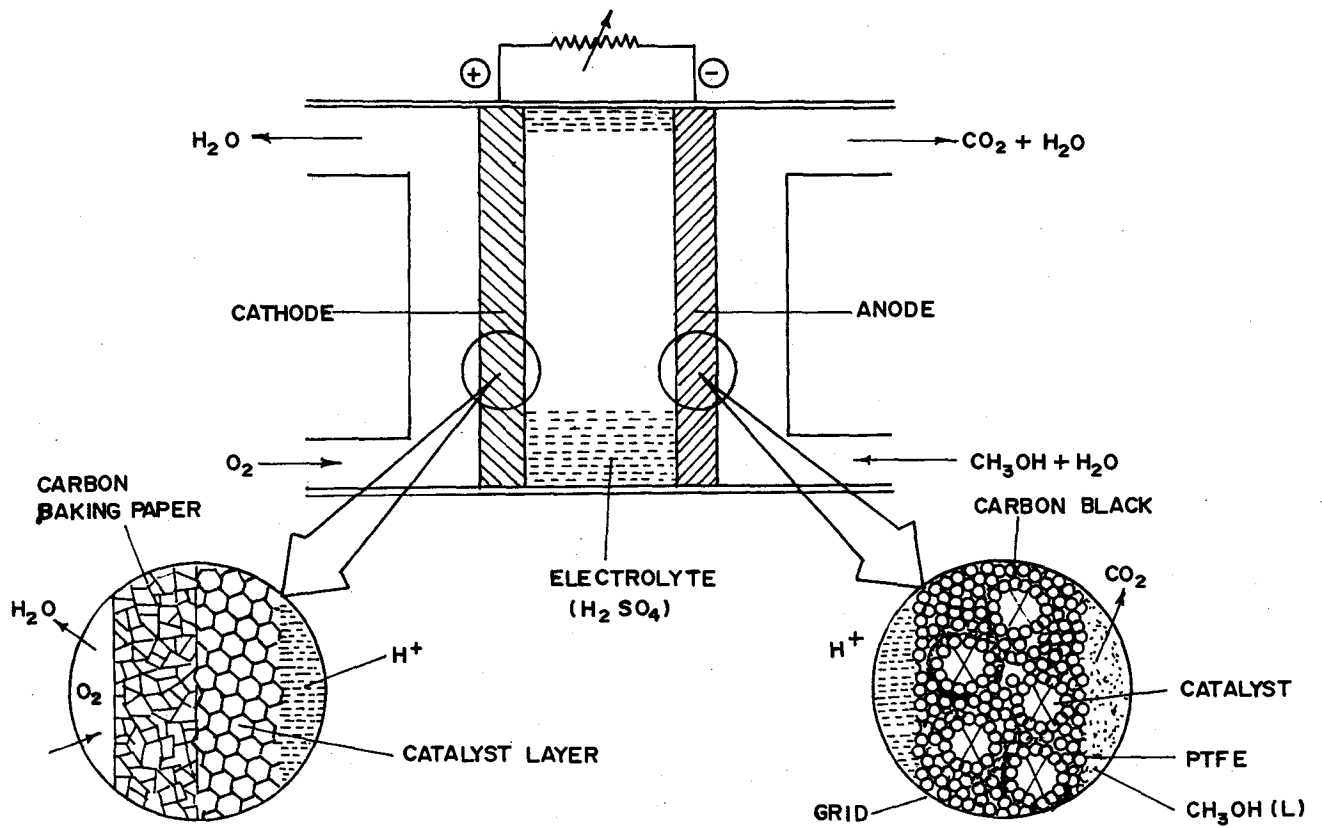


Fig 1.5(A) Typical sketch of $\text{CH}_3\text{OH} / \text{H}_2\text{SO}_4 / \text{O}_2$ fuel cell.

membrane, and eventually loss of its conductivity. Therefore humidifier is used to help keep the membrane in an aqueous environment. However humidifier add additional mass and consume power from the cell.

Another limitation of the PEM is that Pt anodes are extremely CO intolerant. From the cathode and anode reactions traces of CO in reformed gases cannot be avoided. The CO poisoning is due to strong competitive chemisorption of CO to displace H₂ from Pt surface. Chemisorptions of CO, weaken considerably with temperature and efforts are needed to develop higher temperature PEM fuel cells.

Yet another limitation of fuel cell is onboard hydrogen storage; it can be stored in rechargeable metal hydride or in a hydride compound that releases hydrogen when reacted with water. One of the challenges today is to discover a cheap, convenient and efficient way to store enough hydrogen in the vehicle without consuming too much space.

☛ How to Overcome these problems ?

In order to overcome these problems, the major methods being used by auto companies are methanol reformation and gasoline reformation as an alternative for hydrogen. At present methanol is looked upon as attractive fuel for PEM fuel cell, since it being a liquid, is easy to handle and can be supplied from the current network of oil company distribution sites.

Methanol can be made from any renewable resource containing carbon, such as seaweed, waste wood and garbage. It is projected that methanol can make major requirements for road transportation if used in fuel cell vehicle. Thus methanol fuel for a car, powered by fuel cells would be carried in a tank, just as with petrol, and refueling should take no longer than filling up at a petrol station.

Ethanol also stands as a competitive substitute candidate, subject to its state of development of ethanol oxidation catalyst. However its use in fuel cell would be restricted depending upon its cost and availability in a particular country.

At present there are approximately 14,000 methanol fuel cell passenger cars in use, mostly in Federal and private fleets, and about 400 methanol buses in daily operation, mostly in California.

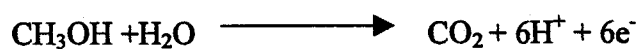
1.2 Direct Methanol fuel Cell:

The direct methanol fuel cell overcomes the hydrogen - specific restrictions. It is based on the direct electrochemical conversion of methanol without an intermediate reforming step. The principle is known for decades, but until now nobody could demonstrate any commercialization.

Steady progress has been made in various fields, such as catalysis electrolytes, electrode structure, theoretical understanding of gas diffusion and fuel cell engineering. This makes direct methanol fuel cell (DMFC), long considered as the most difficult fuel cell technology due to methanol crossover and catalytic inefficiency, a reality.

The direct methanol fuel cell (DMFC) is shown schematically in fig 1.5(A) & (B). It is based on a PEM-type construction with similar materials except the anode catalyst: Pt /Ru alloys are used instead of pure Pt [17].

It consists of an anode at which methanol is electro-oxidised to CO₂ through the reaction.



And the cathode at which oxygen (usually as air) is reduced to water or steam



The electrolyte in the cell can be either aqueous acid or alkali, the former being pioneered in fifties and sixties by Shell, and latter by

Exxon -Alstom. The Exxon program was abandoned in the late seventies, and the Shell program in 1981, both decisions being essentially driven by the realization that oil prices were unlikely to show any substantial rise over the foreseeable future, and the commercialization of the DMFC in traction based application would be extremely difficult.

A number of developments have combined to cause a re-appraisal of the DMFC. There is rising concern over the environmental damage caused by the internal combustion engine, coupled with the realization that the engineering of a truly clean ICE is in itself a major problem. A comparison of the obvious alternative electrochemical technologies reveals that although batteries offer prospects of a true zero emission vehicle, all current batteries have a considerable environmental problem and engineering drawback. The fuel cell likely to be a serious contender for traction is the DMFC, in which the liquid methanol is supplied directly to the anode at which it is oxidized to CO₂.

For the commercialisation of DMFC it is worth emphasizing the areas where improvement would be highly advantageous:

1. The activity of the anode must be further improved, either by increasing the operating temperature or identifying improved electrocatalysts.
2. The current density of the noble metal need to be reduced, even though the economic arguments for very low loading do need to be re-assessed in the light of more realistic views put forward by Stonehart [18.]
3. The membrane properties need to be improved both in terms of water balance sensitivity and by inhibiting the cross - diffusion of methanol.
4. The response of methanol cell to rapid changes in demand needs to be assessed, since the ability to react rapidly will be critical to the success of the cell.

☞ 1.3 Electrocatalysts for DMFC:

This issue contains several different directions which, however merge, as far as the objective is concerned: how to extract best possible performance out of a given amount of noble metal incorporated in a particular catalyst? It can be broken down into catalyst preparation, pretreatment and characterization. Other issues such as possible catalyst support interaction and the choice of a suitable C support are involved directly.

Platinum is widely studied as an electrocatalyst for methanol oxidation, but it is not sufficiently active to be useful commercially, and there has been an intensive search for other active materials [19-22]. Platinum in polycrystalline and nanoparticle form were found to promote methanol oxidation [23-24]. This search has been illuminated by the mechanistic analysis in particular, the bifunctionality has led to the search for materials that might be able to combine with platinum with the later acting to chemisorb methanol and promoter then providing oxygen in some active form to facilitate oxidation of the chemisorbed CO.

The simplest method for enhancing oxidative activity is to generate more Pt-O species on the platinum surface by incorporation of metals as alloys that then dissolve to leave highly reticulated and active surfaces. Alloys such as Pt₃Cr and Pt₃Fe have been shown to be more active than platinum by virtue of this process, as shown in fig 1.6 & 1.7.

And the same may be true in part for Pt Sn, though there is controversy here. The drawback with this method of promotion is the poor long term stability of the particles. In addition, improved methods for platinum particle deposition are important in creating improved surface

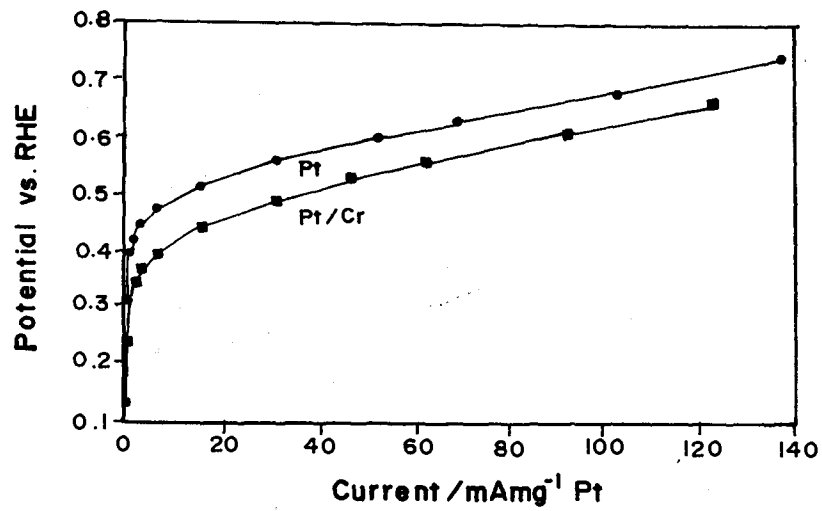


**Fig 1.6 Polarization curves for Pt/and Pt/ Cr
2.5 M H₂SO₄ and 1M CH₃OH at 60°C**

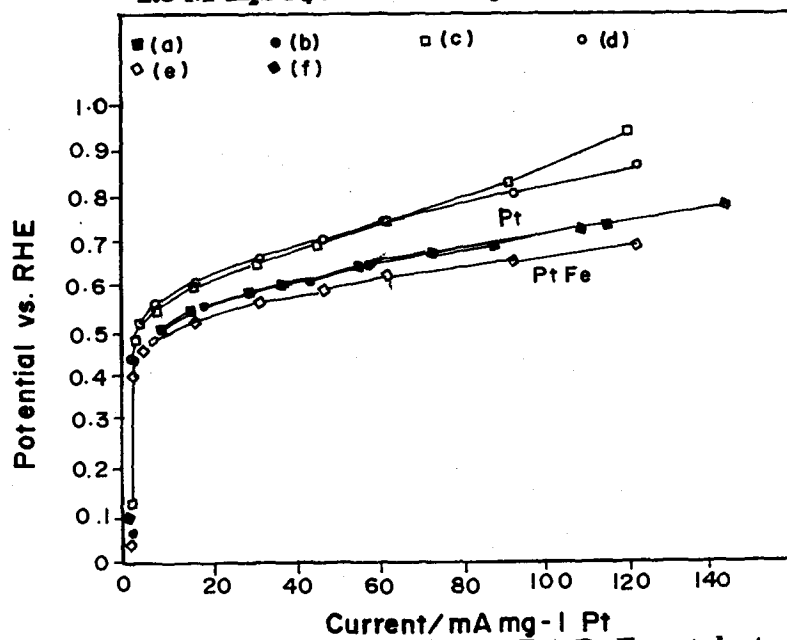


Fig 1.7 Polarization curves for Pt-Ru, Pt-Fe catalyst.

area and surface morphology. The use of more powerful reducing agents can improve performance, as shown in fig 1.8.

And by the use of controlled colloid deposition through the "sulphito" route, extremely high activities can be found at higher loading, fig 1.9.

Second approach has been the use of surface ad-atoms deposited by UPD on the platinum surface. These have been studied extensively [18,25-26], with Au [27] being identified early on, but with most recent attention being on Sn [28-30] and Bi [31]. Several modes of operation have been suggested for these ad - atoms, including the blocking of hydrogen adsorption, the ability to modify the electronic properties of the platinum, the ability to act as redox centers, the blocking of poison adsorption sites or the ability of the ad - atoms to induce Pt-O formation on neighboring sites, creating additional active sites for oxidation of CO ads. The ability of both Sn and Bi ad-atoms to enhance the rate of methanol oxidation has been queried in a recent paper [31]; under very careful conditions, the adsorption of these metals actually inhibited methanol oxidation, even though there is good evidence that Bi adsorption also inhibited formation of adsorbed CO [32].

A third type of promotion is the use of alloys of platinum with different metals which form a surface oxide in the potential range for methanol oxidation. This is the basis for studies of Pt-Sn, Pt-Ru, Pt-Os, Pt-Ir, Pt-Mo, Pt-Re etc [33-38]. The superior performance of binary catalyst relative to platinum is ascribed due to two effects. In the bifunctional model the oxophilic metal is thought to provide sites for H₂O adsorption. In the ligand effect or electronic model, the role of alloying element is to modify the electronic properties of Pt by contributing d-

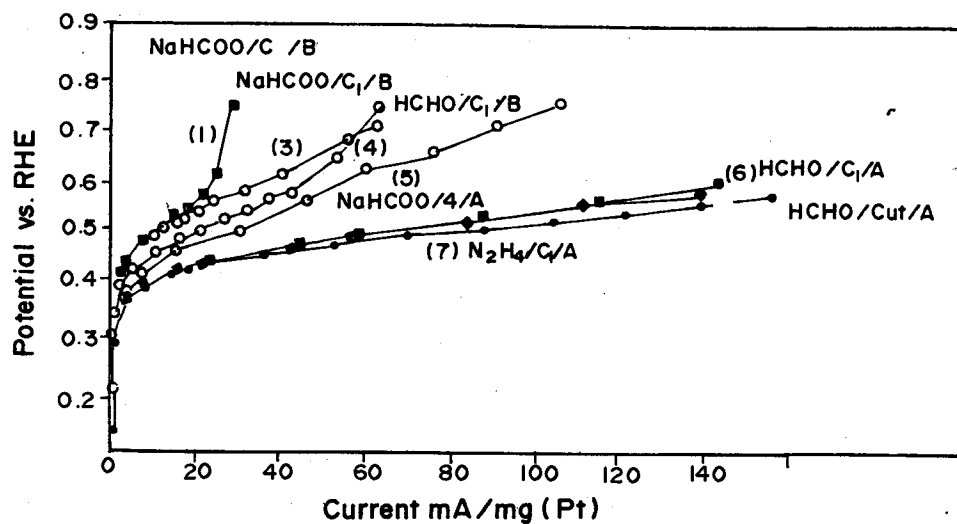


Fig 1.8 Effect of reduction on the activity of Pt particulate in 2.5 M H₂SO₄ and 1M CH₃OH at 60°C

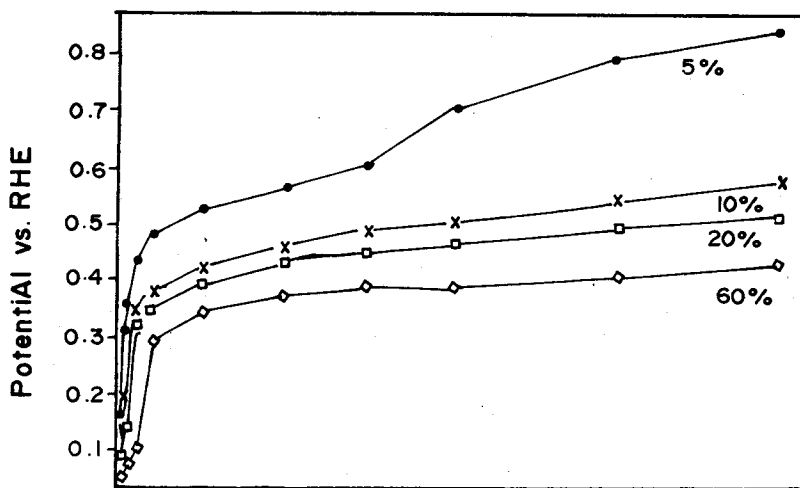


Fig 1.9 Polarization curves for Pt/Ru electrode in 2.5M H₂SO₄ and 1M CH₃OH with increased catalyst loading made by "sulphito" group.

electron density. Thus alloy of platinum with more oxophilic elements have been discovered. Unlike the Sn- ad-atoms [31], there seems little doubt that Pt₃Sn as an alloy does show catalytic behavior [29,39-41] though this may simply derive from the same mechanism as Pt₃Cr, perhaps with the resulting fractal particle surface being stabilized by Sn adsorption. Studies of Pt alloyed with the other noble metals has shown that Ru has by far the largest effect, giving a real catalytic advantage as shown in fig 1.10.

Ir and Os were also found to act as promoters in this study [42], with Au and Pd inhibiting the reaction. Pd was also not found helpful in acidic solutions [43]. Amongst the non noble metals, electrodeposited Pt-Re alloys were reported to show substantial enhancement by Cathro [44]; a result that seems not have been followed up. Reports of very strong enhancement for electrodeposited Mo on Pt have also been reported [45-46], particularly at low currents where there seems to be a different oxidation mechanism operating. Given the effectiveness of binary alloy formation, particularly with Ru / Pt, attention has turned recently to ternary alloys. The apparently different promotion mechanism for Pt / Sn and Pt /Ru led Troughton and Hamnett [41] to explore the Pt / Ru / Sn system, but it was found that alloying Pt /Ru with Sn tends to expel the Ru, leading to no advantage. Of other ternary alloys studied, Pt / Ru / Cr, Pt / Ru / Ni, Pt / Ru / W, Pt / Ru / Mo only Pt / Ru / Ga showed any unequivocal advantage, and this was slight fig 1.11[47].

Recently quaternary alloys such as Pt-Ru-Os-Ir, Pt- Ru-Sn-W, are also found to show great catalytic activity towards methanol [48,105]. Mollouk et. Al. has found a combinatorial screening technique for electrochemical catalyst. Fig 1.12 shows comparison in polarization curves of Pt-Ru-Os-Ir and Pt- Ru-Os.

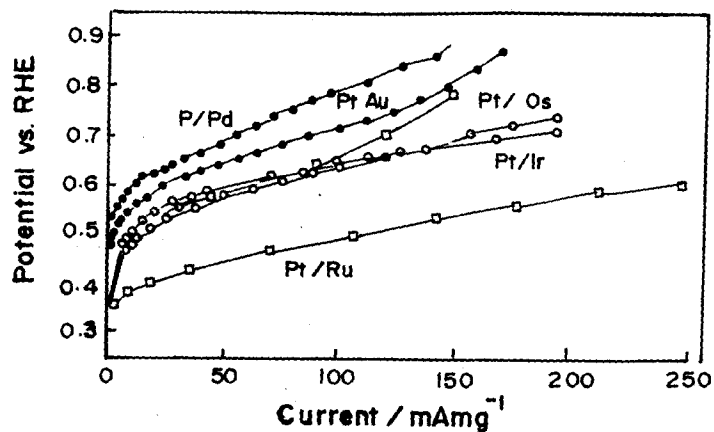


Fig 1.10 Polarization data for Pt/ M [M= Pd, Au, s, Ir] 2.5 M H₂SO₄ and 1M CH₃OH

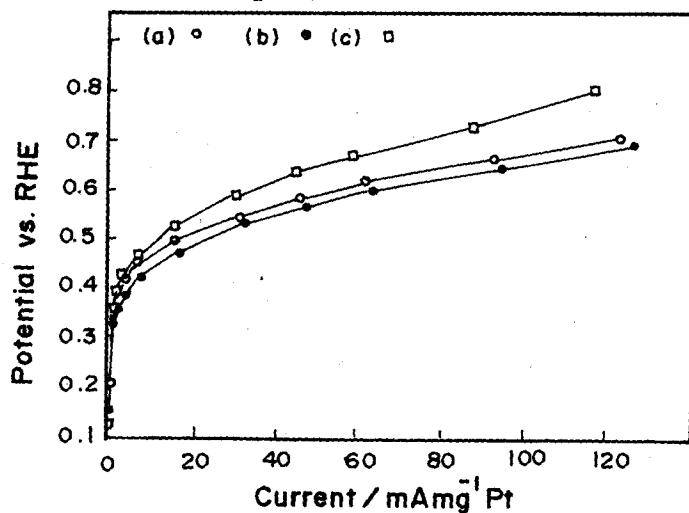


Fig 1.11 Comparison polarization data for Pt-Ru, Pt-Ru-Ga, Pt-Ru-Cr electrode

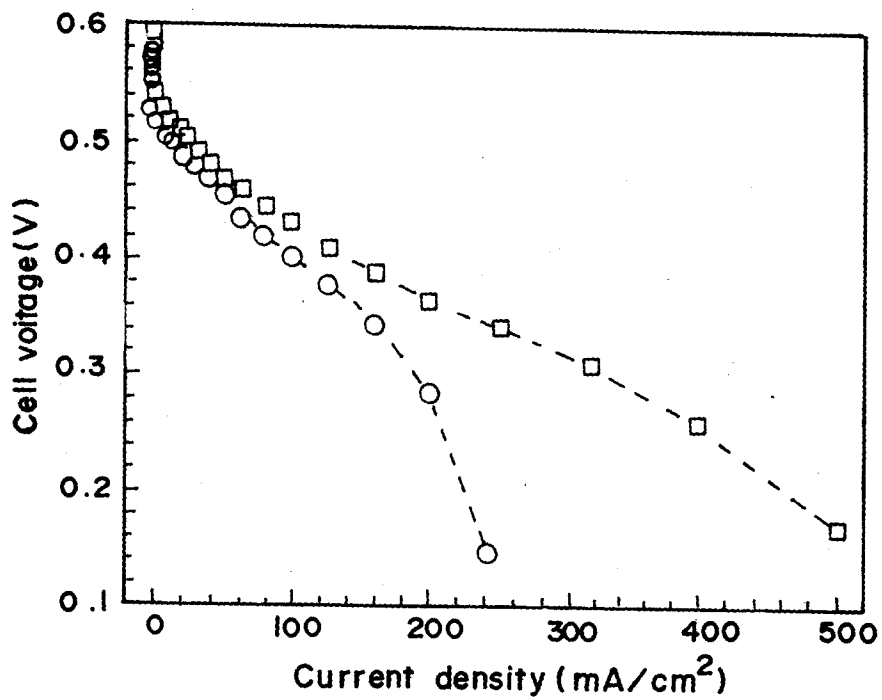


Fig 1.12 Comparison of steady state V-I data for Pt/Ru/Os , Pt/Ru/ Os/Ir.

The fifth type of promoter to be described in the literature is a combination of Pt with a base-metal oxide. Initially these were reported by Hamnett et. al. [49], with Nb, Zr and Ta being found most active for Pt promotion, particularly at higher currents as shown in fig1.13 and 1.14.

However although the effect on Pt itself is clear, attempts to use ZrO_2 to promote Pt / Ru were unsuccessful [50], suggesting that the original mechanism for promotion by these oxides is similar to that for Ru itself [51]. Hamnett et, al. [49] originally identified WO_3 as inhibitor, but more recently, Shen and Tseung [52-53] have identified hydrous WO_{3-x} as a substantial promoter for activity when Pt is electrodeposited on its surface, and this was confirmed separately by Shukla et.al. [54] who reductively codeposited Pt and WO_{3-x} onto a porous carbon substrate. Related catalysts are formed by doping tungsten bronzes of the structure $Ln_{0.1}WO_3$ with Pt. In these catalysts, as in the ones reported by Tseung, W seems to be providing a redox couple, cycling between W (IV) or W (V) and W (VI). Interestingly, the enthalpy of activation is much lower for these catalysts than for Pt itself [55]. There have also been reports of Pt on mixed In / Pb oxides on carbon which showed good activity but poor stability [56].

In addition to the electrodeposition or reductive deposition of Pt on to an oxide surface, it is possible to incorporate the Pt directly into many oxide structures, and these species have been examined recently. Perovskite based oxides, in particular, $SrRu_{0.5}Pt_{0.5}O_3$ were found to give good current densities when used as electrodes in nafion -based cells [57], and similar results were reported for $Dy_xPt_3O_4$ [58]. It is unclear how stable these oxides are for longer terms in acidic environments.

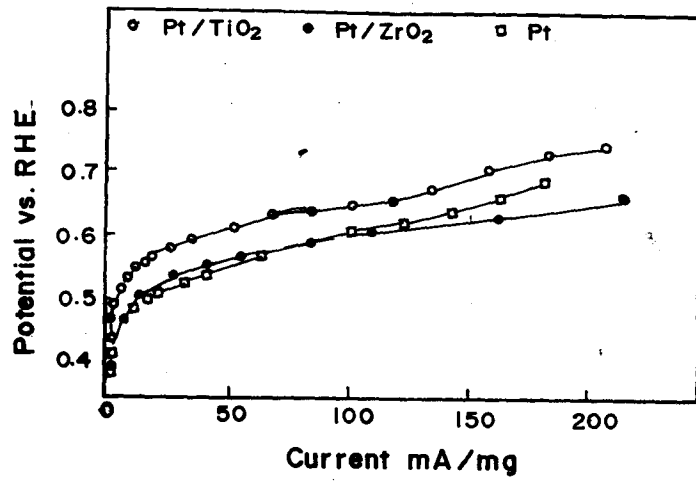


Fig 1.13 Polarization data for Pt/ TiO₂ and Pt/ ZrO₂ in 2.5 M H₂SO₄ and 1M CH₃OH

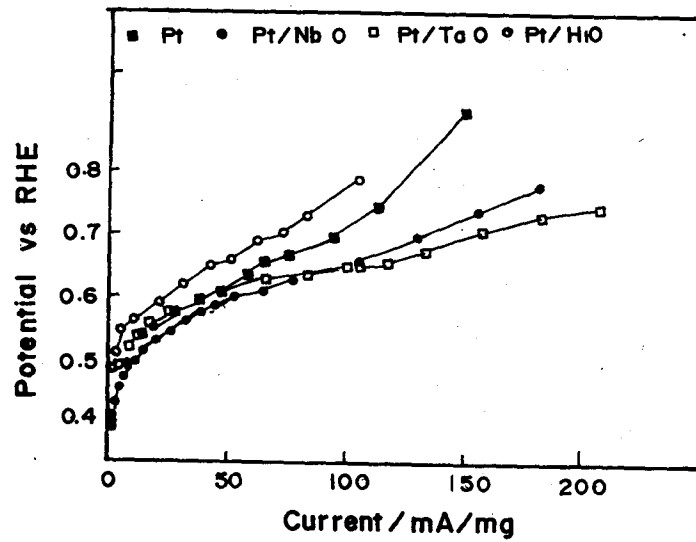


Fig 1.14 Idem for Pt: Pt/ HfO₂, Pt/Nb₂O₅ and Pt/ Ta₂O₅

1.4 Mechanism of anodic oxidation of methanol:

Although there remain areas of controversy over the details of the methanol oxidation process, which are certainly connected with the existence of multiple pathways with similar activation energies on the platinum surface, the primary processes can be represented as follows:

1. Adsorption of methanol, most easily and energetically favoured sites such as steps.
2. Sequential proton stripping from the methanol to give a series of multiply bonded intermediates that eventually convert to linearly bonded CO.
3. Kinetic analysis suggests that there are two extreme types of mechanisms for methanol oxidation on Pt : one involves attack of water on CO molecules on the outside of the chemisorbed CO islands in a type of rapid process and the second involves rate limiting migration of CO from the edges of the islands to the active sites, perhaps Pt -O.

Many mechanisms have been proposed for the anodic oxidation of methanol [64-75]. The complete anodic oxidation of methanol is described by.



The full anodic reaction to yield carbon dioxide [reaction 1] involves a six - electron oxidation of the carbon atom .the thermodynamic equilibrium potential for reaction calculated from the standard chemical potentials at 25 ° C by Pourbaix [76] is 0.03 V v/s [SHE] . However, because of the number of electron involved, equilibrium is not readily realizable, even on the best electrocatalysts so far devised.

Anodic oxidation thus involves a number of steps, all of which produce intermediate products. Some of these intermediate products are themselves relatively stable compounds. Thus it is expected that formaldehyde, formic acid and carbon monoxide would be formed as intermediates, and these may well acquire sufficient stability for further reaction to be difficult. It is well to consider these reactions and their standard thermodynamics, in an attempt to isolate those steps which may prove difficult, at least on thermodynamic grounds.

Equilibrium may be considered between methanol and any number of appropriate intermediate stable phases, or between the stable phases themselves. A succession of anodic reactions involving the stable phases can thus be proposed as a mechanism for the full oxidation of the fuel to CO₂ (with a and b below being alternative oxidative steps).

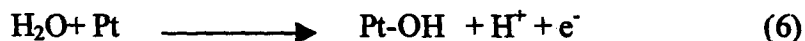


In the above description of the mechanism, the adsorption of the various reacting species is taken for granted, since initial adsorption is necessary for any interfacial reaction. The lowest of the standard equilibrium potentials involving methanol itself is the CH₃OH / CO₂ reaction, the overall reaction. Other reaction involve considerably higher equilibrium potentials, particularly the CH₃OH / HCHO reaction.

It is thus clear that if the mechanism of anodic oxidation were to go through this sequence of relatively stable intermediates, the first step involving formation of formaldehyde, would therefore be thermodynamically the most difficult. The successful running of the methanol fed anode is in fact hampered largely by the fact that an anodic overpotential of some 0.3 - 0.4 V is required to drive the anode at a significant rate; this prominent feature of the reaction was displayed in the work of Hampson et al [77] at c.a 0.55 V (SHE). This poisoning by early stage intermediates is the exclusive reason for the overpotential barrier. The sequence 2→3a or 3b→4b or 4b represents a possible mechanism based only on intermediates, which are relatively stable and which can exist as separate entities without a stabilizing surface.

There have been many discussions in the literature [73,78 -79] as to whether these intermediates form in parallel with the oxidation to CO₂, essentially as side reaction, or whether they are formed as intermediates in CO₂ production (series reaction) , but with no suitable conclusion. The implication of the formation of these relatively stable oxidation states as intermediates in series or in parallel are clear. By running a parallel, the anodic reaction is no longer 100% current efficient, since some of the oxidation product would escape the electrode in an oxidation state lower than CO₂. By running in series, such stable oxidation states of carbon must add to the overpotential required to drive the reaction.

The above mechanism, based only on the stability of the intermediates, is in broad agreement with Breiter's work. It is however, quite different from that of Bagotsky and Vassilyev [67], where only unstable adsorbed intermediates are formed.

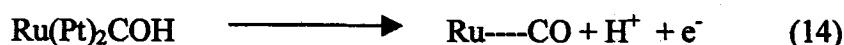


In this process, step (6) precedes each step of steps 7,8 and 9 in providing the electron transfer, and carbon is then oxidized by the adsorbed OH radical.

Other features of this complex electrochemical mechanism concern surface intermediates acting as poisons for the electrocatalyst, hence retarding the overall reaction. It is generally agreed that there is some poison for the anode electrocatalyst, but the identity of the poison is uncertain. The poison is commonly perceived as an adsorbed layer of CO, CHO or COH formed as intermediates in the anodic reaction, these species being chemisorbed to the platinum and difficult to remove [67-75,77-83]. The curious feature of these adsorbed species in terms of being poisons is that they are also expected to be intermediates in the anodic reaction to give CO₂. Their accumulation on the catalyst surface to high coverage may imply that their further oxidation and / or desorption is the slow step in the reaction [67,68,69,70]. If these intermediates function exclusively as poisons (imply parallel path reaction), as their high steady - state implies a smaller remaining surface area available for the reaction to CO₂. Other steps such as C-H bonds scission are also proposed as rate determining [73,75,79]. These issues remain to be resolved.

The most successful anode catalyst for the methanol fuel cell is the mixture of platinum and ruthenium. One of the proposed roles for ruthenium used in conjunction with platinum as an anode electrocatalyst for methanol is its ability to aid the desorption of the catalyst poison from the platinum surface [78-87], there by increasing the effective surface area available for the oxidation reaction to proceed. The optimum ratio of Pt-Ru in these alloy electrocatalysts has been variously cited as between 9 : 1

and 1:1 [86,88-90]. The enhanced desorption from the surface as imparted by ruthenium can be envisaged as follows:



The metal atoms in parentheses are surface catalyst atoms onto which the oxidising carbon atom of the reacting fragment is adsorbed. Here the reaction passes through a series of adsorbed intermediates via successive deprotonation steps (step 10-14) one of which is the COH (formed in step 12), pyramidally bonded over by three surface catalyst atoms. If Ru aids the desorption as proposed then this mechanism would imply that a Pt / Ru atomic ratio of 2 could be optimum. Such a notion, however, would require that the solid solution of Ru in Pt has a perfect structural distribution of Ru in Pt .

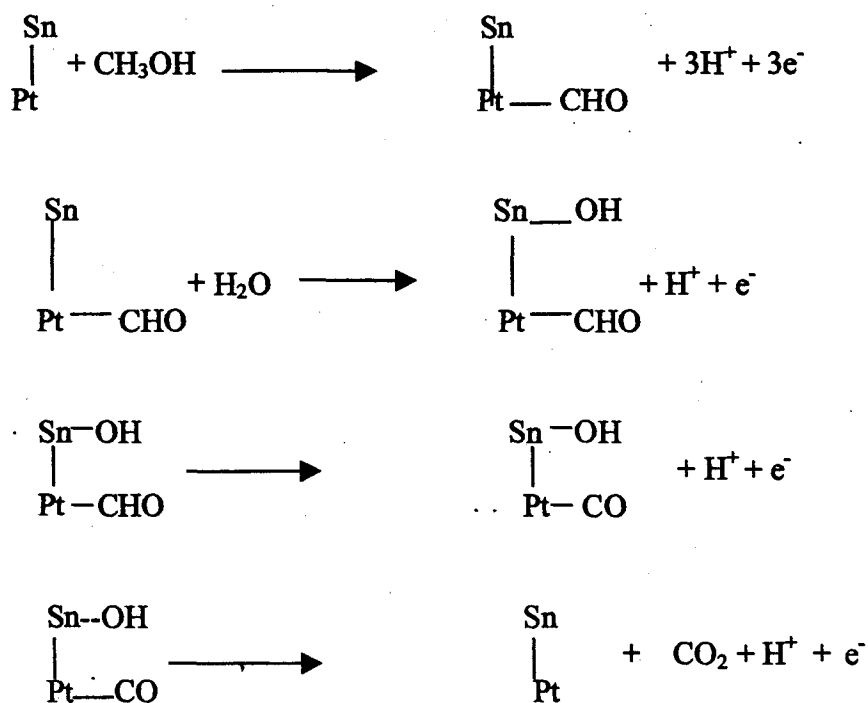
The alloying of Ru and Pt has been postulated to give rise to an electronic effect in which electrons are transferred from Ru to Pt [95]. However, the suggested direction of electron donation has been challenged recently, particularly from FTIR studies on well defined bulky alloy [96], and on Pt-Ru particles [97] both of which show reduction in the coverage of the electrode by CO_{ads} at any given potential, and an increase in the absorption frequency of the bound CO. This latter effect must be electronic in origin and is consistent with CO being less strongly adsorbed through a reduction in the back π bonding from Pt to the CO π^* orbital. The reduction in the π back bonding will also lead to a higher positive charge on the carbon atom, rendering it more liable to nucleophilic attack by water, and permitting oxidation of CO at lower potentials. This effect has been verified by DEMS studies [98], which also demonstrated that at pure Ru at room temperature though CO is oxidised at Ru at potentials 200mV more negative than Pt alloy; formation of Pt - Ru alloy shifts the CO oxidation maximum in cyclic voltammetry to more negative potentials, again suggesting an electronic effect.

The second major effect of Ru is to increase the coverage of Pt- Ru surfaces by oxy - species. An XPS study [99] showed that the presence of Ru significantly enhanced the amount of Pt-O species present, a result confirmed by latter work [100-102].

The studies on well defined alloy surfaces, with known surface composition [103-104] have shown that low Ru coverage lead to facile chemisorption of methanol, but as expected to rate- limiting oxidation of CO_{ads} , with RDS being CO migration to active Ru clusters.

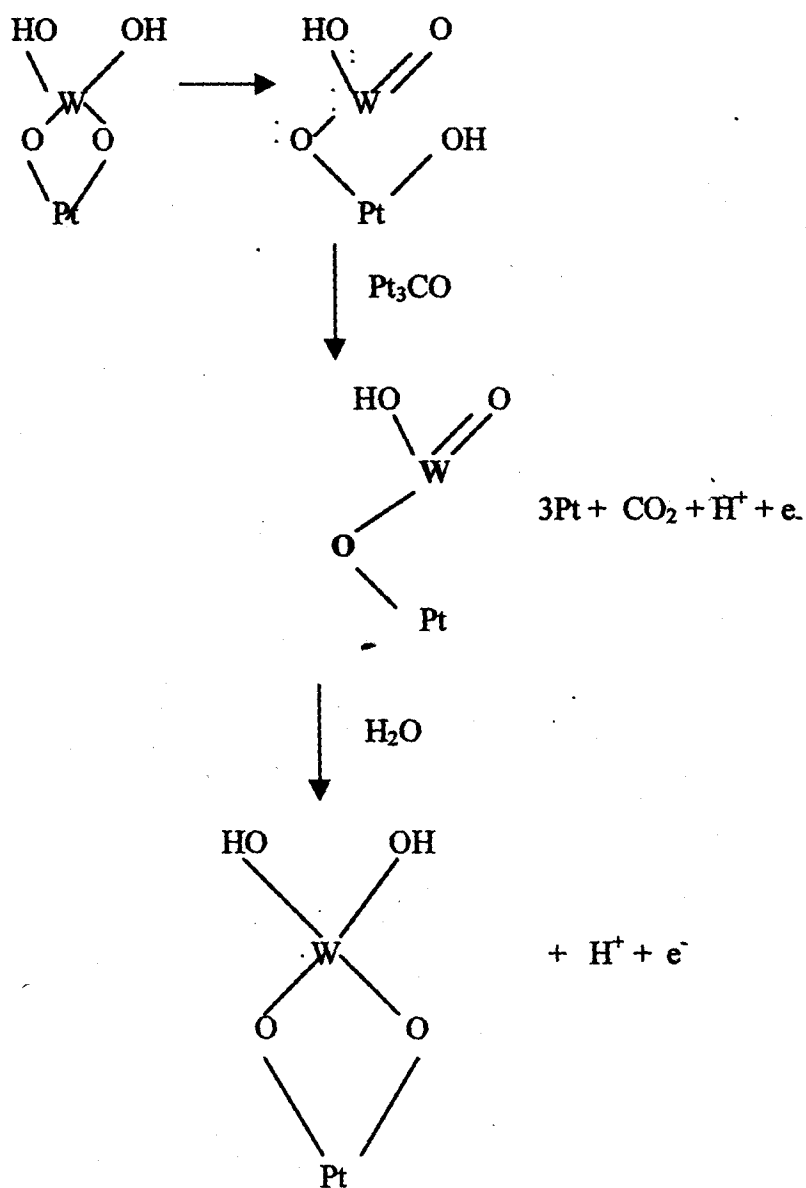
Pt / Sn catalyst is also found to enhance methanol oxidation, because the charge transfer from Sn to Pt for Pt-Sn catalyst is found to be maximum [91-92]. It is speculated that the charge - transfer from Sn to Pt

within this bimetal catalyst and partial scavenging of oxidic platinum impurities from platinum are the determining factors for the observed synergistic promotion of methanol oxidation reaction. This is because during the methanol oxidation reaction, the catalyst is operated in a regime in which oxides should not be present but where supply of oxygen to the surface is of paramount significance. Following scheme is envisaged for methanol oxidation by Shukla et. al.



The methanol oxidation is also found to be increased by using Pt-WO₃ as reported in [93], it is speculated that the WO_{3-x} is present as an oxyhydroxide, which can promote surface oxy-species on platinum by

proton transfer .it is argued that promotion of platinum by base metal is bounded to the platinum surface through M-O-Pt bonds which can breaks as follows:



Anodic oxidation of methanol using base electrocatalysts:

Base electrocatalysts have been suggested earlier for the DMFC. Electrocatalysts made from base materials must be able to resist the corrosive action of the acidic electrolyte used. Acidic electrolytes are a requirement for all high temperature direct methanol fuel cell, chiefly in order to reject CO₂, which would otherwise dissolve in neutral or alkaline solution. Since base materials are themselves thermodynamically unstable in acidic solutions, the requirement for any base electrocatalyst is that it is passive towards corrosion. Tungsten and molybdenum carbides have been shown to have some electrocatalytic activity towards methanol oxidation [94].

A similar material using a mixture of nickel and tungsten in the mole ratio 1:1 was also made. The material showed high a high degree of passivity towards corrosion and modest electrocatalytic activity towards methanol oxidation up to potential of ~ 0.6 V (SHE).

Similar material was also prepared using ruthenium tungstate to generate an electrode from reduced ruthenium and tungsten in an atomic ratio Ru / W \cong 1. The carburised Ru /W electrocatalyst showed poor performance for methanol oxidation.

The basic mechanism of the process is sketched in fig1.15

The intervening oxide film between the catalyst particles and electrolyte / methanol must provide an electron conducting path for fuel oxidation to occur. Methanol is initially adsorbed onto the passivating oxide surface in order for its anodic oxidation to take place. It can then be oxidised using ions obtained from the aqueous phase as shown in the

reaction schemes above (2-4 or 13) alternatively, oxide ions can in principle be taken from the passivating oxide surface, and the anion vacancies in the film thus generated, can be annihilated via the aqueous phase after, desorption of the reaction products. For example, if it is imagined that CO is adsorbed to the passivating oxide surface, and the anodic reaction to CO₂ is to occur, then the following reaction scheme would describe the process:



Where MO represents the oxide film and V^o is an oxide ion vacancy in the film. The same mechanism can be applied to any step in the reaction which requires oxide anion. This mechanism is similar to reaction 5-9, with the oxide anion supplied by the surface of the catalyst rather than from the solvent. Loss of anion from the surface by reaction 15 could alternatively be succeeded by dissolution of the associated metal cation. There is no evidence for this: the presence of methanol reduces the rate of catalyst dissolution. The rise in rate of methanol oxidation in the transpassive region does not violate the mechanism.

Many forms of tungsten have been observed to operate in an electrocatalytic manner with either the methanol or the hydrogen oxidation reaction. This is particularly due to high degree of stability of tungsten based materials in acidic solutions; for tungsten carbide this is due to the passivity of the material towards corrosion in strongly acidic electrolytes and its ability to impart passivity to other components such as nickel. Multiple oxidation states of oxidized tungsten, such as W(V) and W(VI) and its ability to form labile hydrogen atoms in HWO₃, may be responsible for this electrocatalytic activity.

🏆 1.5 Conclusion:

Electrocatalytic oxidation of methanol in direct methanol fuel cells operates *through a complex mechanism*. Several relatively stable intermediates, such as formadehyde and formic acid believed to be formed, at the electrode surface, cause anodic current efficiency for the oxidation less than 100% . It is observed that anodic oxidation of formic acid requires initiating overpotential. Some of this initiating overpotential is of kinetic origin, and it is consequently capable of being reduced through suitable electrocatalysis at anode.

It has to be evaluated whether there are any better catalysts than Pt-Ru. *The best strategy for this search is a combined approach of theoretical and fundamental electrochemical studies and a modern screening method like combinatorial analysis*. It is desirable that catalyst manufacture process and associated physical data be well established in the open literature in order to make inter-catalyst comparisons possible. In order to reduce the usage of the precious metals and thus cost, the best possible performance has to be extracted from a given amount of catalyst. This involves mainly catalyst preparation techniques, pretreatment, electrode preparation and in the case of supported catalysts, also choice of suitable support.

The possibility of using anode electrocatalysts of *base metal* origin is raised. This possibility warrants much further investigation towards the search for the potentially very much cheaper electrocatalysts for the direct methanol fuel cell. In acidic solutions, nickel can be made very passive towards corrosion by suitable reaction with tungsten, and the consequent material is anodically active towards methanol oxidation. Although the rates of reaction are modest, these materials have not yet

been optimised. The incorporation of ruthenium with tungsten in a similar preparation gives negligible catalysis of the methanol reaction, although a modest hydrogen electrode was generated.

High degree of stability of tungsten based materials such as *tungsten carbide* in acidic solution is due to its passivity of the material towards corrosion in strongly acidic electrolyte and its ability to impart passivity to other components such as nickel. Multiple oxidation states of oxidised tungsten as W (V) and W (IV) and its ability to form the labile hydrogen atom as in HWO_3 is believed to be responsible for this electrocatalytic effect. *Nickel -tungstate system* as anode material have also found to give high electrocatalytic activity. It contains no precious metal at all, and it can be made simply and cheaply.

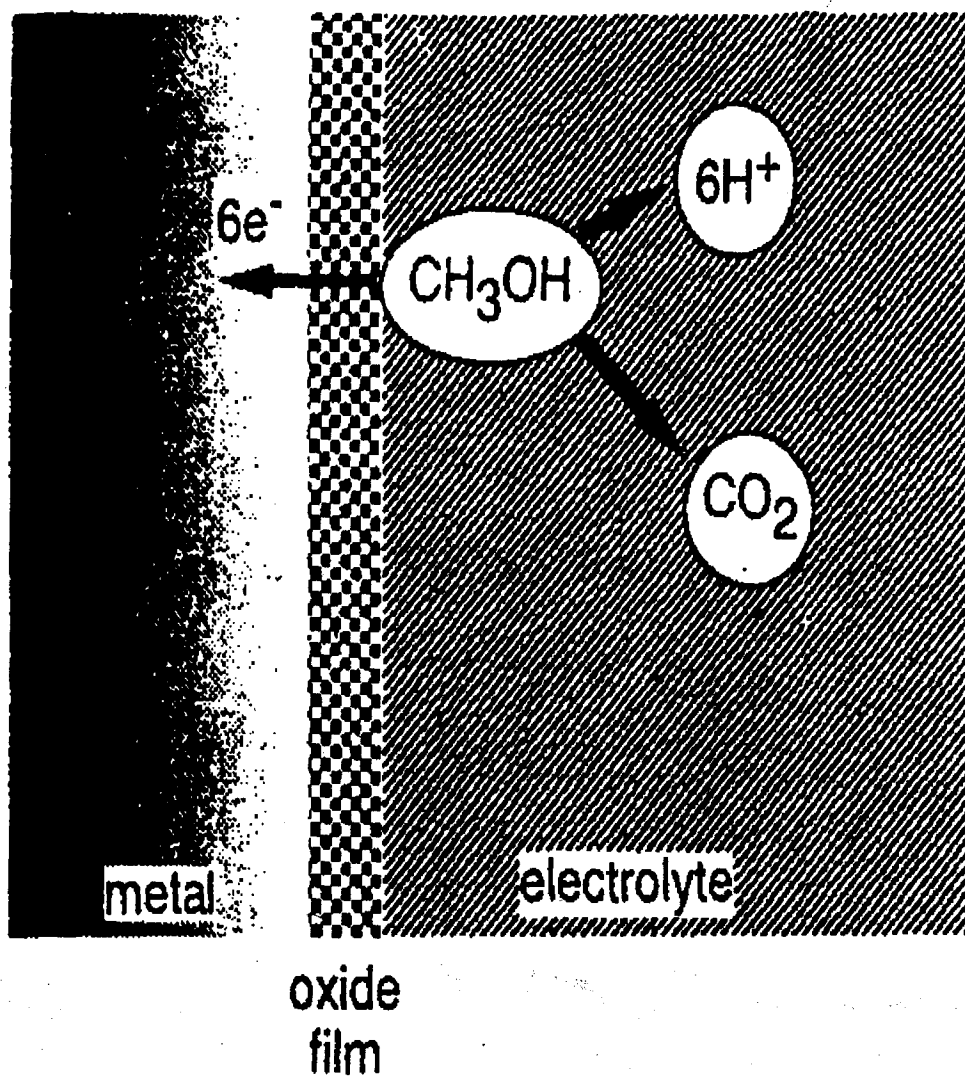
The most urgent task to be faced by in further development of the DMFC is probably improvement *in the membrane properties needed to prevent depolarisation of the cathode and dehydration effects at and near anode.*

The second task that needs to be carried out is the investigation of the speed of response of a simple fuel cell to changing demand. *The thermal fluxes in such cells have not yet been explored*, but are likely to be considerable, and the stability of the membrane to such fluxes also need to be established.

In terms of the supporting work, it would be highly desirable to pin down unequivocally the mechanism of ruthenium promotion, in order that further improvements in catalyst design can be carried out. The possibility of discovering a wholly novel catalysts for methanol oxidation

by establishing the mechanism, of activity of current catalyst, appear to be very high.

The DMFC has reached an important watershed in its development. It is likely that working stacks will be constructed within the next few years, and the research impetus is gathering pace very quickly, bringing new challenges for the engineer as well as new demands on the electrochemists. *This development represents a remarkable achievement in combining catalytic insight and practical manufacture: the fruits of the combined scientific and engineering programme may well revolutionize the way in which we power our cars.*



1.15 Basic model for methanol oxidation through an electrocatalytic surface generated by passivating the surface with an oxide film.

References:

1. F. Du Melle, J. Power Sources, 71 (1998) 7.
2. L. Sjunnesson, J. Power Sources, 71 (1998) 41.
3. S.G. Chalk, J. Milliken, J.F. Miller S.R. Venkateswaran, J. Power Sources 71 (1998) 26.
4. P. Patil, P. Zeger, J. Power Sources, 49, 1-3, (1994) 169.
5. K. Trosst, J. Power Sources 49, 1-3 (1994) 185.
6. Kwa - Sur Tam, J. Power Sources 71 (1998) 190.
7. W. P. Teagan, J. Bentley, B. Barnett, 71 (1998) 80.
8. S. G. Chalk, P.G. Patil, S. R. Venkateswaran, 61 (1996) 7.
9. F. Panik, J. Power Sources, 71 (1998) 36.

10. A. P. Ficket, D. Linden (Ed) "Handbook of batteries and Fuel Cells", Mc Graw Hill Book Company, 1984.
11. R. Pattbiraman, Transaction of the SAEST, Vol 27, No 4(1992) 161.
12. A. Tseung, Chemistry in Britian., Vol 33, No 2, (1997) 19
13. R. Beesten Mater. World ., 5,3, (1997) 150
14. F. Standaert, K. Hemnes, N. Woudstra, Electrochem Soc181th spring Meeting Extended Abstr Reno, Nevada 15, 1, 1995 May 21-6, 713.
15. S. Srinivasan, R. Mosdale, Bull Electrochem., 12, 3-4, (1996) 170.
16. A.J Appleby, J. Power Sources 49, 1-3, (1994) 15.
17. M. Waidhas, W. Drenckhahn, W. Preidel, H. Landes J. Power Sources 61 (1996) 91.
18. P. Stonehart, in: J. Drake (Ed). Electrochemistry and clean Energy of chemistry, Cambridge, 1994.
19. G. Kokkinidis, J. Electroanal. Chem., 201 (1986) 217.
20. B. D. Mc Nicol, J. Electroanal. Chem ., 118 (1981) 71.

21. A. Hamnett, S. A. Weeks, B. J. Kannedy, G. Troughton and P.A. Christensen
Ber. Bunsenges. Phys. Chem., 94 (1990) 1014.
22. J. M. Leger, and C. Lamy, Ber. Bunsenges. Phys. Chem., 94 (1990) 1021.
23. R. Parsons and T. Vander Noot, J. Electroanal Chem., 257 (1988) 9.
24. X. H. Xia, T. Iwasha, F. Ge and W. Vielstich, Electrochim Acta, Vol 41, No5
(1996) 718.
25. F. Gloaguen, J. M. Leger, C. Lamy, J. Appl., Electrochem., 27 (1997) 1052.
26. R. R. Adizic, H. Gerischer, C.W. Tobias (Eds), Advances in Electrochemistry
and Electrochemical Engineering, Vol 13 1984.
27. M. Watanabe, S. Motoo, J. Electroanal. Chem, 60(1975) 259.
28. M.M.P. Janssen, J. Moolhuysen, Electrochim Acta 21 (1976) 289.
29. M. Watanabe, Y. Furuuchi, S. Motoo, J. Electroanal. Chem 191(1985) 367.
30. S. A. Campbell, R. Parsons, J. Chem. Soc. Farad. Trans, 88 (1992) 833.
31. E. Herrero, A. Fernandez-Vega, J. M. Feliu, A. Aldaz, J. Electroanal. Chem.,
350 (1993) 73.
32. Rauhe, B. R. Jr; Mc Larnon, F. R.; Crain E. J, J. Electrochem., Soc., 142 (1995)
1073.
33. Fremlink T. Visscher W; Cox A. P., van Veen J.A.R, Electrochim Acta 40
(1995) 1537.
34. R. Ianniello, V. M. Schmidt, V. Stimming, J Stumper, Electrochim Acta, Vol
39, No11/12 (1994) 1863.
35. M. M. Hefny and S. Abdel-Waneest, Electrochim Acta, Vol 42, No 9 (1996)
1419.
36. J O M's Bockris; J. H. Wroblowa , J. Electroanal Chem 7 (1964) 428.
37. Ross P.N. In the proceedings of the workshop on Direct Methanol Air fuel Cell
A. R. Sen, R.K. Eds; The electrochemical Society Pennington NJ 1992 Vol 92-

38. B. Beden, F. Kadirgan, C. Lamy, J. M. Leger, *J. Electroanal. Chem.*, 127 (1981) 75.
39. A. S. Arico, V. Antonucci, N. Giordano, A. K. Shukla, M. K. Ravikumar, A. S. Roy, S. R. Barman, D. D. Sharma, *J. Power Sources* 50 (1994) 295.
40. K. Wing, H. A. Gastiger, N.M. Markovic and P.N. Ross, *Electrochim Acta* Vol 141, No16 (1996) 2587.
41. G. L. Troughton, A. Hamnett, *Bull Electrochem.* 7 (1991) 488.
42. A. Hamnett, B. J. Kennedy, *Electrochim Acta* 33 (1988) 1613.
43. F. Kadiram, B. Beden, J. M. Leger, C. Lamy, *J. Electroanal. Chem* 125 (1981) 89.
44. K.L. Cathro, *Electrochem Tech*, 5 (1967) 441.
45. J. Wang, H. Nakajima, H. Kita, 5 (1967) 441.
46. H. Nakajima, *J. Chem. Tech. Biotechnol.*, 50 (1991) 555.
47. G. L. Troughton , Ph.D. Thesis , Newcastle-Upon -Tyne 1993.
48. E. Reddington, A. Sapienza, B.Gurau, R. Vishwanathan, E. S. Smotkin, T.E. Mallouk Vol 280, *Science* (1998) 1375.
49. A. Hamnett, B. J. Kennedy, S. A. Weeks, *J. Electroanal. Chem* 240 (1988) 355.
50. A. Hamnett, P. Stevens, G. L. Troughton, *Catalysis Today* 7 (1990) 219.
51. B. J. Kennedy, A. Hamnett, *J. Electroanal Chem*, 283 (1990) 271.
52. P.K. Sen, A.C.C. Tseung, *Pocceedings of the 186th Meeting of the Electrochemical Soc 93-1, Spring Meeting Extended Abstract 576,Hawaii, 16-21 may,1993.*
53. P.K. Sen, A.C.C. Tseung, *Pocceedings of the 186th Meeting of the Electrochemical Soc 93-1, Spring Meeting Extended Abstract1778,Hawaii, 16-21 may,1993.*
54. A. K. Shukla, M. K. Ravikumar, A. S. Arico, G. Candiano, V. Antonucci, N. Giordano, A. Hamnett, *J. App. Electrochem.*, 25 (1995) 528.

55. K. I. Machida, M. Enyo, G.Y. Adachi, J. Shiokawa, *Bull. Chem., Soc* 135 (1998) 528.
56. P.C. Biswas, T. Ohmori, M. Enyo, *J. Electroanal. Chem.*, 305 (1991) 205.
57. J. H. White, A. F. Sammells, *J. Electrochem. Soc.*, 140 (1993) 2167.
58. K. I. Machida, M. Enyo, G.Y. Adachi, J. Shiokawa, *Bull. Chem, Soc. Jap.*, 60 (1987) 411.
59. R. Ya Shaidullin, A. D. Semenova, G.D Vovchenko, Yu. B. Vasil'ev, *Zh. Fiz. Khim.* 57 (1983) 1019.
60. M. S. Ureta- Zanartu, P. Bravo, J. Zagal, *J. Electroanal. Chem.*, 337 (1992) 241.
61. S. Ya Vasina, S. A. Stuken, O. A. Petrii, I.L Gogichadze, V. A. Mukhin, *Electrokhimiya* 23 (1987) 1127.
62. C. C. Hays, R. Manoharan, J.B. Goodenough, *J. Power Sources* 45 (1993) 291.
63. A. Kawahima, T. Kanda, K. Hashimoto, *Mat. Sci Eng.*, 99(1988) 521.
64. F. T. Bacon, in: G. J. Young (Ed), *Fuel Cells*, Reinhold, New York,(1960) 51.
65. A .J. Appleby, F. R. Foulkes, *Fuel Cell Handbook*, Van Nostrand Reinold, New York. 1989.
66. R. P. Buck, L.R. Griffith, *J. Electrochem. Soc.*, 109 (1962) 1005.
67. V. S. Bagotsky, Y.B. Vassilyev, *Electrochim Acta* (1967) 1323.
68. T. Biegler, D. F. Koch, *J. Electrochem Soc.*, 114 (1967) 904.
69. M. W. Breiter, *Disk. Farad Soc.*, 45 (1968) 79.
70. P. Sidheswaran, H. Lal. *J. Electroanal Chem.*, 40 (1972) 143.
71. R. Inada, K. Shimazu, H. Kita, *J. Electroanal Chem.*, 277 (1990) 315.
72. B. Beden, J.M. Leger, C. Lamy, in: J.O'M Bokckris, B. E. Conway, R. E. White (Eds), *Modern Aspects of Electrochemistry*, Vol 22, Plenum, New York, 1992, p.97.
73. E. Herrero, K. Franaszezuk, A. Wieckowski, *J. Phys. Chem.*, 98 (1994) 5074.
74. A. Papoutsis, J. M. Leger, C. Lamy, *J. Electroanal Chem* .,359 (1993) 141.

75. P.C. Biswas, Y. Nodasaka, M Enyo, *J Appl. Electrochem.*, 26 (1996) 30.
76. M. Pourbaix, *Atlas, of Electrochemical Equilibria in Aqueous Solution*, Pergamon, Oxford 1966, p. 450, 330. 280.
77. N. A. Hampson, M. J. Willars, B. D. McNicol, *J. Chem. Soc. Faraday Trans.*, (1979) 10421.
78. W. Vielstich, X. H. Xia, *J. Phys Chem.*, 99 (1995) 10421.
79. E. Herrero, W. Chranoswski, A. Wieckowski, *J. Phys Chem.*, 99 (1995) 10423.
80. C. Pu, W. Huang, K.L. Ley, E. S. Smotkin, *J. Electrochem Soc.*, 5(1995)119.
81. K. Kunimatsu, *Bar. Bunsenges. Phys.*, 94 (1990) 1025.
82. K. Chandrasekaran, J.C. Wass, J.O'M. Bockris, *J. Electrochem. Soc.*, 137 (1990) 518.
83. A. Hamnett, S. A. Weeks, B.J. Kennedy, G. Troughton, P.A. Christensen, *Ber. Bunsenges, Phys. Chem.*, 94(1990) 1014.
84. N.M. Markovic, H. A. Gasteiger, P.N. Ross, X. D. Jiang, I. Villegas, M. J. Weaver, *Electrochim Acta*, 40 (1995) 91.
85. N. A. Hampson, M.J. Willars, B. D. Mc Nicol, *J. Power Sources*, 4 (1979) 191.
86. V.M. Schmidt, R. Ianniello, H.F. Oetjen, H. Reger, U. Stimming, in: G. Halpert, A. Landgrebe (Eds) *Proton Conducting Membrane Fuel Cell 1*, PV 95-23, The Electrochemical Soc, Pennington , New Jersey, 1995, p. 267.
87. M. Watanabe, M. Uchida, S. Motoo, *J. Electroanal. Chem.*, 229 (1987)395.
88. J.O'M Bockris, H. Wroblowa, *J. Electroanal. Chem.*, 7 (1964) 428.
89. J.B. Goodenough, H. Hamnett, B.J. Kennedy, R. Manoharan, S. A. Weeks, *J. Electroanal. Chem.*, 240 (1988) 133.
90. H. A. Gasteiger, N. Markovic, P.N. Ross, E.J. Cairns, *J. Phys Chem.*, 97 (1993) 12020.
91. Z. Wei, H. Guo, Z. Tang, *J. Power Sources*, 58 (1996)239
92. S. R. Wing and P.S. Fedkiw, *J. Electrochem Soc.*, 139 (1992) 3151.

93. A. K. Shukla, M. K. Ravikumar, A. S. Arico, G. Antonucci, N. Giordano A. Hamnett, *J. Appl. Electrochem.*, 25 (1995) 528.
94. G. Bronoel, S. Besse, N. Tassin, *Electrochim. Acta* 37 (1992) 1351.
95. B.J. Kennedy and A.W. Smith, *J. Electroanal Chem.*, 293 (1990) 913.
96. I. Iwasita, F.C. Nart, W. Vielstich, *Ber. Bunsenges Phys Chem.*, 94 (1990) 1030.
97. P.A. Christensen, A. Hamnett, J. Munk, E. Skou, *J. Appl. Electrochem.*, 40 (1996) 215.
98. M. Krausa, W. Vielstich, *J. Electroanal. Chem.*, 379 (1994) 307.
99. B.J. Kennedy, A. Hamnett, *J. Electroanal Chem.*, 283 (1990) 271.
100. B.J. Kennedy, A. Hamnett, *J. Electroanal Chem.*, 283 (1990) 271.
101. J. B. Goodenough, B.J. Kennedy, A. Hamnett, R. Manoharan, S. A. Weeks, *J. Electroanal Chem.*, 240(1988) 133.
102. K. Franaszczuk, J. Sobkowski, *J. Electroanal Chem.*, 327 (1982) 235.
103. H. A. Gasteiger, N. Markovic, P.N. Ross, E.J. Crains, *Electrochem Soc.*, 141 (1994) 1795.
104. H. A. Geasteiger, *Interface*, 3 (3)(1994) 49.
105. A. S. Arico, Z. Pottazeski, H. Kim, A. Marna, N. Giordano, *J. Power Sources*, 55 (1995) 159.

CHAPTER 2
EXPERIMENTAL
(Synthesis and Characterization of Catalysts)

EXPERIMENTAL

(Synthesis and Characterization of Catalyst):

This chapter is divided into following sections:

2.1 Synthesis of Catalyst.

2.2 Characterization of catalyst by instrumental methods.

2.3 Hydrogen peroxide decomposition studies.

2.1 Synthesis of catalysts:

This section gives the details of chemical synthesis of the electrocatalysts of various type.

- (a) Synthesis of nickel and iron doped manganese oxides.
- (b) Preparation of copper oxides and copper oxide /Y zeolite hybrid catalysts.
- (c) Synthesis of HY, Pt (HY), Pt-Ru(HY)^b and Pt-Ru(HY)^b.
- (d) Synthesis of Pt-Pd (HY) , Pt-Sn/Y and Pt-Ni/Y.

All the chemicals used as reactants or reagents were of Analar grade.

The source of Chemicals is given below.

Chemicals	Source
Pt(NH ₃) ₄ Cl ₂	Aldrich
H ₂ PtCl ₆ .xH ₂ O	Arora-Matthey Ltd
RuCl ₃ .3H ₂ O	Loba Chemie
PdCl ₂	Loba Chemie
SnCl ₂	Qualigens
NaBH ₄	S.D.Fine
(CH ₃ COO) ₂ CuH ₂ O	S.D.Fine
Mn(NO ₃) ₂ .xH ₂ O	Fluka
Ni(NO ₃) ₂ .xH ₂ O	Loba Chemie
Fe(NO ₃) ₂ .xH ₂ O	Aldrich
NaY	UCIL(India)
NiCl ₂	Loba Chemie
N ₂ H ₄	Qualigens

Table 2.1 source of chemicals

2.1.1 Synthesis of Ni²⁺ and Fe³⁺ doped manganese oxides.

The above catalysts were prepared by thermal decomposition of mixed metal nitrate salts on the platinum substrate [detail given section 3.1(b)].

2.1.2 Synthesis of Cu₂O, CuO and Cu₂O/NaY.

(a) Cu₂O was synthesized by dropwise addition of 250 ml of hydrazine hydrate to calculated amount of cupric acetate at 80°C. The powder obtained was washed several times with hot water and dried at 110°C and stored under vacuum desiccator[1].

(b) CuO was obtained by thermal decomposition of Cu (NO₃)₂ at 250°C. The product was washed several times with distilled water, dried at 110°C and stored as above.

(c) Cu₂O/ NaY was obtained by taking calculated amounts of Cu₂O and NaY in isopropyl alcohol and stirred for 1 hour. The sample was dried and stored.

2.1.3 Synthesis of platinum and platinum bimetallic catalysts:

(A) Preparation of HY zeolite by ion exchange process:

Commercially obtained NaY zeolite (UCIL) is converted to HY by conventional ion exchange using 5 M NH₄Cl solution. 20 grams of NaY were shaken with 1000 ml of 5 M NH₄Cl for 48 hours followed by filtration and washing with hot distilled water till free from chloride. The product was dried at 110°C, followed by calcination at 500°C for 12 hours and stored.

1. Nakawa, M. Achi, I. Ogino, Mat. Res. Bull, 20 (1985) 293.

(B) Synthesis of Pt (HY):

3 grams of HY was washed with 800 ml of demineralized water and dried at 110°C for 2 days. The zeolite powder was then dispersed by sonication in 1 litre of water. An aqueous solution of Pt (NH₃)₄Cl₂.H₂O (0.1 g/cm³) was added dropwise whilst stirring; the stirring was continued for 10 hours and then the suspension was filtered. The product was repeatedly suspended in water, centrifuged and separated from the supernatant until the latter was free from unused Pt(NH₃)₄⁺ which is evident by the disappearance of the UV absorbance at 290 nm. The reduction of the incorporated platinum complex within the zeolite was carried out using NaBH₄. The Pt(NH₃)₄⁺ exchanged zeolite powder was kept under flowing nitrogen at 40°C for 16 hours and then suspended in 700 ml of water, the reduction was carried out by dropwise addition of 500 ml 0.1 M aqueous NaBH₄. After 10 hours, platinised zeolite was filtered and washed with hot water and dried at 110°C and stored in vacuum dessicator [2].

(C) Synthesis of Pt-Ru (HY)^b: Reduction by NaBH₄

3 g of HY zeolite was dispersed in 1L distilled water. An aqueous solution of 0.1 g Pt (NH₃)₄Cl₂ and 0.26143 g RuCl₃ in 100 cm³ water was added dropwise to the suspension of HY(3g / L) and the stirring was continued for 10 hours. The suspension was filtered and centrifuged till free from unused Pt(NH₃)₄⁺ and RuCl₃. The reduction of Pt-Ru complex was carried out using 0.1 M NaBH₄ as described above. The resulting catalyst Pt-Ru (HY)^b was washed with water dried at 110°C and stored as before.

2. White et al., Inorganic Chem, Vol 26, No 22, (1987) 3823.

(D) Synthesis of Pt-Ru (HY)^h : Reduction by hydrazine hydrate

For this synthesis procedure similar to that of Pt-Ru (HY)^b is followed , except that the reduction was carried out using hydrazine hydrate. This catalyst is stored as Pt-Ru (HY)^h.

(E) Synthesis of Pt-Sn/Y and Pt-Pd /Y:

Calculated amounts of Pt(NH₃)₄Cl₂, SnCl₂ or PdCl₂ in H₂O were taken and the suspension was stirred for 10 hours .The suspension was filtered, washed and dried ,followed by reduction with 0.1M NaBH₄.The powder was washed with water and dried at 110⁰C and stored as Pt-Sn(HY) and Pt-Pd(HY).

(F) Synthesis of Pt-Ni/Y :

The procedure included the following two stages:

1] Preparation of [Ni(en)₂]Cl₂

1.240 g of [Ni (en)₂]Cl₂ and 0.480 g of NiCl₂ were dissolved in small quantity of water. The resulting blue coloured solution was gently refluxed and evaporated to dryness on water bath. Crystals are seeded with hot mixture of acetone and water. The crystals obtained were greenish blue in colour [3].



2] Preparation of Pt-Ni /Y:

Calculated amounts of [Ni(en)₂]Cl₂ and 0.1 g of Pt(NH₃)₄Cl₂ were dissolved and added dropwise to HY zeolite (3g /100 ml of water). The suspension was continuously stirred for 10 hours and then filtered, washed several times with hot water and finally dried in an air oven at 110⁰C for 6 hours.

3. E. G. Rochow, Inorganic synthesis, Vol (IV)198.

2.1.4 Synthesis of Pt / C :

Appropriate quantity of vulcan XC -72 carbon is boiled at 90 °C in water for about 30 minutes. To this, calculated amount of $\text{Pt}(\text{NH}_3)_4\text{Cl}_2$ dissolved in 100 ml of water is added. Resulting solution is then kept for stirring for 2 hours at 90°C. 250 ml of 0.1M NaBH_4 is added dropwise and stirring is continued for 6 hours. The above solution is then filtered, washed and dried in an oven at 110°C.

2.1.5 Synthesis of Pt-Ru / C:

Appropriate quantity of vulcan XC -72 carbon is boiled at 90 °C in 100ml of water for about 30 minutes. To this, is added an aqueous solution obtained by dissolving calculated amounts of $\text{Pt}(\text{NH}_3)_4\text{Cl}_2$ (50mg) and RuCl_3 (50mg), in 100 ml of water. The resulting solution is then stirred for 2 hours at 90°C. 250 ml of 0.1M NaBH_4 is added dropwise and stirring is continued for 6 hours. The above solution is then filtered, washed and dried in an oven at 110°C.

2.2 Characterisation:

2.2.1 X ray diffraction:

X ray diffraction studies were carried out on a PW1710 X ray diffractometer using Cu K α radiation ($\lambda = 1.544\text{\AA}$), the samples were scanned from 5° to 100° , 2θ . XRD pattern and the data of the various samples is presented in fig 3.18 and discussed in chapter 3.3

2.2.2 Scanning Electron Microscopy (SEM) :

SEM micrograph of the platinised zeolite and platinised bimetallic zeolite catalysts were taken on a JOEL scanning electron microscope. The catalyst sample was spread on alumina foil and coated with a thin film of gold to protect material from thermal damage by the electron beam. SEM micrographs are presented in fig 3.19 and the values of particle size calculated from SEM micrographs are discussed in chapter 3.3

2.2.3 Cyclic Voltammetry:

Cyclic voltammograms of the catalysts HY, Pt(HY) and Pt-Ru (HY) were carried out using 273 Princeton potentiostat / galvanostat using manual recorder. Calomel was used as reference electrode and platinum electrode was used as counter electrode. The working electrode was prepared by mixing 10 mg of the above samples with 0.5 ml of paraffin and applying the paste on to a small platinum substrate (0.25 cm x 0.25 cm) and subsequently drying in an oven at 100°C for 10 minutes. Experiments were carried out at room temperature and at 60°C using 5 ml of 2.5 M H_2SO_4 and 1.0 M CH_3OH .

The cyclic voltammograms of the samples are discussed in section 3.4

2.2.4 *In situ* fourier transform infra red spectroscopy :

In situ FTIR spectroscopic studies following CO or methanol adsorption carried out on Pt-Ru (Y) and Pt(Y) in the temperature range 270 and at pressures 10- 100 torr . The self supporting samples wafers of 25 mm diameter and weighing about 80 mg were mounted in a high temperature high pressure IR cell fitted with water cooled CaF₂ window. A Mattson model Cygnus 100 FTIR equipped with a DTGS detector is used in this study.

The samples were heated in with or without hydrogen atmosphere *in situ* to remove adsorbed oxygen at 250⁰C for 2 hours and they were further heated in vacuum at 300⁰C to remove adsorbed hydrogen. Samples were cooled under vacuum up to room temperature. Scans for background spectrum were recorded with pellet as reference. CO is then introduced at desired pressure and temperature. Various scans of the spectrum at different time intervals were recorded. The spectra due to adsorbed species were then plotted by subtracting the CO gas spectrum of appropriate intensity from the IR spectrum of the samples. The overlapping spectral bands were separated using computer software of FTIR in order to determine the number and the position of the individual peaks.

Carbon monoxide (99.9% purity , from Arico,USA) was purified before use by enclosing in a solid carbon dioxide trap in order to remove the traces of the metal carbonyl and moisture impurities. Samples were evacuated and heated at 300⁰C and methanol absorption studies were carried out with or without passing oxygen into the reactor.

Each sample was exposed by injecting 10 microlitre of distilled methanol followed by 4ml of oxygen. The absorption spectra were scanned for 30 minutes. The details regarding information of the spectra are discussed in section 3.5.

2.3 Hydrogen peroxide catalytic decomposition studies:

H₂O₂ decomposition activity of the catalysts (25 mg) was measured in 25 ml 0.1 M H₂SO₄ solution using 1ml of 1.013 M H₂O₂ (6% w/v, 20 volumes). The reaction kinetics were followed isothermally at three different temperature (30-40 °C) by determining the volume of oxygen released (Vt) as a function of time in a gasometer assembly. Arrhenius parameters were determined using first order equation. The plots are shown in fig 3.14 and 3.15.

The experimental details regarding electrode fabrication, fuel cell design fabrication and testing are given in appropriate sections of chapter 3 and chapter 4.

CHAPTER 3

ELECTROCATALYSIS

ELECTROCATALYSIS

This chapter is divided into following sections:

3.1 General method for fabrication of electrode.

3.2 Electrochemical measurements towards methanol oxidation.

3.3 Results and discussions.

3.4 Cyclic voltammetric studies.

3.5 *in situ* FTIR studies.

This chapter describes evaluation of electrocatalytic activity of the various catalysts prepared in this work, by the use of conventional three electrode assembly as shown in fig 3.1.

Working electrodes were prepared from the catalyst and half cell polarization studies were carried out to give measure of electrocatalytic activity.

The various catalysts are grouped below.

Group A : Ni-manganese oxides,

Group B : HY, Cu₂O, Cu Y and Cu₂O(NaY),

Group C : Pt/ C, HY, Pt (HY),and Pt-Ru (HY),

Group D: Pt-Ru (HY), Pt-Ni (HY), Pt- Sn (HY) and Pt-Pd (HY).

3.1(a) General method for fabrication of gas diffusion porous carbon electrodes:

The catalysed porous electrodes were obtained by the following procedure: An appropriate amount of Vulcan XC 72 which was previously activated at 450 ° C for 5 hours in a furnace, was suspended in 50 ml of conductivity water and boiled at 85-90 ° C for nearly 1 hour. The resultant slurry was mixed by grinding in mortar and pestle for 3 hours with appropriate amount of catalyst material. To this mixture (20mg) 5% by wt teflon binder was added along with 5ml of isopropanol and mixed thoroughly for 30 minutes. The putty like mixture thus obtained was stretched on a platinum collector. It was then converted into pellet by pressing in a die (fig.3.32) of diameter (1.4 cm²) using pressure of 115 kg / cm² for 3 minutes and further heated at 340 °C at the pressure 200 kg/cm².

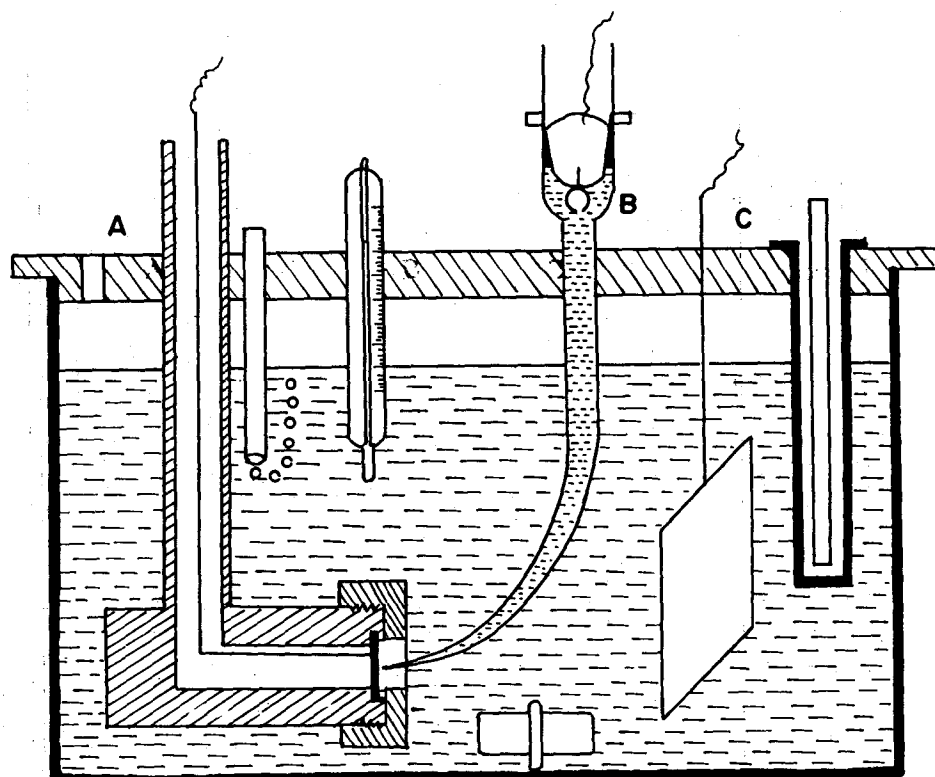


Fig3.1 Conventional three electrode set up
A= working electrode, B= Reference electrode , C= counter electrode

Adopted from :

Shukla et. al. J. Electrochem. Soc., 141 (1994) 1517

(b) Preparation of Nickel- manganese oxides electrodes:

These electrodes were prepared by adopting the following procedure;

In this work Nickel- manganese oxide electrodes are prepared by the following method:

Thermal decomposition of catalyst precursors on a platinum substrate for all modifications was performed using the following procedure:

- i) An appropriate amount of metal nitrate or mixed metal nitrate in aqueous form was impregnated with a suitable oxidizing agent.
- ii) Thin layers of the above mixtures were applied to platinum foil.
- iii) The composite from (ii) were gradually dried in a furnace at different temperatures. A platinum plate of size 1cm x 2.2 cm x 2.2mm was used as the substrate. A solution of 0.1 M $\text{Mn}(\text{NO}_3)_2$ prepared in 0.1M HNO_3 aqueous solution was applied to one side of substrate in several successive coatings, the solution was dried at 100°C in an oven and decomposed in a furnace at 170°C for 10 minutes. The geometric area exposed to the solution was 1cm^2 .

Nickel modified manganese oxide catalysts were prepared by taking an appropriate amount of salt typically 0.1M nickel nitrate or Ferric nitrate, 0.1M $\text{Mn}(\text{NO}_3)_2$ and sodium chlorate and applying this mixed solution to a platinum substrate using the above procedure.

Electrochemical measurements were carried out as described in section 3.2

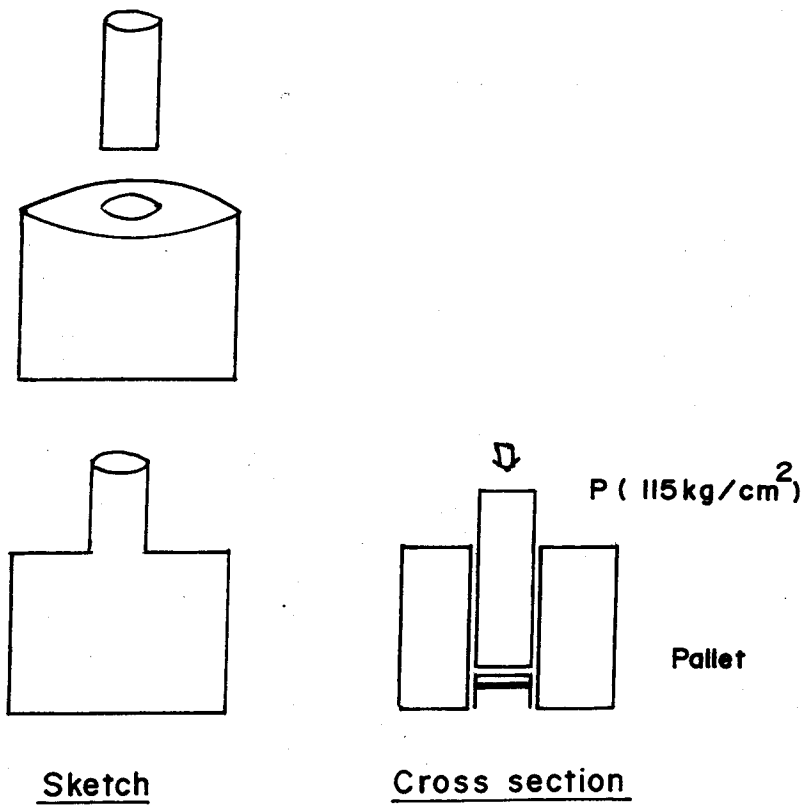


Fig3.2 Schematic diagram of die for pressing electrode powder into pellet

3.2 Electrochemical measurements towards methanol oxidation :

The catalyst gas diffusion electrode was mounted on teflon holder and assembled in three electrode system as shown in fig. 3.1. The steady state polarization tests were carried out in 100 ml solution of 1.0 M CH_3OH in 2.5 M H_2SO_4 at 60°C . The working electrode area exposed to the electrolyte was 1.020 cm^2 . A large area platinum foil was used as counter electrode. The reference electrode was saturated calomel electrode whose tip was placed appropriately close to the working electrode through luggin capillary. Steady state measurements were carried out and presented as C-V curves of η v/s $\log i$ tafel plots.

3.3 Results and Discussions:

3.3.1 Nickel modified manganese oxide as an active electrocatalyst.

Polarization curves are presented in fig 3.3-3.7. Fig 3.3 makes a comparative study of Fe³⁺ doped Ni²⁺ doped manganese oxides for methanol oxidation at 25⁰C and 60⁰C. The activity of the catalyst is measured in terms of minimum overpotential required to generate a fixed value of current density.

Thus at a current density of 100 mA cm⁻², it can be seen that the Ni²⁺ doped manganese oxide has a superior electrocatalytic activity by 140 mV i.e., it gives a higher current output at an overpotential which is 140mV less than that of the Fe³⁺ doped samples (Table3.1). Therefore, the nickel/manganese oxide were investigated further. The electrocatalytic activity was also dependent on the temperature at which the deposited electrodes were heat treated. Hence, they were subjected to heat treatment between 250⁰C and 450⁰C. The activity was found to increase with increasing temperature of heat treatment. At a current output of 100 mA cm⁻², for example, the 450⁰C heated samples exhibit an overpotential which was 100 mV less than that for the 250⁰ C heated samples, when a comparison is made between the potential curves at 60⁰ C (fig 3.4 and table3.2). Heat treatment beyond 450⁰C was not undertaken since manganese oxides are known to undergo phase changes at such temperatures.

Catalyst	Temp ⁰ C	Overpotential obtained at 100 mA / cm ²
Mn- Fe	25 ⁰ C	610
Mn-Fe	60 ⁰ C	580
Mn-Ni	25 ⁰ C	550
Mn-Ni	60 ⁰ C	440

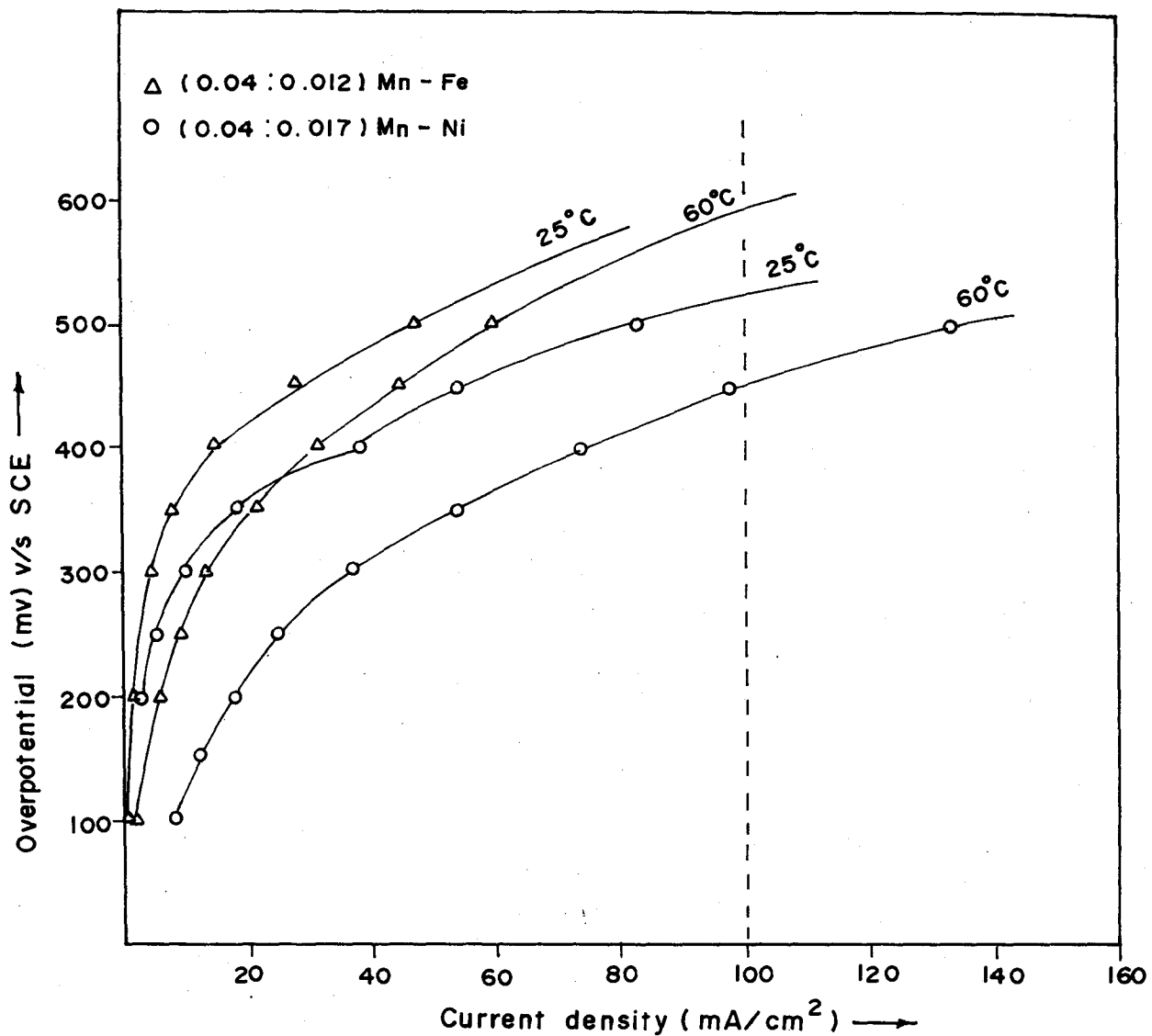


Fig.3.3 Anodic polarisation curves (2.5M H₂SO₄, 1M CH₃OH) for electro-oxidation of methanol on modified manganese dioxide electrodes as a function of nature of dopant Fe³⁺ and Ni²⁺

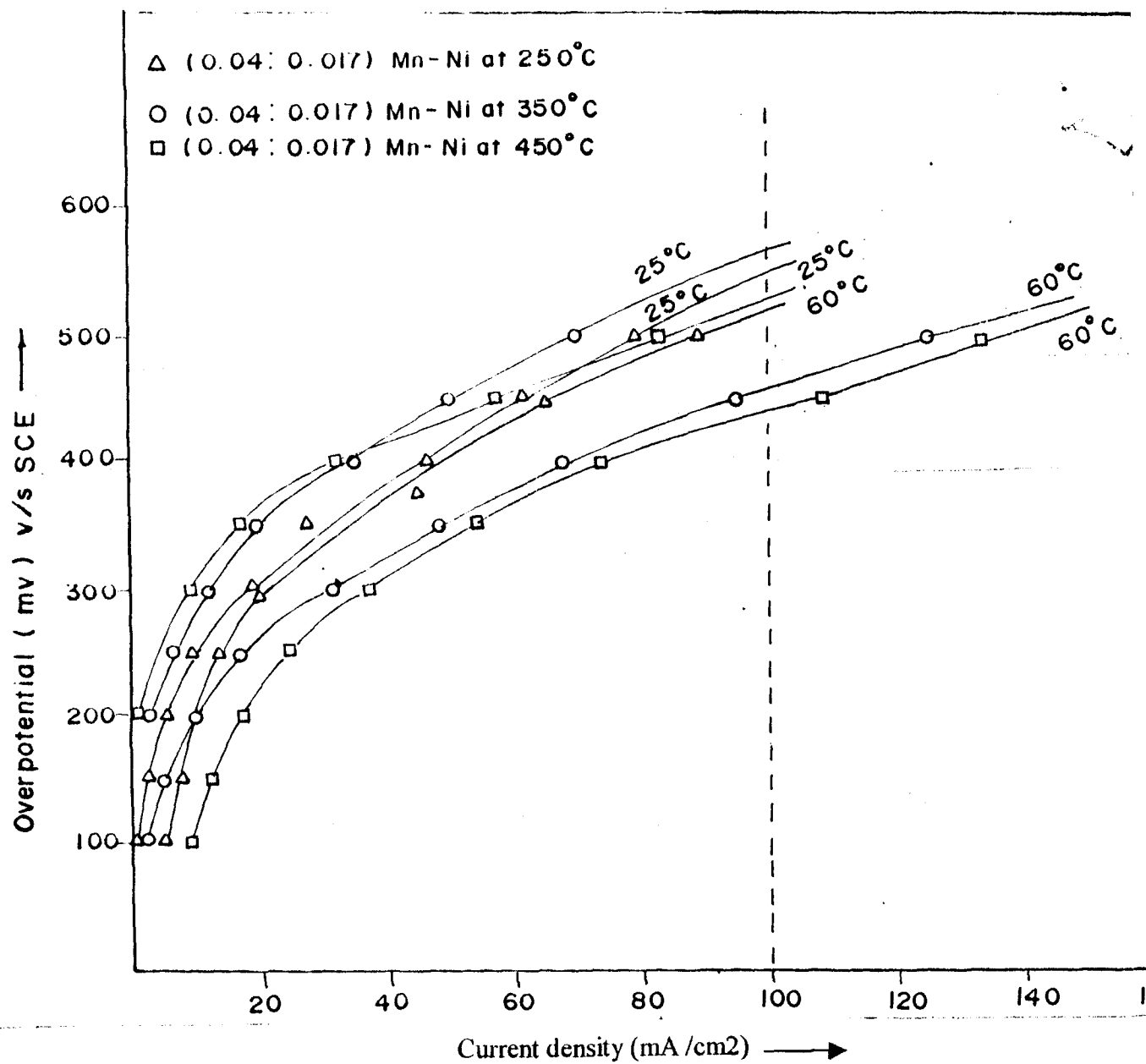


Fig 3.4 Polarization curves (1M CH₃OH/ 2.5M H₂SO₄) for electrooxidation of methanol on modified manganese dioxide electrode at 25°C and 60°C as a function of heat treatment

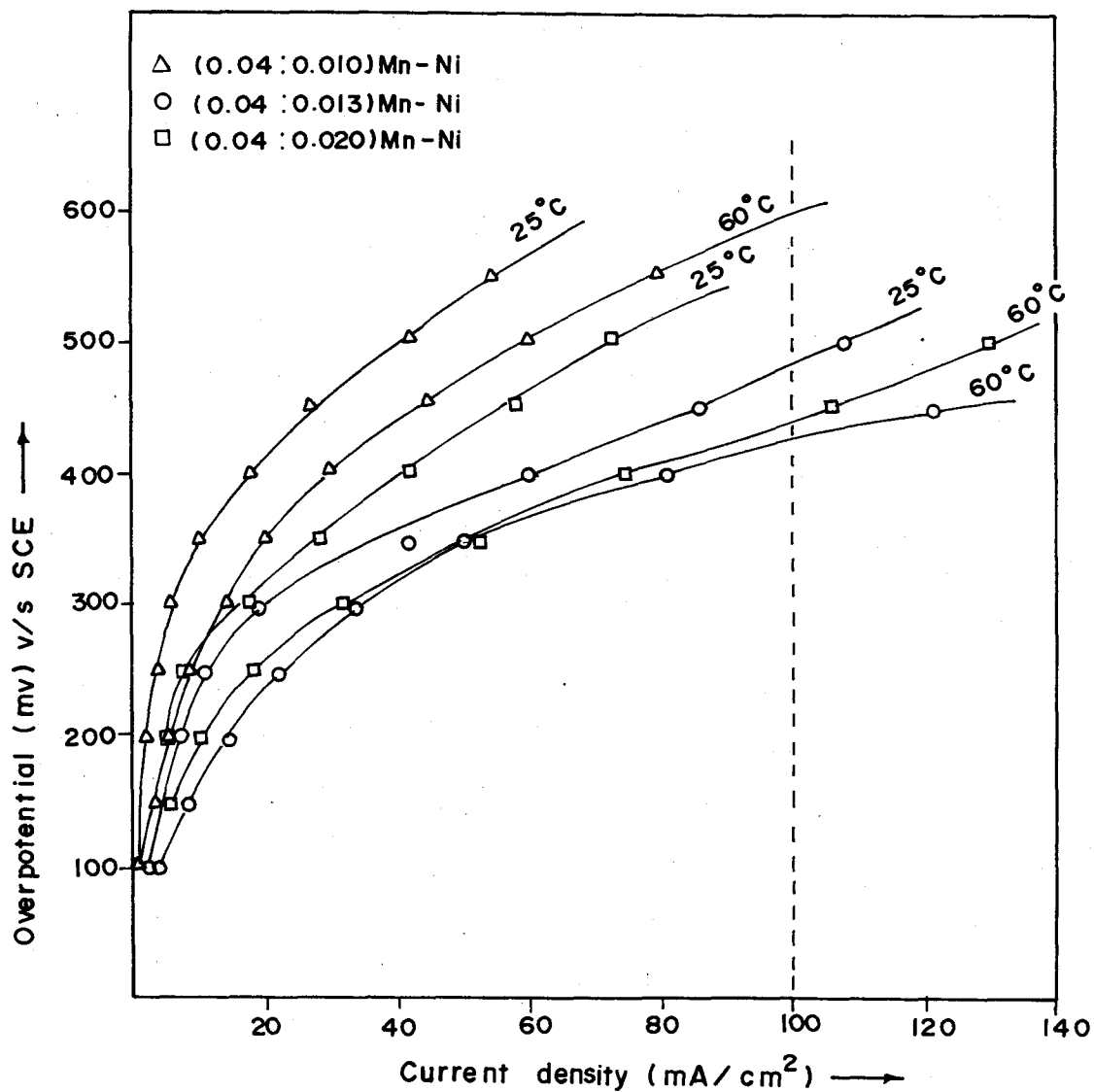


Fig.3.5 Anodic polarisation curves (2.5 M H₂SO₄, 1M CH₃OH) for electro-oxidation of methanol on modified manganese dioxide electrodes as a function of molar composition of Ni⁺²

Table 3.1. Variation of overpotential at different temperature as a function of modified manganese dioxide at current density of 100 mA / cm².

Calcination Temp °C	overpotential obtained at 100 mA / cm ²
250 ⁰	525
350 ⁰	450
450 ⁰	425

Table 3.2 . Variation of overpotential as a function of heat treatment on Mn-Ni catalyst at a current density of 100 mA/cm² measured at 60⁰C .

In order to elucidate the effect of the amount of Ni²⁺ in the manganese oxide, an investigation was performed by preparing manganese oxides which contained varying amounts of Ni²⁺, viz Mn:Ni composition of 0.04:0.010, 0.04:0.013 and 0.04:0.020. The polarization curves for these samples are given in fig 3.5. The samples with 0.04:0.013 Mn : Ni display better characteristics than the 0.04: 0.010 or 0.04:0.020 samples .Thus, an optimum amount of Ni²⁺ in manganese oxide is desirable. A comparison of the curves at 60⁰ C (current density = 100mA cm⁻²) for the 0.04: 0.010 and 0.04:0.013 samples showed that the overpotential of the latter samples was lower by 225 mV, for the 0.04: 0.013 and 0.04:0.020 samples, the overpotential of latter is less by 20 mV.

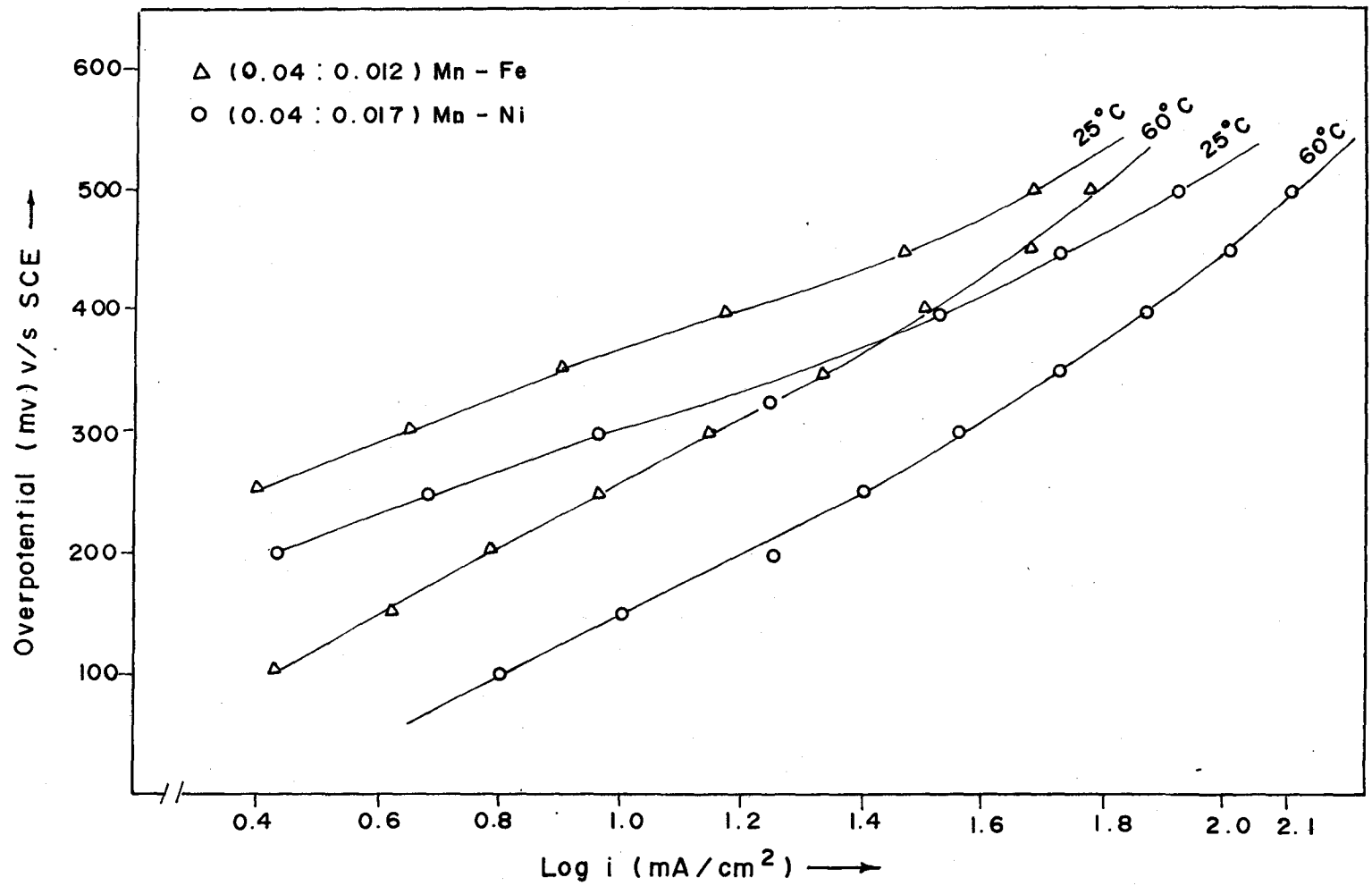


Fig.3.6 Tafel plots (2.5 M H₂ SO₄, 1M CH₃ OH) of Fe⁺³ and Ni⁺² doped manganese dioxide

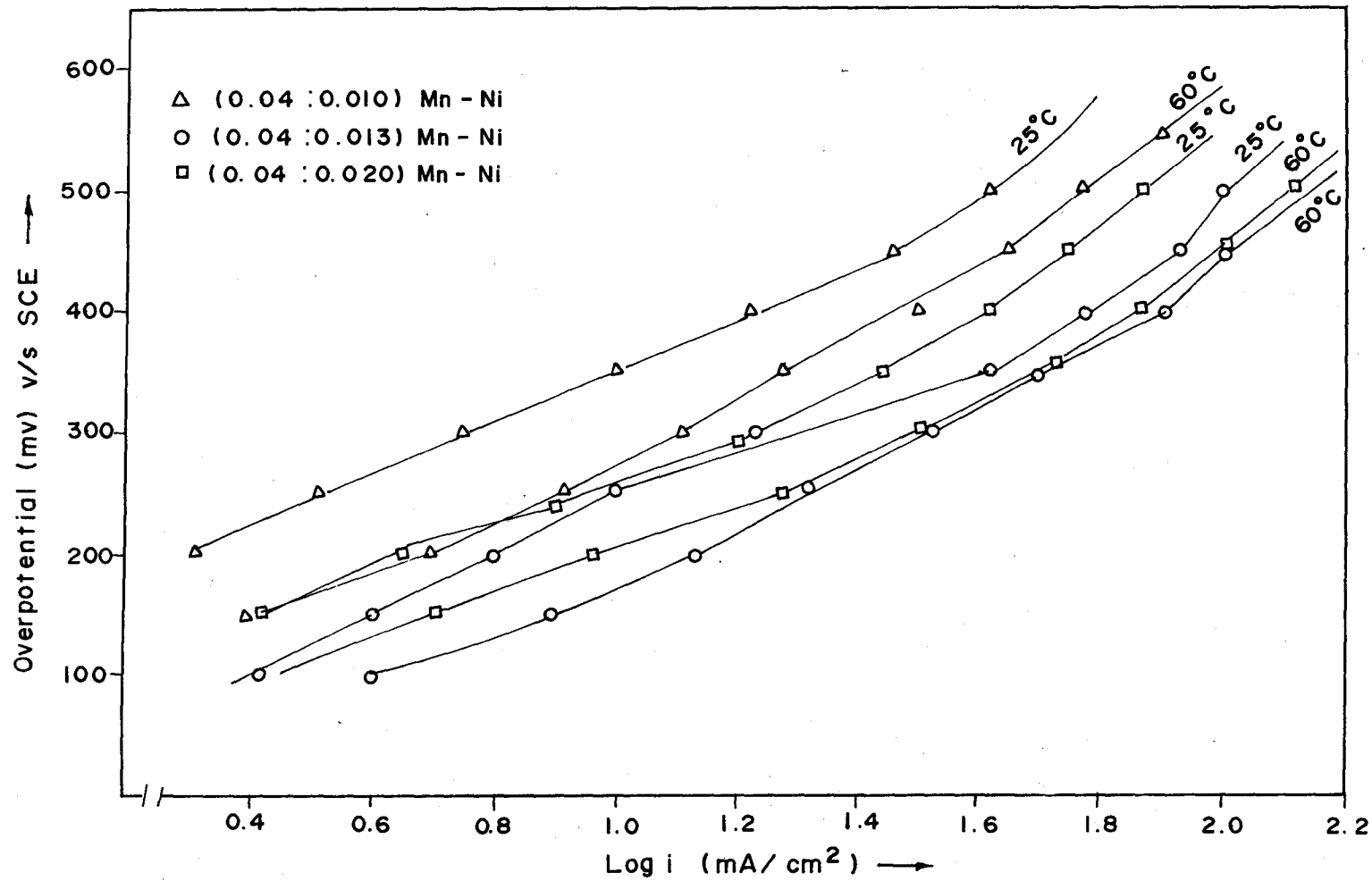


Fig.3.7 Tafel plots (2.5M H₂SO₄, 1M CH₃OH) of manganese dioxides containing varying amounts of Ni²⁺

Catalyst composition	Overpotential obtained at 100mA/cm ²
4 : 1	510
4 : 1.3	430
4 : 2	410

Table 3.3. Effect of catalyst composition of Mn-Ni on overpotential measured at 60°C.

A comparative study of Tafel plots of Fe³⁺ doped and Ni²⁺ doped manganese oxides of composition 0.04: 0.012 Mn-Fe and 0.020 Mn - Ni is given fig 3.6. The data are in agreement with the above observations that Ni²⁺ doped samples are superior to Fe³⁺ doped samples as the latter showed a significantly higher overpotential at low current density.

Tafel plots for various Ni²⁺ doped manganese dioxides (0.04:0.010, 0.04:0.013, 0.04:0.020) are given in fig 3.7. The Tafel slopes of the various plots are all around 180mV, i.e. about twice that reported for the conventional platinum based electrocatalyst (~95 mV) for the electro-oxidation of methanol. The magnitude of the Tafel slopes is known to depend on the electrocatalytic reaction mechanism and the adsorbed states of the methanol and its decomposition products. We therefore predict that new type of mechanism is occurring on the modified manganese dioxide electrodes. In fact, in a recent investigation of Pt-WO₃ electrodes for methanol electrooxidation, Hamnett et al [1] predicted an oxyhydroxide surface structure which can be associated with proton insertion electrode [2-6] and has an active hydroxylated surface. Experiments with Ni²⁺ doped manganese oxide samples, indicated a rich hydroxylated surface. We

therefore suggest simultaneous proton – electron intercalation of the nickel – manganese electrode which favours the electrooxidation of methanol.

Conclusions:

- 1.) A new Ni^{2+} modified manganese oxide electrode is investigated for the first time, for the anodic oxidation of methanol.
- 2.) Ni^{2+} modified electrode is found to be quite active for methanol oxidation. By contrast Fe^{3+} modified oxide exhibited poor electrocatalytic activity.
- 3.) The activity of Ni^{2+} modified electrodes is dependent on (i) the temperature of the thermal treatment of electrodes; (ii) the amount of Ni^{2+} in the electrode; and (iii) the nature of dopant.
- 4.) The anodic oxidation of methanol on oxide intercalation electrodes, such as modified manganese dioxide, is believed to follow a mechanism, which is different from that on conventional platinum – based electrodes.

Published in *J. Power Sources*, 79 (1999) 114.

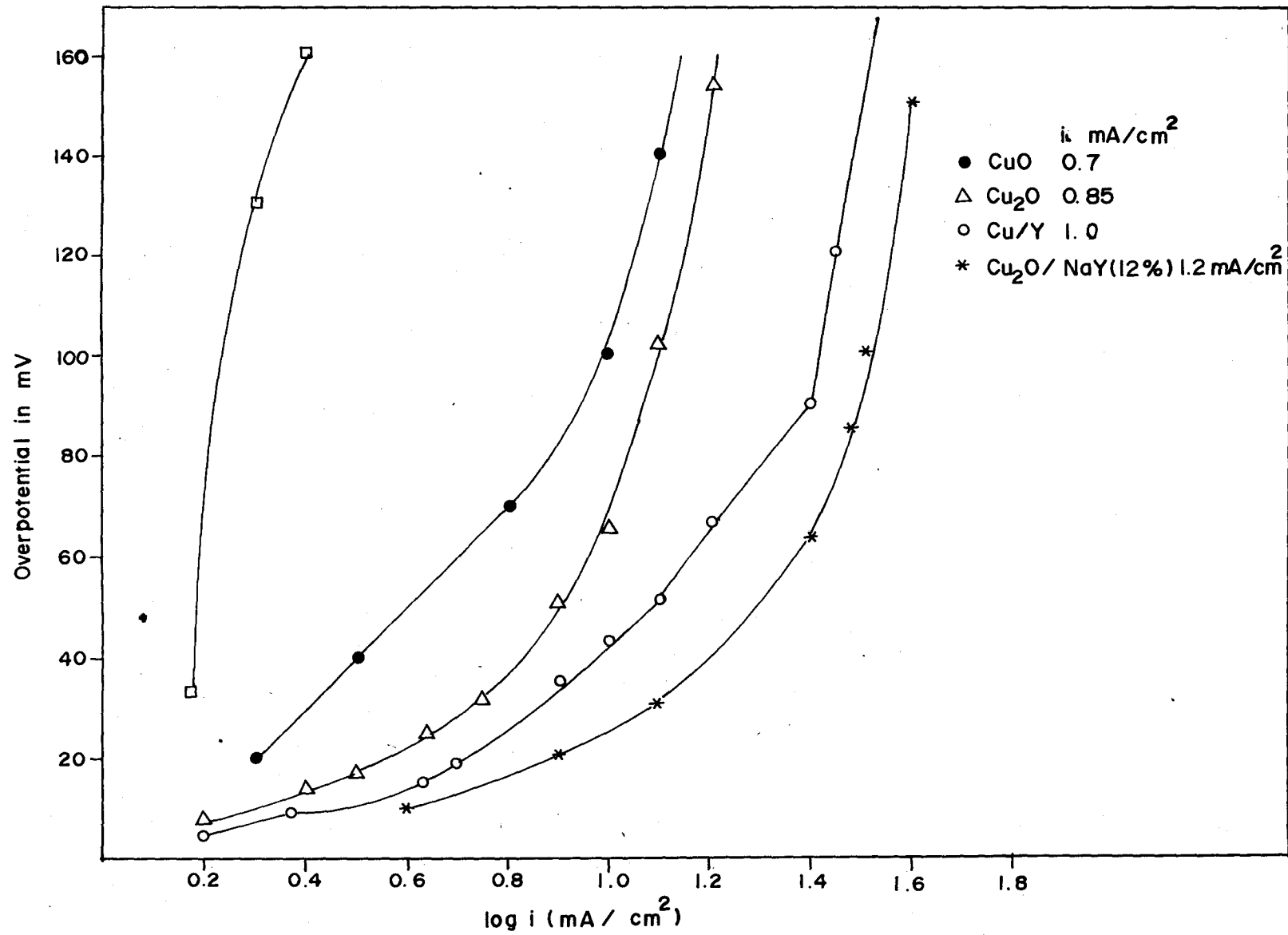


Fig.3.8 Tafel plots (2.5 M H₂SO₄, 1M CH₃OH) of different Catalyst materials

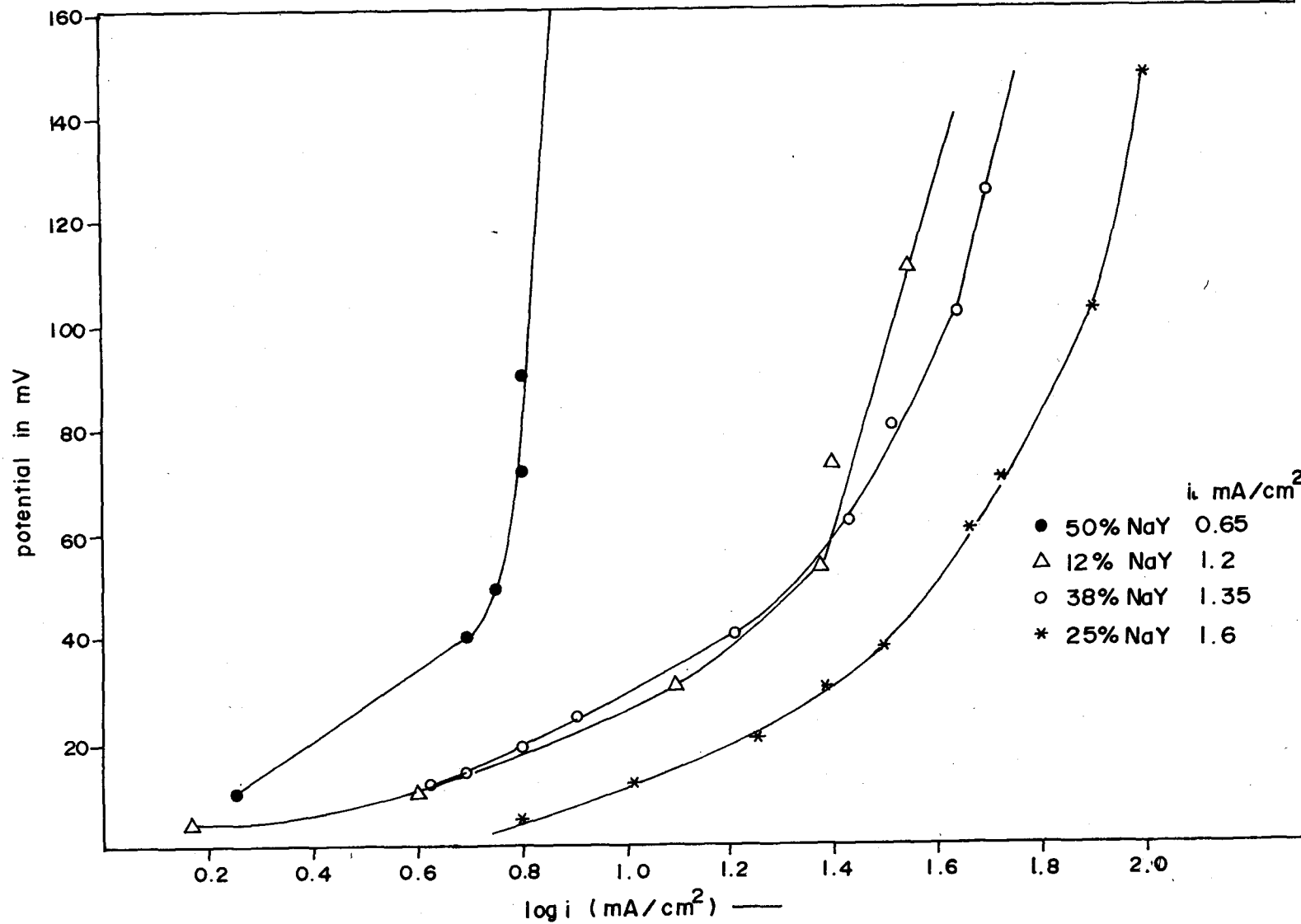


Fig.3.9 Tafel plots ($2.5 \text{ H}_2\text{SO}_4$, $1 \text{ M CH}_3\text{OH}$) for electro-oxidation of methanol a function of catalyst composition (w/w) with respect to $\text{Cu}_2\text{O}/\text{Y}$

3.3.2 Electrocatalytic activity of CopperY based zeolite catalyst:

Tafel plots for the various catalysts HY, Cu₂O, CuY and Cu₂O(NaY) are given in fig 3.8. Tafel plots for Cu₂O (NaY)in various proportions are given in fig 3.9. The intercept on the log i axis give a measure of electrocatalytic activity .It is clear from Fig 3.8 that Cu₂O is more active than CuO. Similarly Cu₂O NaY mixed catalyst showed better activity towards methanol oxidation. The electro-oxidation of methanol, is therefore favoured by copper oxide catalyst in which copper is in monovalent state, and the electrocatalytic activity is enhanced in the presence of Y zeolite. In general the catalytic activity followed the order:



Further it is seen from fig 3.9 that an optimum level of ~25% NaY by weight in relation to Cu₂O is desirable for the best catalytic activity, probably to stabilize Cu¹⁺ in the zeolite matrix. Activity decreased if the percentage of NaY was increased beyond 30% or decreased below 20%. Higher methanol oxidation rate is mediated by Cu¹⁺ in the catalyst would imply corresponding reduction of Cu¹⁺ to metallic copper. An intrazeolite ion diffusion mechanism is believed to occur in Cu²⁺- NaY modified glassy carbon electrode [7] wherein Cu²⁺ diffuses through the zeolite framework to undergo reduction at the electrode surface to Cu¹⁺ state .In the next step Cu¹⁺ could either diffuse back into the zeolite bulk or undergo further reduction to Cu⁰ as shown in fig 3.10. The cation migration from the electrolyte into the zeolite bulk for charge compensation is believed to be rate the limiting step. In the present investigation, since experiments are carried out in sulfuric acid, one does not expect the cation migration to be the rate limiting step, as proton

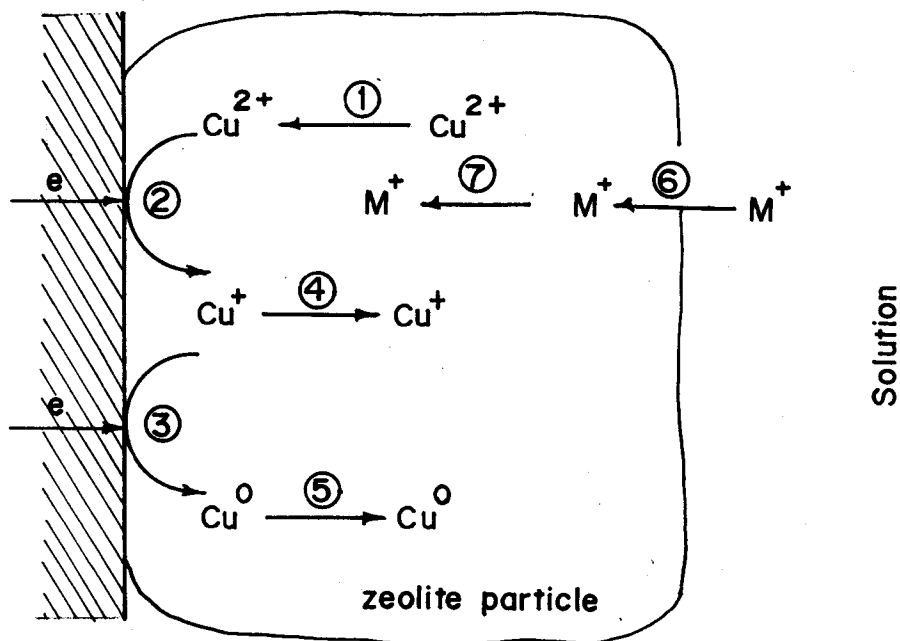
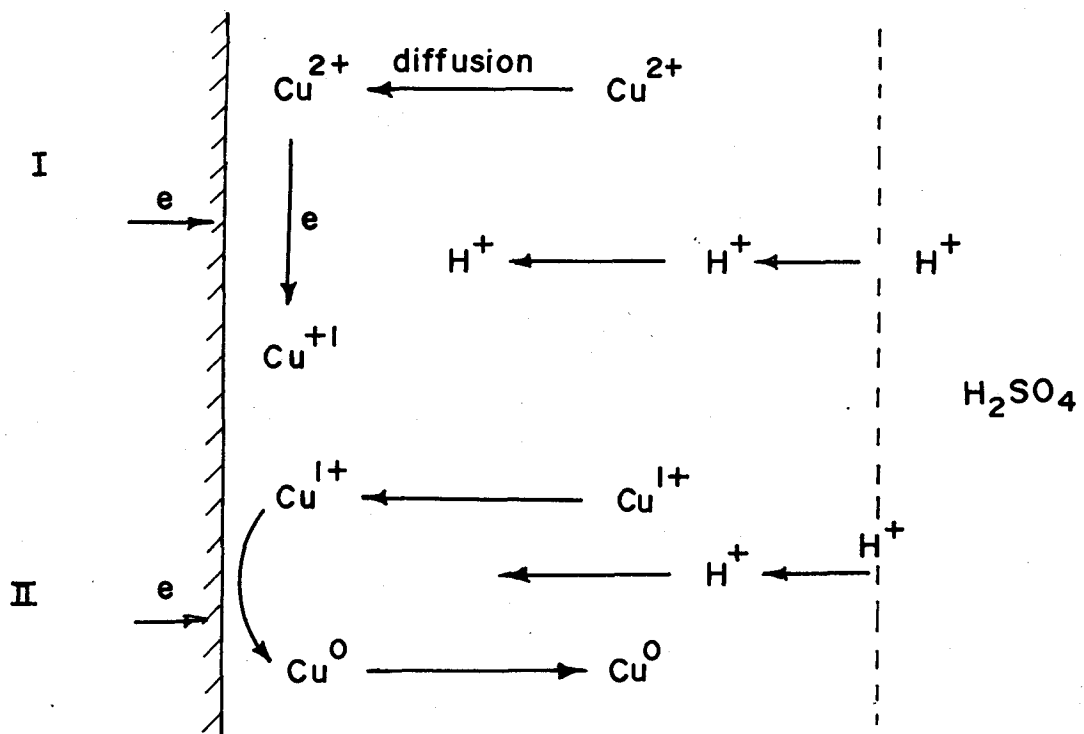


Fig.3.10 Possible rate-limiting steps in electrochemical reduction

- 1 Diffusion of Cu^{2+} ions from the bulk of zeolite to the surface
- 2 Reduction of Cu^{2+} to Cu^+
- 3 Reduction of Cu^+ to Cu^0
- 4 Diffusion of Cu^+ into the bulk of zeolite
- 5 Diffusion of Cu^0 into the bulk of zeolite
- 6 Movement M^+ into the zeolite to maintain charge neutrality
- 7 Diffusion of M^+ within the zeolite

Adopted from :

Jian-wei Li et.al, J. Electroanal. Chem., 377 (1994) 163



For $\text{Cu}^{2+} \rightarrow \text{Cu}^{+1}$ is R.D.S.

in Cu_2O ; $\text{Cu}^{+1} \rightarrow \text{Cu}^0$ is R.D.S.

$\therefore \text{Cu}_2\text{O}$ is more active Cu O

Fig 3.11 Possible intrazeolite mechanism for reduction of Cu_2O during electrooxidation of methanol

mobilities are comparatively low activation energy processes . Further since CuO is less active catalyst than Cu₂O with or without zeolite , it is reasonable to conclude that Cu¹⁺ to Cu⁰ process can be rate limiting rather than operation of Cu²⁺/ Cu¹⁺ redox couple during methanol electro-oxidation (fig 3.11).

Further the enhancement of activity, both in case of Cu²⁺ and Cu¹⁺ catalysts in presence of Y zeolite could be merely due to the stabilizing effect of the matrix on the copper cation and to make the catalyst less susceptible to CO poisoning by facilitating its oxidation to CO₂

Conclusion:

1. Cu₂O mixed with NaY electrode is an active catalyst for methanol oxidation.
2. An optimum amount of 25% NaY in Cu₂O is desirable for better activity.
3. Intrazeolite transport mechanism is believed to occur in Cu²⁺ NaY and Cu¹⁺ to Cu⁰ is the rate limiting step.

Published in "*Recent Trend in Catalysis*" ,V. Murugesan, B. Arbindo, M. Palamchamy, (eds) , Narosa publishing house (1999)230.

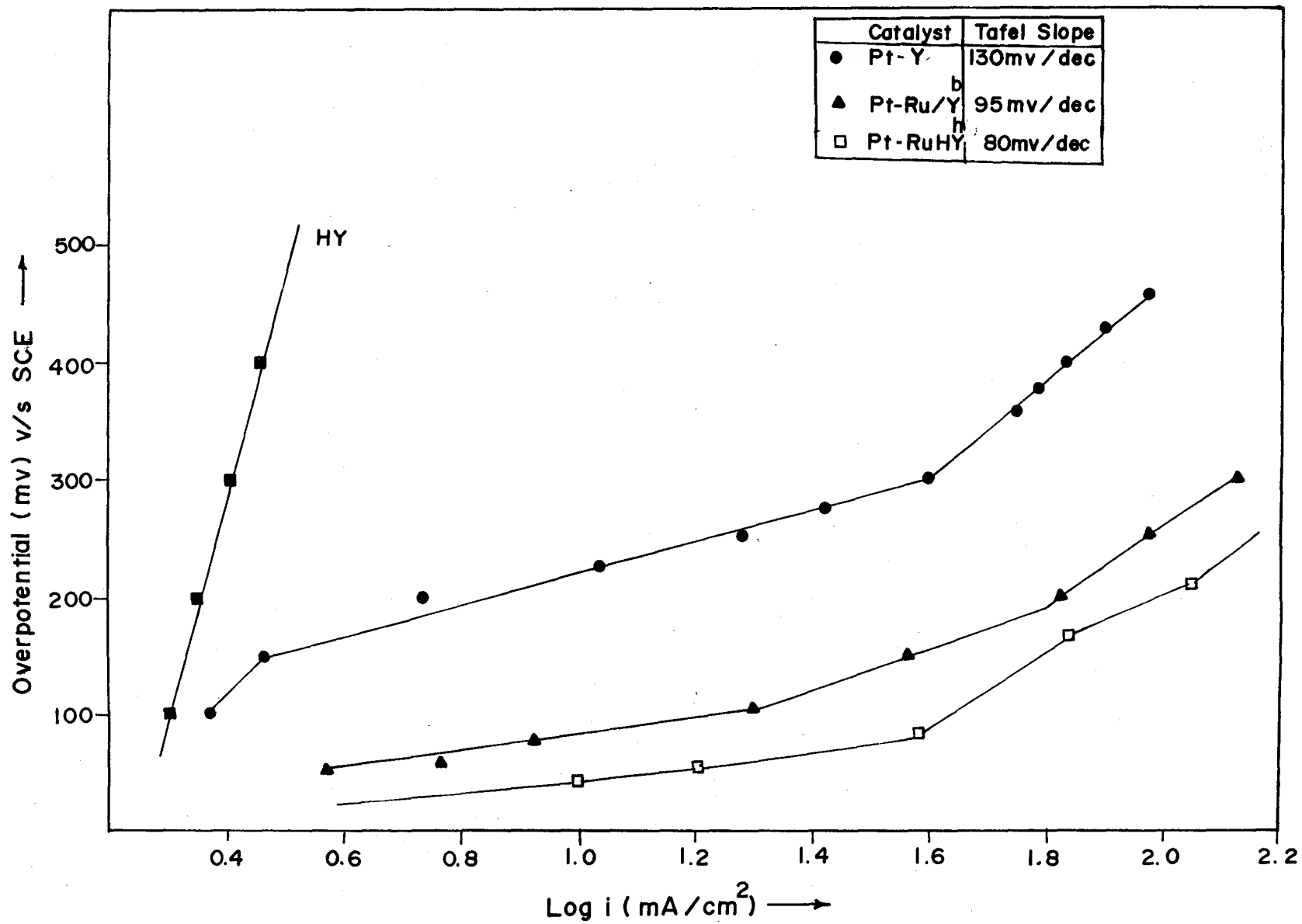


Fig. 3.13 Tafel plots ($2.5 \text{ mol dm}^{-3} \text{ H}_2\text{SO}_4$, $1 \text{ mol dm}^{-3} \text{ CH}_3\text{OH}$) for methanol oxidation on various electrocatalysts at 333 K.

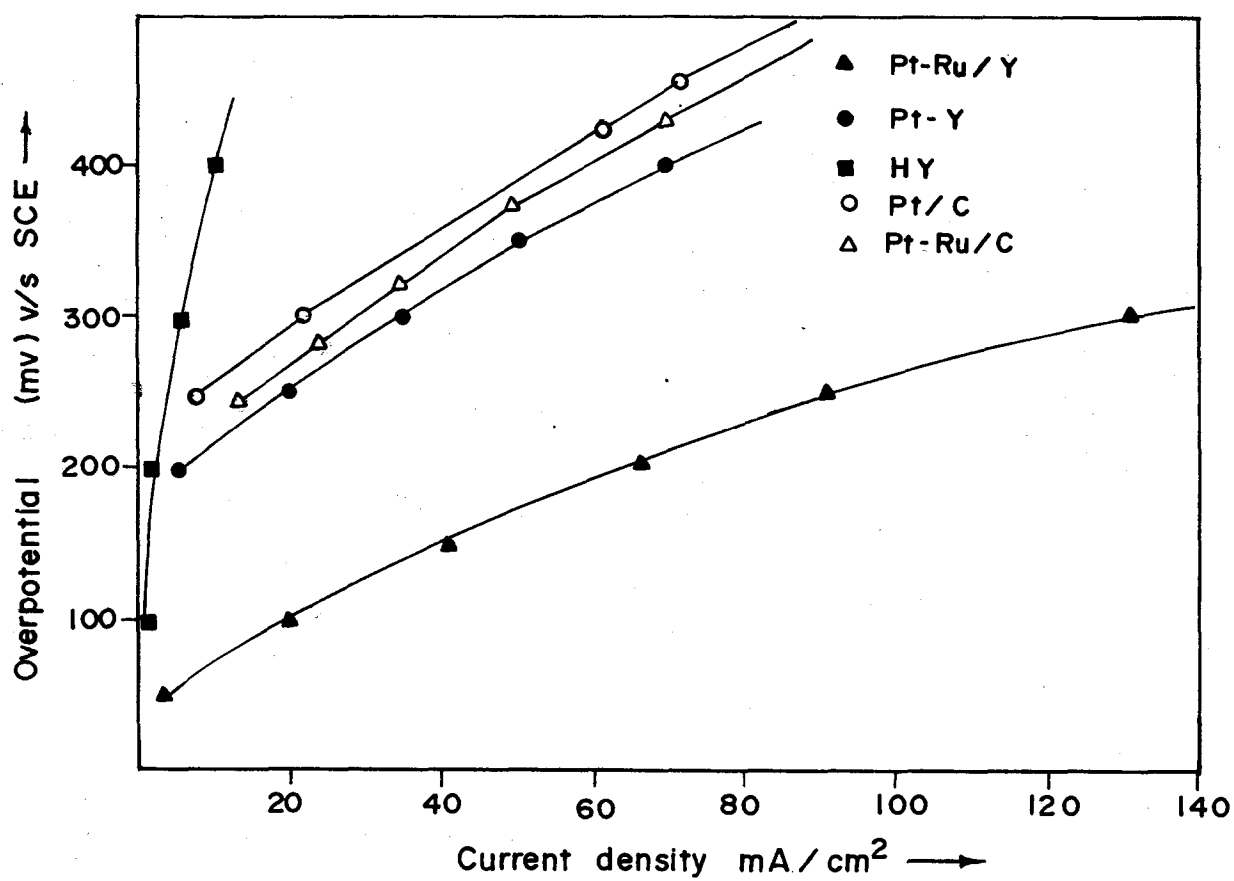


Fig 3.12 Polarization curves ($2.5 \text{ mol dm}^{-3} \text{ H}_2\text{SO}_4$, $1 \text{ mol dm}^{-3} \text{ CH}_3\text{OH}$) for oxidation of methanol at 333 K on various electrocatalyst.

3.3.3 Enhanced electrocatalytic activity of Pt (HY) and Pt-Ru (HY):

The previous two sections described the activity of new electrocatalysts, synthesised in this work which are found effective for methanol oxidation. It is reported therein for the first time the favourable role of Y zeolite during electrocatalysis of methanol. This section describes electrocatalysis by noble metal catalysts in presence of Y zeolite.

The activity of the electrocatalysts for methanol oxidation may be considered to be a measure of its ability to decompose methanol to carbon dioxide by preventing the accumulation of partially oxidized intermediates or poisons such as adsorbed CO and/or COH. Fig.3.12 and 3.13 gives the current voltage (I-V) and Tafel plots η v/s $\log i$ respectively for methanol oxidation on various electrocatalysts. For convenience, the activity of the catalysts may be compared with respect to the current densities produced at some fixed overpotential. Thus at an overpotential of 250 millivolts the following current densities are observed (the values derived from Fig.3.12).

Catalyst	HY	Pt(HY)	Pt/ C	Pt-Ru(HY)	Pt-Ru / C
Current density mA/cm ²	03	18.62	7.94	87.09	15

Table 3.4 : Comparison of current densities versus catalyst at an over potential of 250 mV at 60⁰C in 1M CH₃OH and 2.5M H₂SO₄.

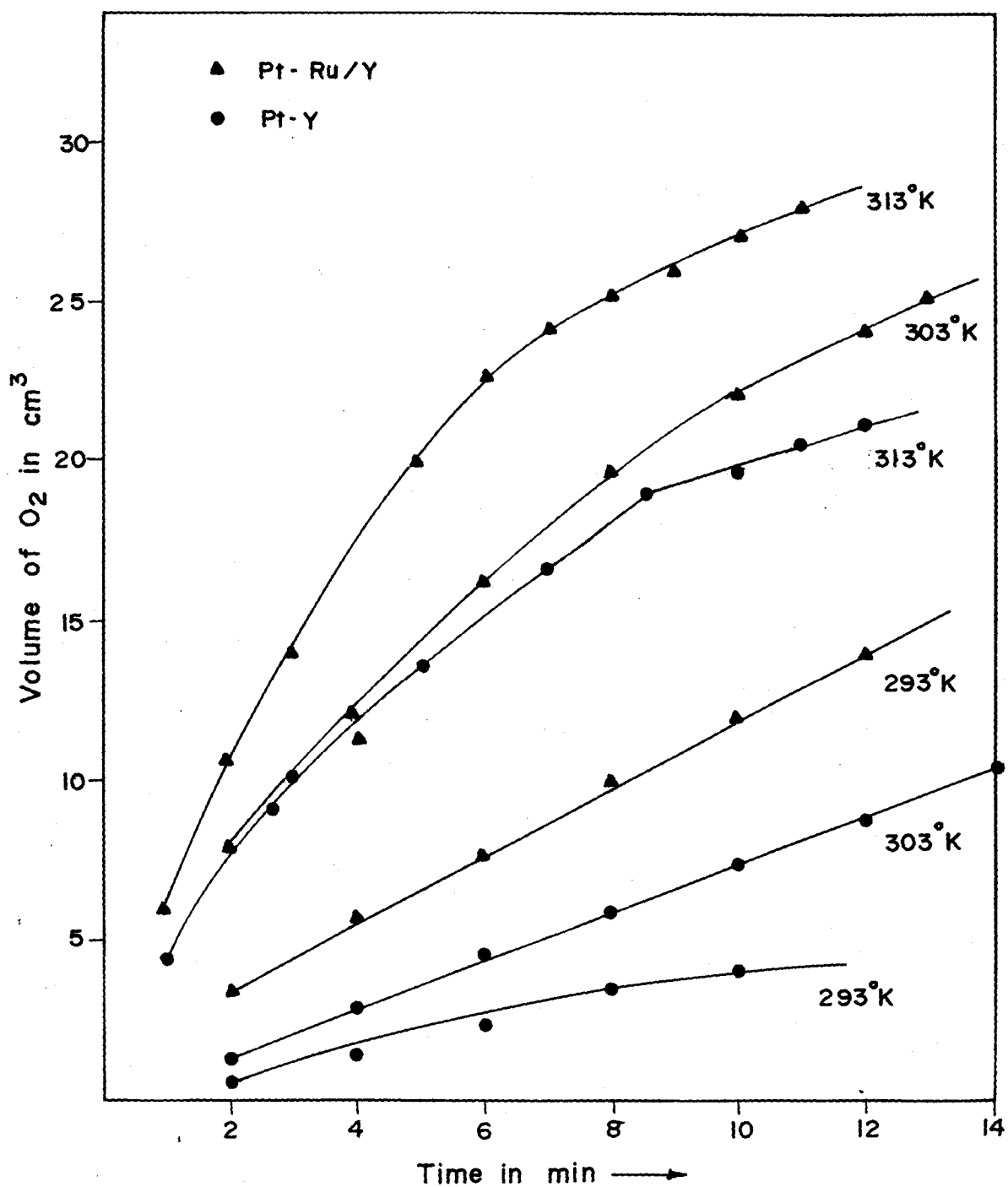


Fig.3.14 Peroxide decomposition profiles with different catalysts at the initial concentration of $0.13 \text{ mol dm}^{-3} \text{ H}_2\text{O}_2$ in $0.1 \text{ mol dm}^{-3} \text{ H}_2\text{SO}_4$ recorded as a function of temperature.

zeolites. Since in case of methanol oxidation, which precedes methanol adsorption on platinum sites, carbon monoxide type adsorbed species will necessarily have to cluster on metal sites at specific location / cages in zeolites. This assumption is justified considering recent theoretical studies that CO adsorption is sensitive to electronic state of platinum in zeolite [14]. It is shown that synergistic effect for methanol oxidation is observed only on sputtered Pt-Ru alloy and not on its annealed form [11]. It is therefore reasonable to conclude that zeolite Y provide an environment analogous to formation of sputtered or dispersed Pt-Ru alloy, specially at low metal loading (~5 %) in the catalyst used in the present work. Also we believe that the formation of ruthenium clusters as a nanoelectrode as in case of annealed alloy within platinum in the zeolite cage is not desirable, as adsorbed OH groups on adjacent ruthenium atoms could undergo mutual dehydration, and not available for decomposition of adsorbed CO species. Thus based on the above discussion a plausible explanation for superior oxidation kinetics in presence of zeolite Y could be due to *“preferential formation of CO clusters on platinum, limited by the steric constraints imposed by the zeolite framework, followed by its facile oxidation to CO₂ by interaction with the surface or bridged hydroxyls of the zeolite and/or dispersed Ru OHads species.”*

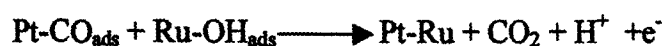
That platinum and Pt-Ru are better oxidation catalysts in presence of zeolite Y is confirmed by the fact that these catalysts are also highly active in H₂O₂ decomposition reaction. Just as HY is not active in methanol electrooxidation, it also does not have any activity for H₂O₂ decomposition to oxygen; the catalytic activity for H₂O₂ decomposition followed the order



The relative activity of these catalysts in terms of rate of decomposition of H₂O₂ is illustrated in fig 3.14 at different temperatures. The activation energies for decomposition of H₂O₂ calculated from Arrhenius

It is immediately clear from the above data that metal catalysts in zeolite Y matrix cause profound enhancement in electrocatalytic activity. HY zeolite used in the present work by itself did not have any significant activity. This fact was also reported earlier [8] hence for identifying the role of zeolite Y, one may recall in brief the current state of understanding of the mechanism of methanol electrooxidation.

Synergistic increase in electrocatalytic activity of platinum electrodes by ruthenium in carefully prepared Pt-Ru alloys seems to be well-understood [9] and elaborated in the further sections. It is however not clear the manner in which ruthenium promotes platinum activity whether less CO is generated, or absorption of CO is reduced or whether CO is more readily oxidized anodically [10] on Pt-Ru catalyst. It is reported that ruthenium does not favour adsorption of methanol, but favours nucleation of oxidized species such as Ru-OH, whose exact molecular identity is not clear [11] but whose formation is possible in electrochemical environment; the decomposition of the adsorbed carbonyl follows the reaction.



No previous reports however are available on the role of zeolite Y in methanol electrooxidation. However recently on the basis of detailed infrared spectral studies of adsorbed CO in pure and cation exchanged Y zeolites, Gupta [12-14] have shown the existence of CO clusters which are not specific to specific zeolites site interaction, but influenced by zeolite cage effect, although the electrostatic zeolite cation field could play an important role in stabilization of these clusters. They interpreted CO₂ formation could be the result from strong interaction of CO with framework oxygen site or the surface hydroxyls. These studies however were with respect to alkali and alkali earth metal cation exchanged

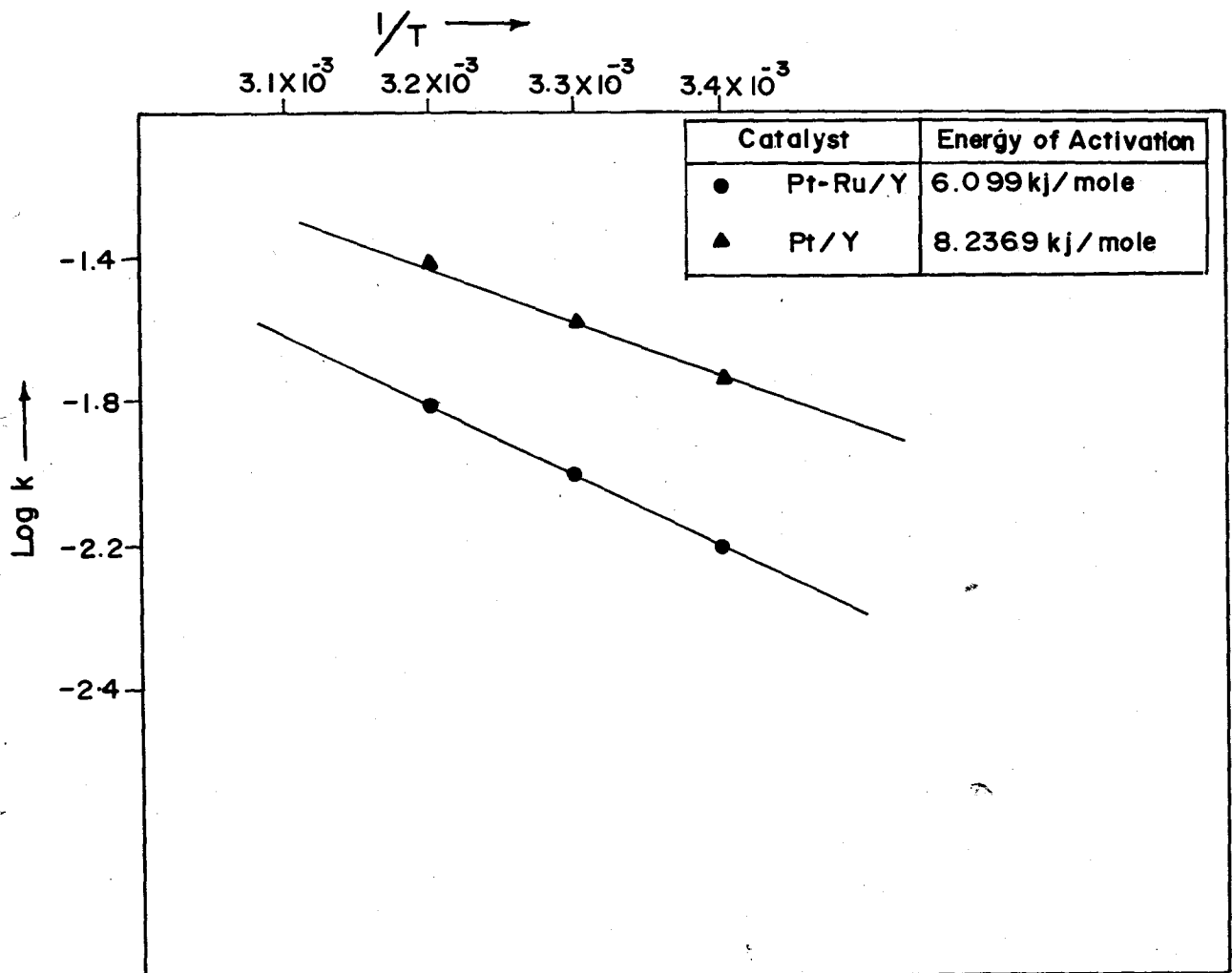


Fig.3.15 Arrhenius plots for catalytic decomposition of H₂O₂

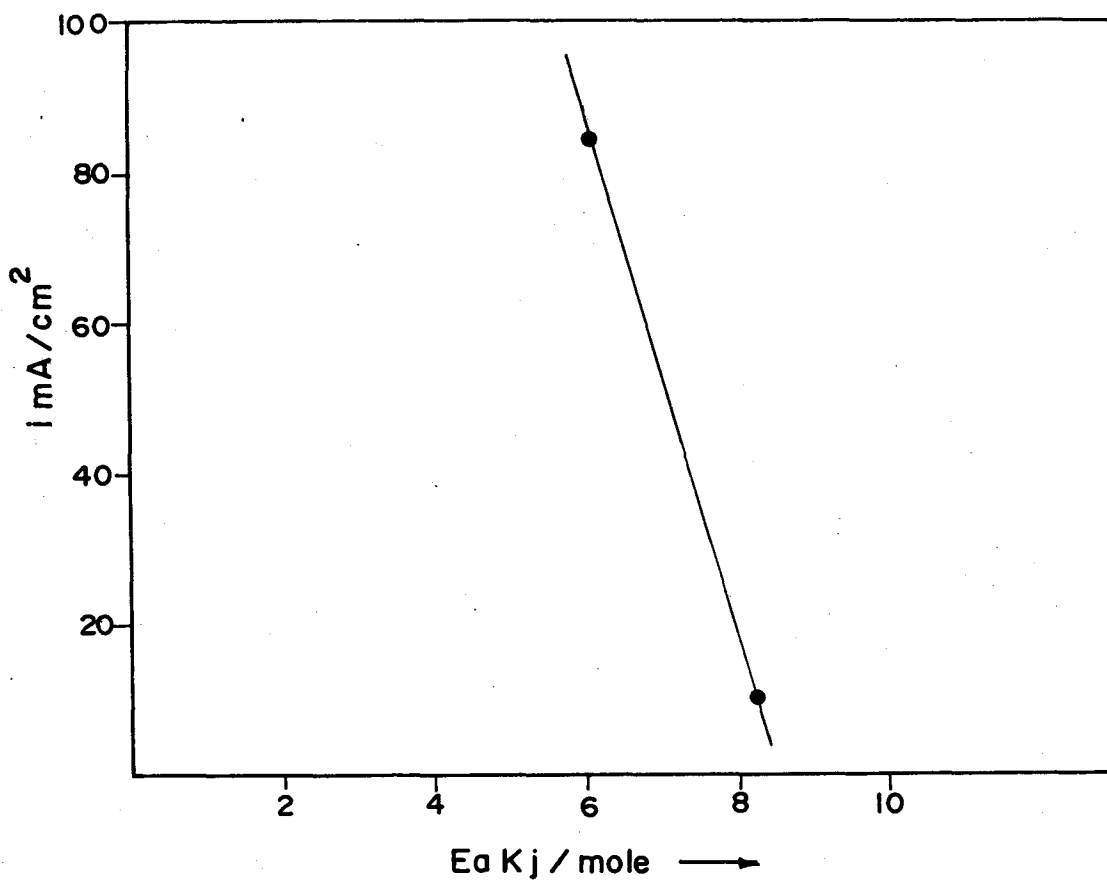


Fig. 3.16 Correlation between rate of methanol oxidation in terms of current density and energy of activation.

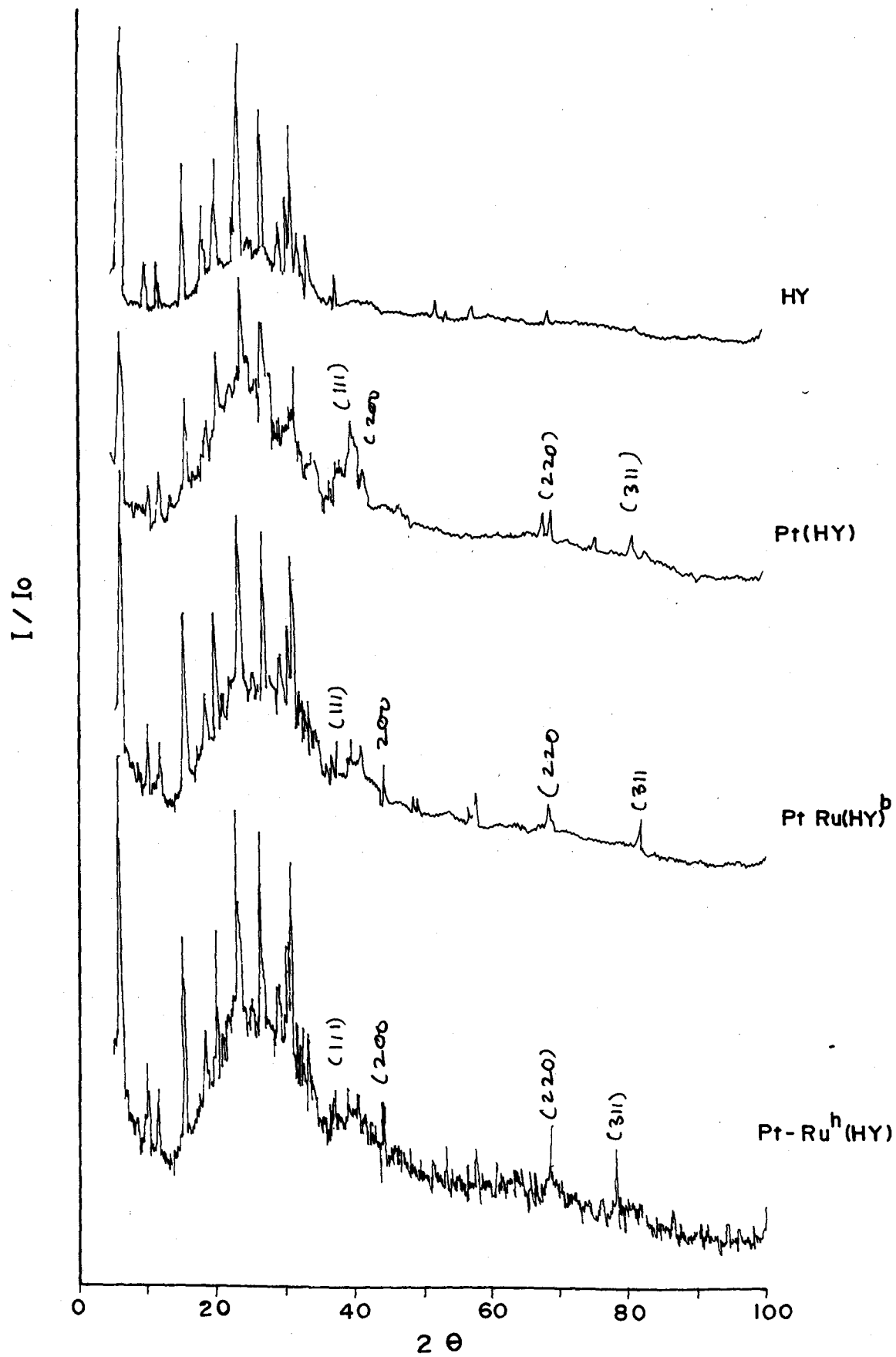
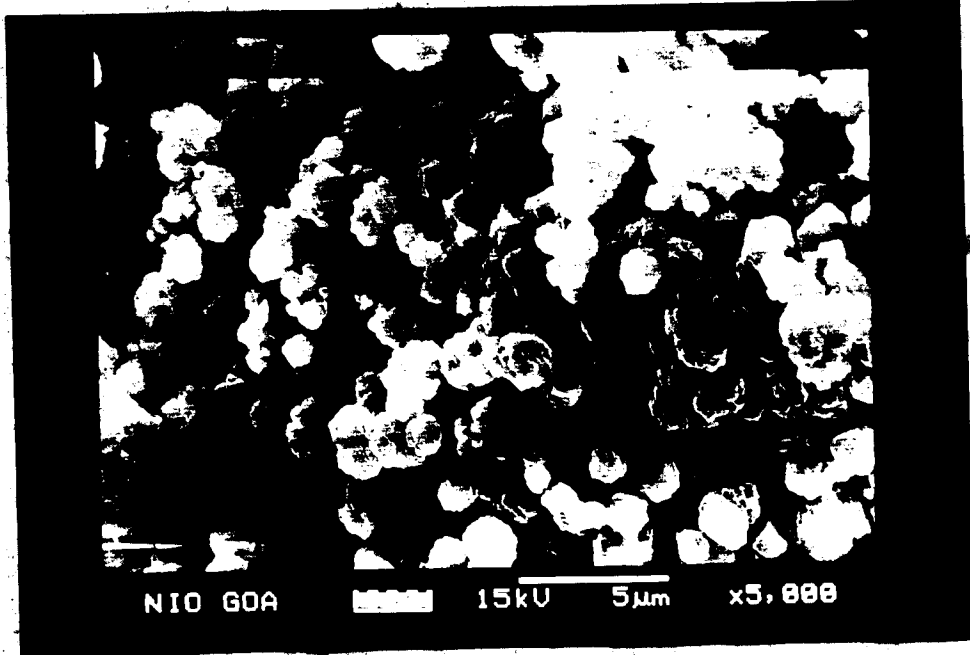
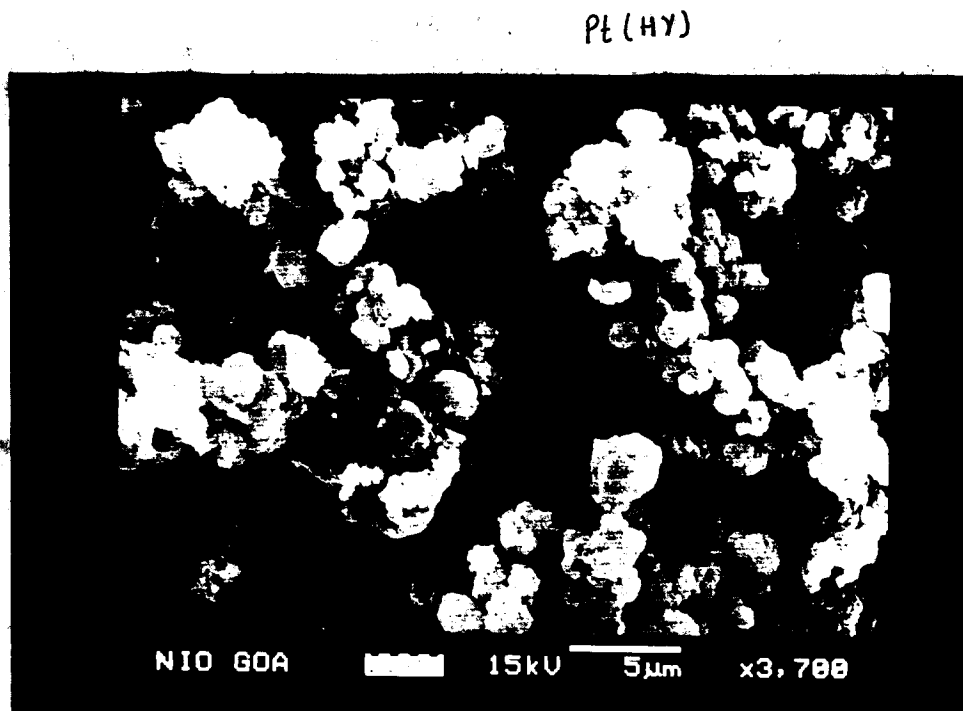


Fig. 3.18 XRD Pattern of HY, Pt(HY), Pt Ru(HY)^b & Pt-Ru^h(HY)

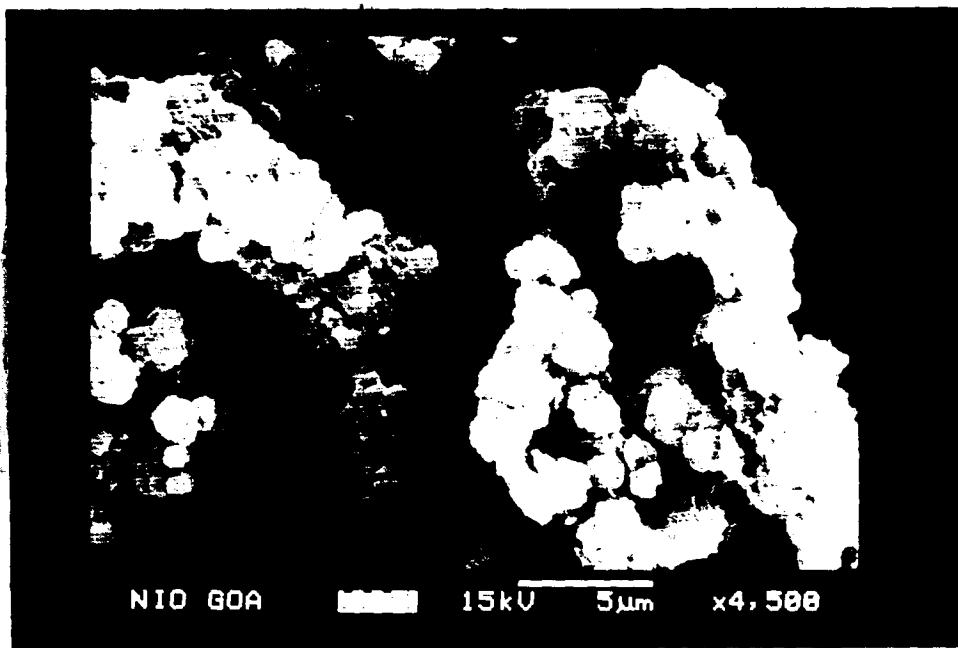


HY



Pt(HY)

3.18 (B) S.E.M micrographs of HY, Pt(HY)



3.18 (B) S.E.M micrographs of Pt -Ru(HY)

plots ($\log K$ v/s $1/T$) were 8.2369 and 6.099 kJmol^{-1} for Pt(Y) and Pt-Ru (HY) catalyst respectively as shown in fig 3.15 and thus could account for the facile oxidation of methanol on the latter. Fig 3.16 shows the correlation between rate of methanol oxidation (electrocatalytic activity expressed as current density $i_d, \text{mA/cm}^2$) versus heterogeneous catalytic activity for H_2O_2 decomposition expressed as activation energies E_a , kilojoules per mole. As expected, catalysts with high catalytic and electrocatalytic activity show corresponding low activation energy values. Further, structural studies and infrared spectroscopy of CO and / or methanol adsorption on Pt or Pt-Ru entrapped in zeolites is expected to throw more light on intricate structural features vis a vis activity of these catalysts. Fig 3.18(A), 3.18(B) and table 3.7 give XRD and SEM data of Pt(HY) and Pt.Ru(HY)^h samples. Particle sizes determined by XRD and SEM analysis reveal lower particle size and lattice parameters for Pt-Ru catalyst, implying greater dispersion of Pt-Ru alloy particles and hence enhanced electrocatalytic activity.

Catalyst	X.R.Dat220 <i>a_{fcc}</i>	Average size	S.E.M	Ref ^d Av. Part Size	Report ^a <i>a_{fcc}</i> 220
Pt (HY)	10.031	4.0484	4.9978	23A ⁰	3.921 A ⁰
Pt-Ru (HY)	9.574	9.368	2.0588	20 A ⁰	3.870 A ¹

Table 3.7

¹ A. S. Arico, et al. *Electrochim Acta* vol 23 (1998)3791

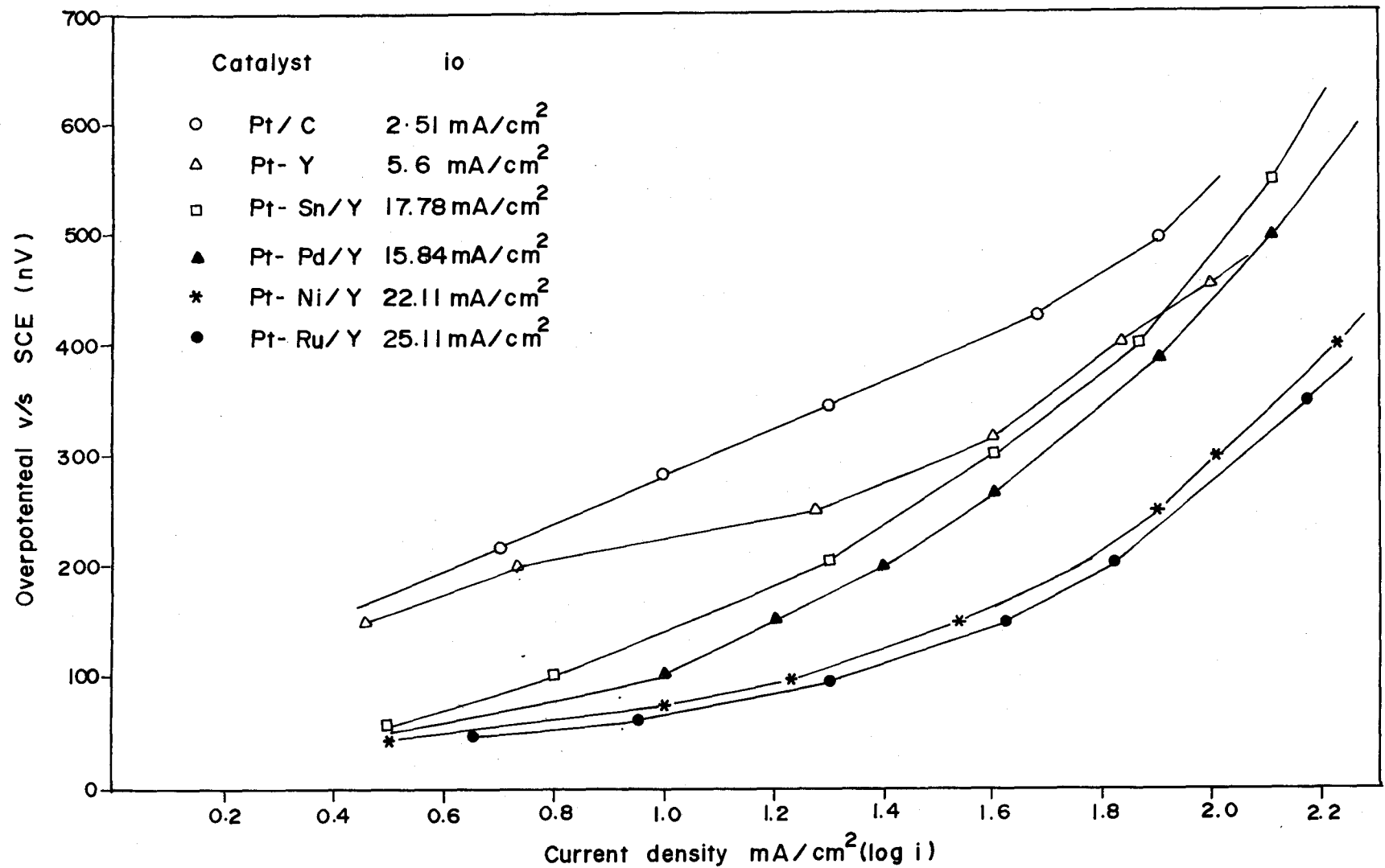
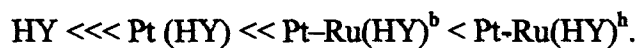


Fig.3.17 Tafel curves for various catalysts in 1.25 M H₂SO₄ and 0.5 M CH₃OH at 60°C

Conclusions:

Pt and Pt-Ru catalyst are prepared in HY zeolite and their electrocatalytic activity is evaluated for methanol oxidation in H₂SO₄.

The activity followed the order



The same activity trend was followed in heterogeneous catalytic decomposition of hydrogen peroxide in acidic medium. The enhanced electrocatalytic activity is explained on the basis of specific CO cluster formation in zeolite cages.

Paper communicated for Electrochem. Comm.

3.3.4 Pt-M (M= Ru, Ni, Sn, Pd) as active electrocatalyst:

The activity of the electrocatalysts is measured in terms of its ability to decompose methanol to CO₂. The bifunctional model for methanol electrooxidation suggests that effective catalysts should contain at least two types of surface elements. Those that bind methanol and activate its C-H bonds and those that adsorb and activate water. Pt-Ru (HY) and Pt-Ni (HY) shows higher catalytic activity as compared to other catalysts. This can be observed from Tafel curves (fig.3.17). The table 3.8 below gives comparison of overall electrocatalytic activity of various samples

Catalysts	Pt/C	Pt(HY)	Pt-Pd(HY)	Pt-Sn(HY)	Pt-Ni(HY)	Pt-Ru(HY)
Current density in mA/cm ²	7.94	18.62	26.32	35.48	79.43	87.09

From the table, it is clear that Pt-Ni(HY) and Pt-R(HY) are better catalysts than Pt-Sn(HY) and Pt-Pd (HY). The alloying of Ru and Pt has been postulated to give rise to an electronic effect in which electrons from Ru are transferred from Ru to Pt and thus CO is less strongly adsorbed permitting oxidation of CO at lower potential. Ru is also known to increase the coverage of Pt-Ru by oxy species, presence of Ru significantly enhances the amount of Pt-O species. The enhanced electrocatalytic effect in presence of Y zeolite is attributed to unique effect of cage structures to readily decompose CO clusters adsorbed on Pt sites into CO₂. The relatively high activity of Pt-Ni catalyst is believed to be

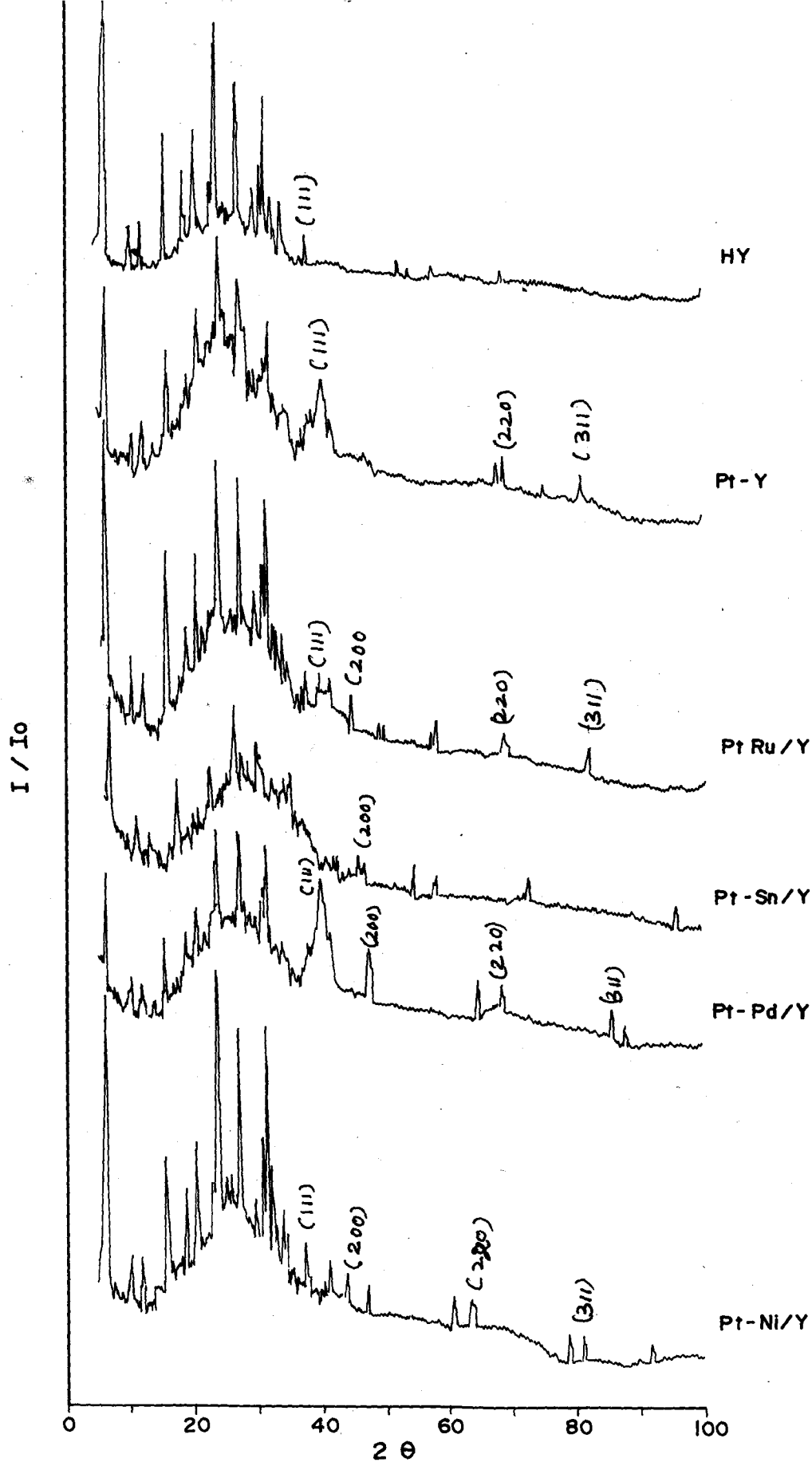
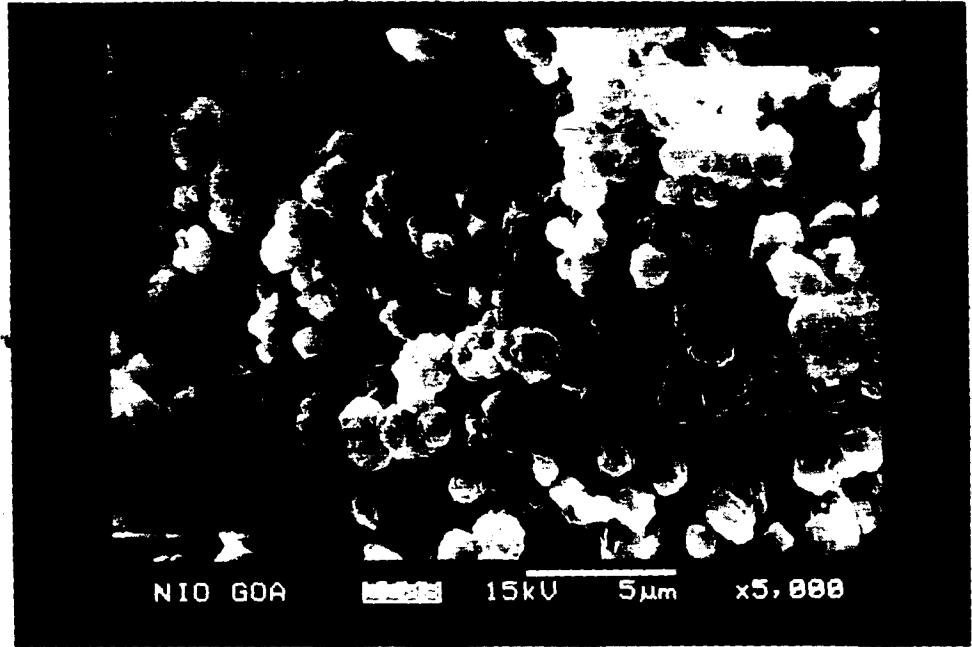
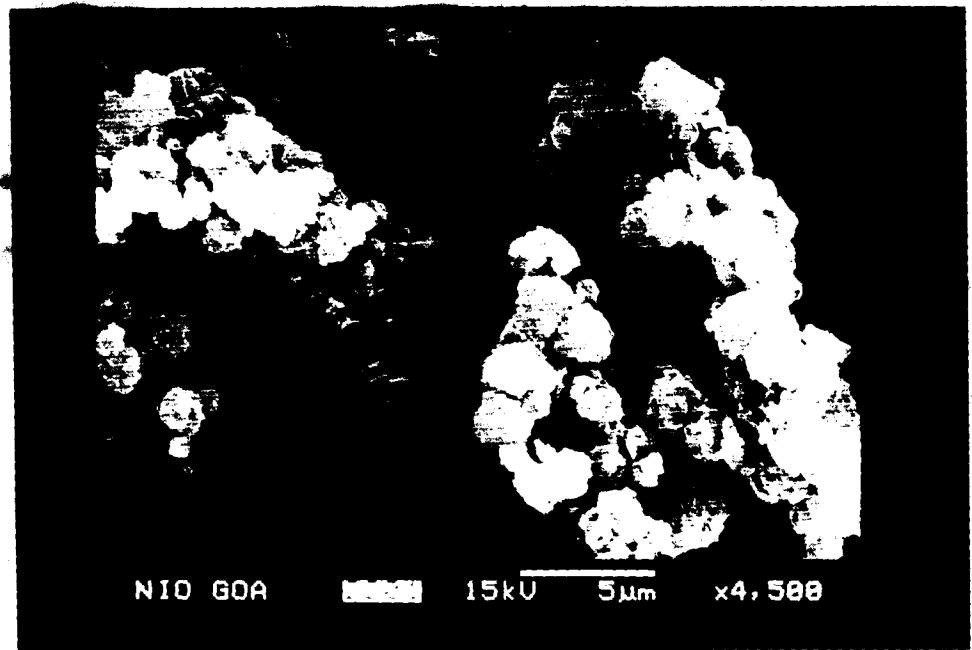


Fig 3.18 XRD Patterns of HY, Pt/Y & Pt-M (M = Ru, Pd, Sn, & Ni) Catalys

HY

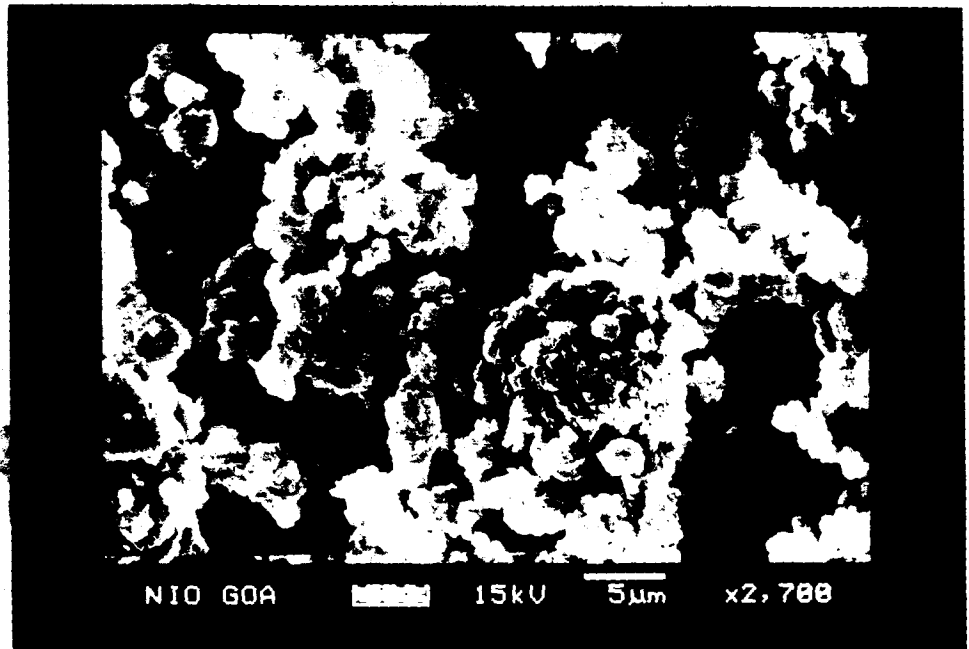


Pt-Ru (HY)^b

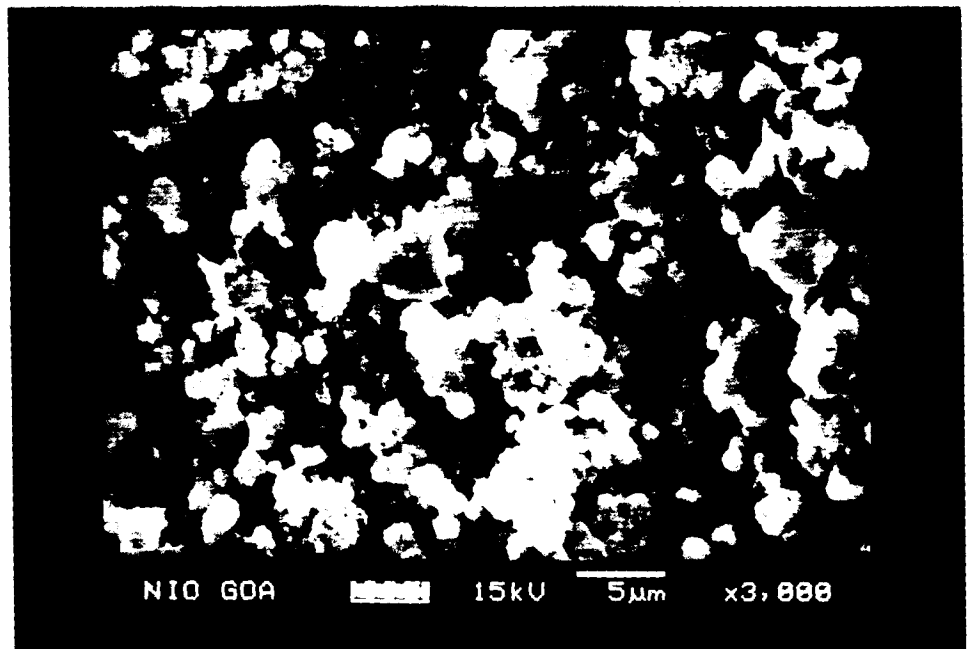


3.19 S.E.M micrographs of Pt -M (HY)

Pt-Ni (HY)



Pt-Sn (HY)



3.19 S.E.M micrographs of Pt -M (HY)

through electron donor property of Ni in comparison to the more electronegative Pt. The Ni component would readily adsorb water and help in decomposing the carbonyl species on Pt.

The relatively lower activity of Pt-Sn(HY) zeolite may be discussed in the light of its XRD pattern. Comparison of XRD pattern of HY and Pt-Sn(HY) indicate that zeolite has considerably lost its crystallinity, as pattern of Pt-Sn(HY) appears very diffuse. The sharp peaks seen in HY in the 2θ range 15 to 35, have become broad and diffuse in the Pt-Sn (HY). Hence presence of Sn has possibly distorted the zeolite structure either by dilation of framework bonds due to high atomic size of Sn or by its substitution in zeolite lattice sites.

In that case it is expected that Pt and Sn in zeolite is not present as Pt-Sn alloy. This assumption is supported by the fact that peaks of Pt-Sn alloy as reported in the literature [15] at 2θ around 30° , 42° and 43° are not seen in the present case. However peaks due to Pt at 2θ 39° , 68° and 87° have been observed. This suggests that Pt is present in zeolite independently or not close enough to Sn as an alloy.

This is correlated with the fact that Pt-Sn (HY) catalyst did not show particularly good electrocatalytic activity as would be normally expected. In fact its activity is almost similar to Pt (HY) catalyst. This needs to be particularly noted since many workers have reported synergistic effect for Pt-Sn alloy on carbon support; which is not found to be true when Pt-Sn is dispersed in zeolite, even though enhanced effect due to zeolite seen is seen in case of Pt -Ni and Pt -Ru as shown below in fig [3.18].

Pt-Pd (HY) zeolite shows poor activity though its XRD pattern shows significant crystallinity. It is reported [16] that Pd show very little tendency to oxidise methanol in acid solution, they act by simply blocking

the otherwise active sites for methanol adsorption. For very small crystallites this blocking effect may be amplified if Pd atoms preferentially reside on planar regions which would otherwise be active for methanol adsorption.

Even though small amount of Pt - M active sites are present in Y zeolite structure, the SEM photographs of each binary catalyst show a unique morphology and particle size Fig 3.19 [A,B,C,D]. Pt- Ni (HY) and Pt- Ru (HY) show well defined crystallites and these catalysts are shown significantly superior activity as compared to say Pt-Sn (HY) samples, which shows diffuse morphology.

Conclusion:

Pt and Pt-bimetallic catalyst are prepared in HY zeolite and their electrocatalytic activity is evaluated for methanol oxidation .The activity followed the order

$Pt(HY) \ll Pt-Pd (HY) < Pt-Sn (HY) < Pt-Ni (HY) \sim Pt-Ru (HY)$

The enhancement of electrocatalytic activity is explained on the basis of unique structure of zeolite which readily convert CO_{ads} to CO_2 .

Pt-Ni (HY) catalyst is also found to possess high catalytic activity almost comparable to Pt-Ru (HY).

Paper presented at *Catalysis conference Uni. Witwatersand for catalysis society of South Africa 30th Oct -Nov'99*

3.4 Cyclic Voltammetry:

As shown in the previous section, Pt-Ru (HY) catalysts showed better electrocatalytic activity for methanol oxidation and activity followed the order



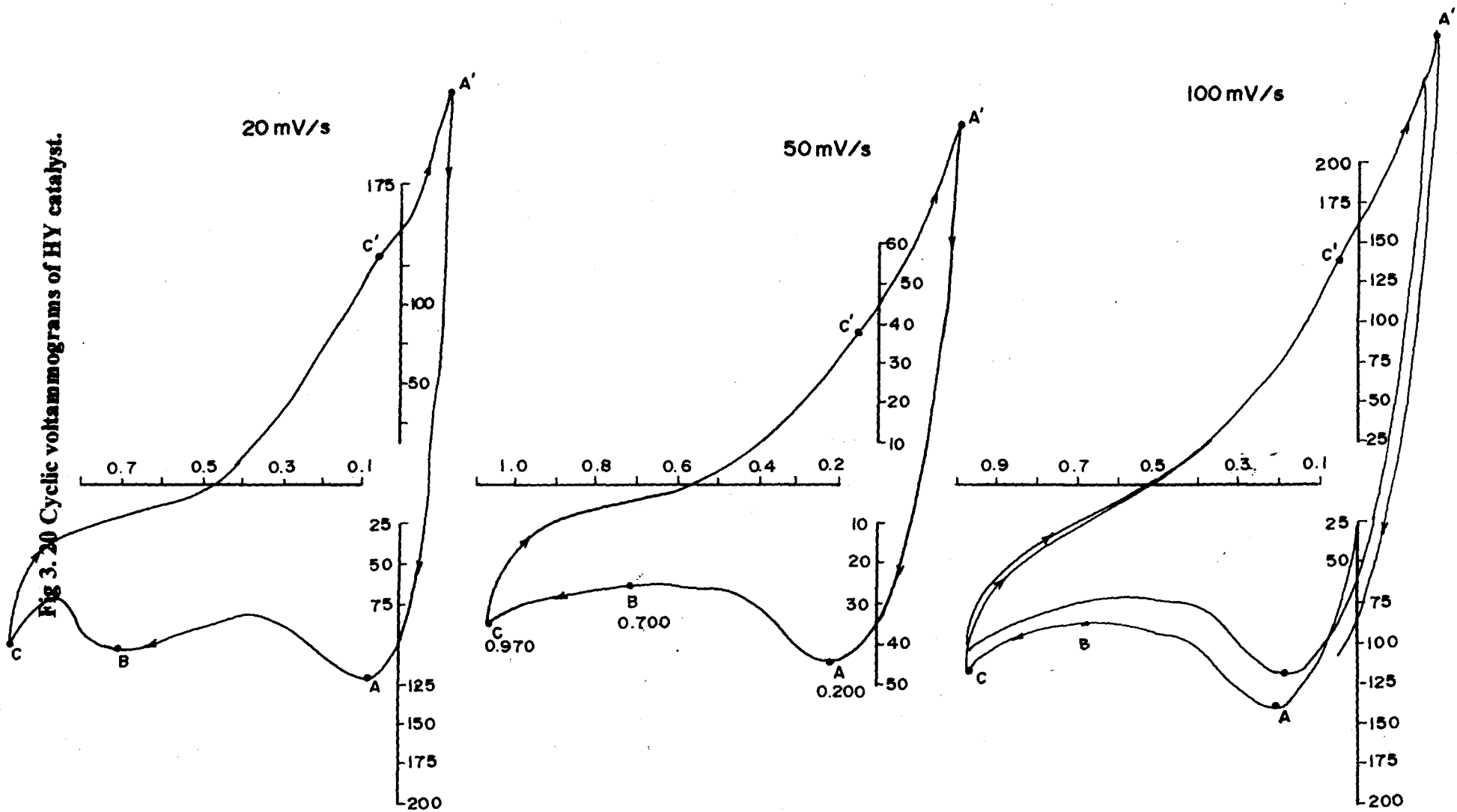
It was also observed that the HY supported catalysts were generally superior to the corresponding carbon supported catalysts. The relative electrochemical behaviour of these catalysts is further studied by cyclic voltammetry.

The experimental techniques of cyclic voltammetry are discussed in detail in 2.2.3

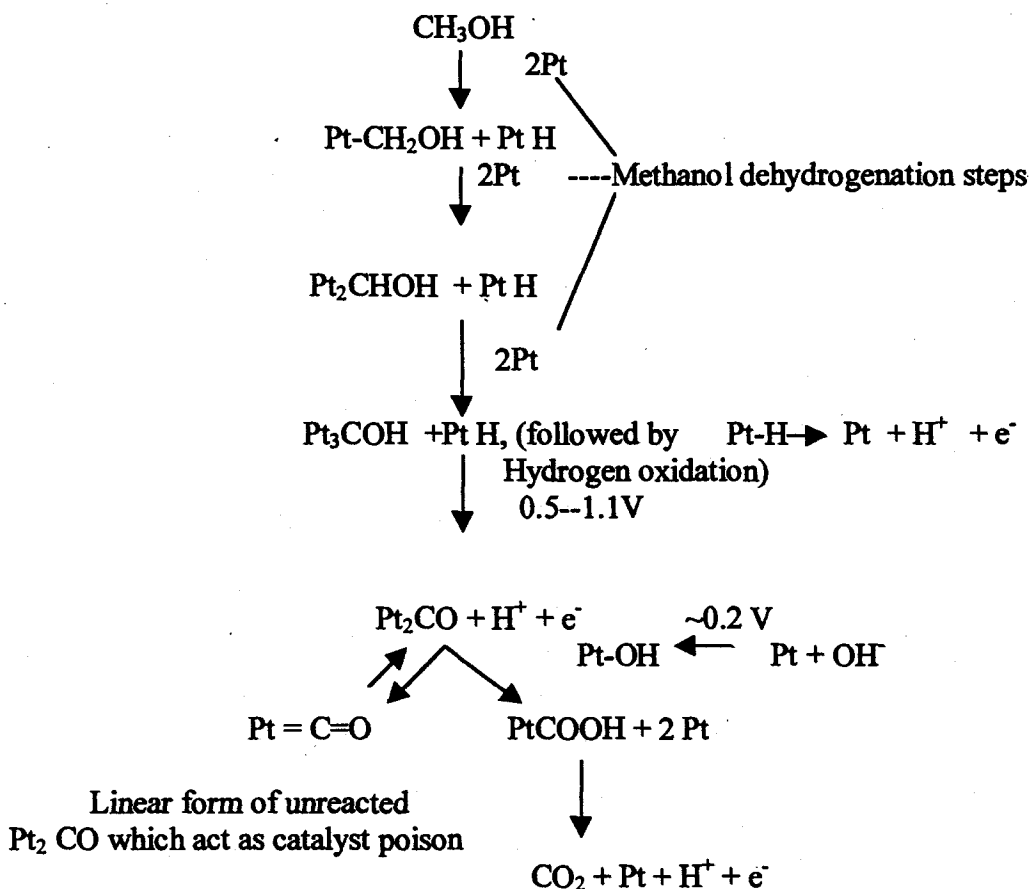
The cyclic voltammogram thus obtained are presented through figures 3.20 to 3.24. The CV profiles of the active samples are studied and compared with that of HY zeolite support.

CV studies (General): While several mechanisms for methanol oxidation have been proposed as discussed in section 1.4, it is felt desirable to briefly sum up the same here in relation to some recent CV studies with platinum as methanol oxidation catalyst (17-19) in acid media.

Fig 3. 20 Cyclic voltammograms of HY catalyst.

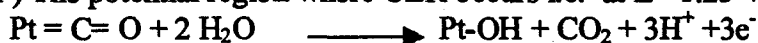


Dissociative Chemisorption of methanol at $E < 0.5 \text{ V}$

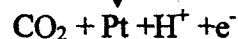
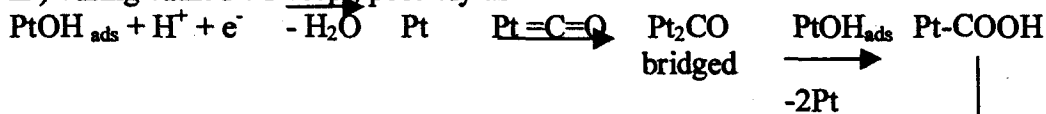


This linear species $\text{Pt} = \text{C} = \text{O}$ may be oxidized by either of the following two processes.

I) The potential region where OER occurs i.e. at $E > 1.23 \text{ V}$



II) during cathodic sweep, possibly as



Various other oxidation products may also be formed as

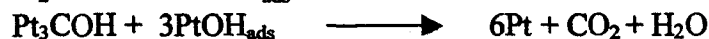
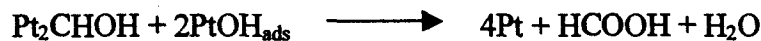
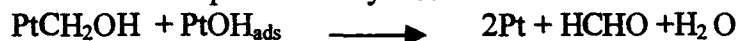
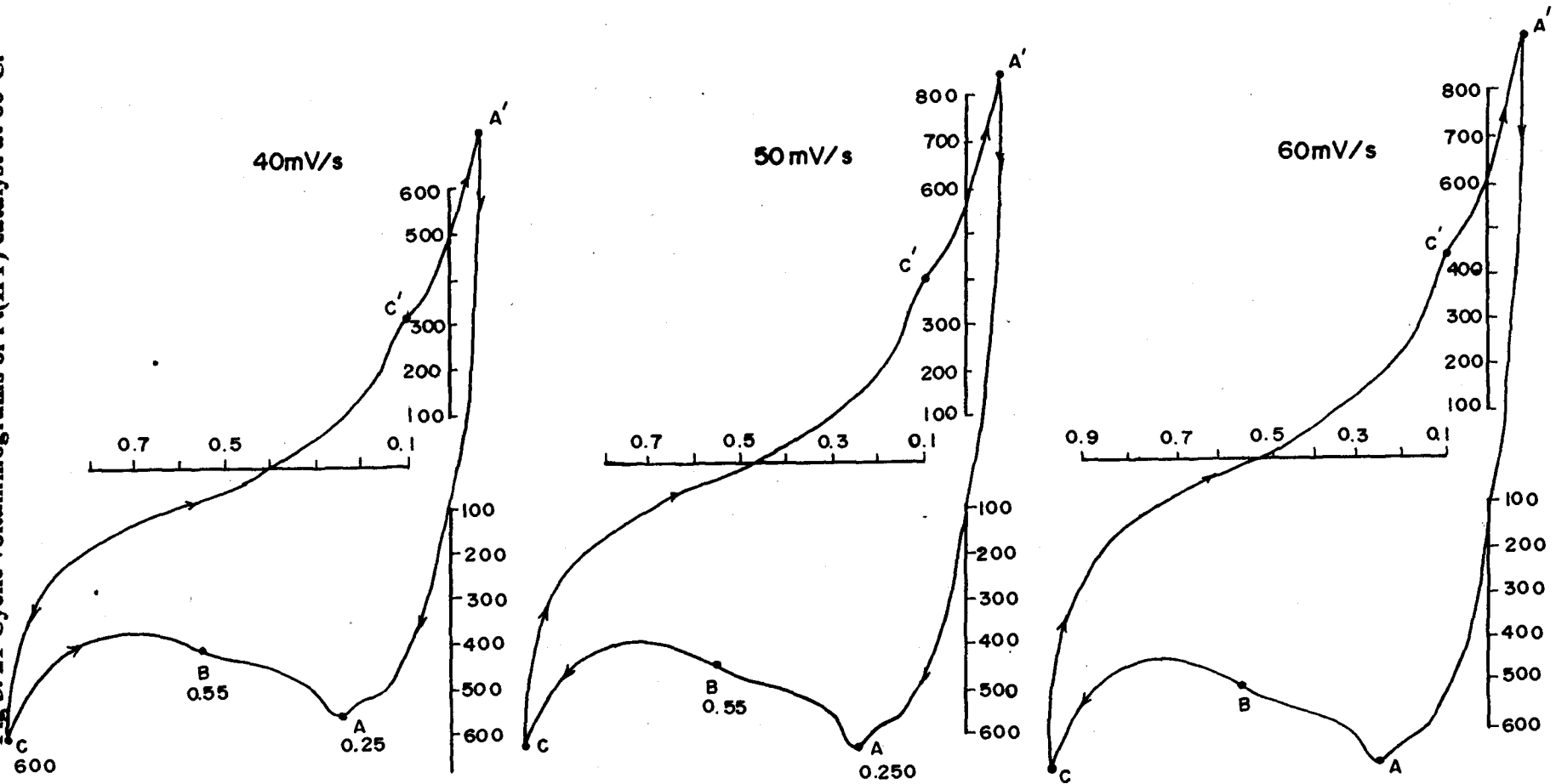
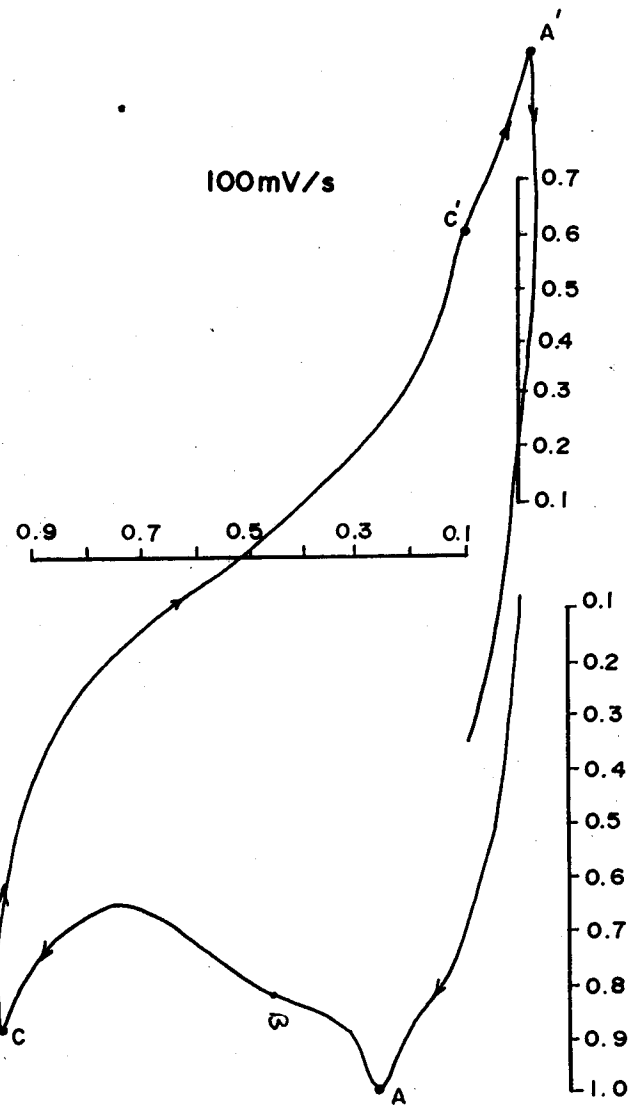
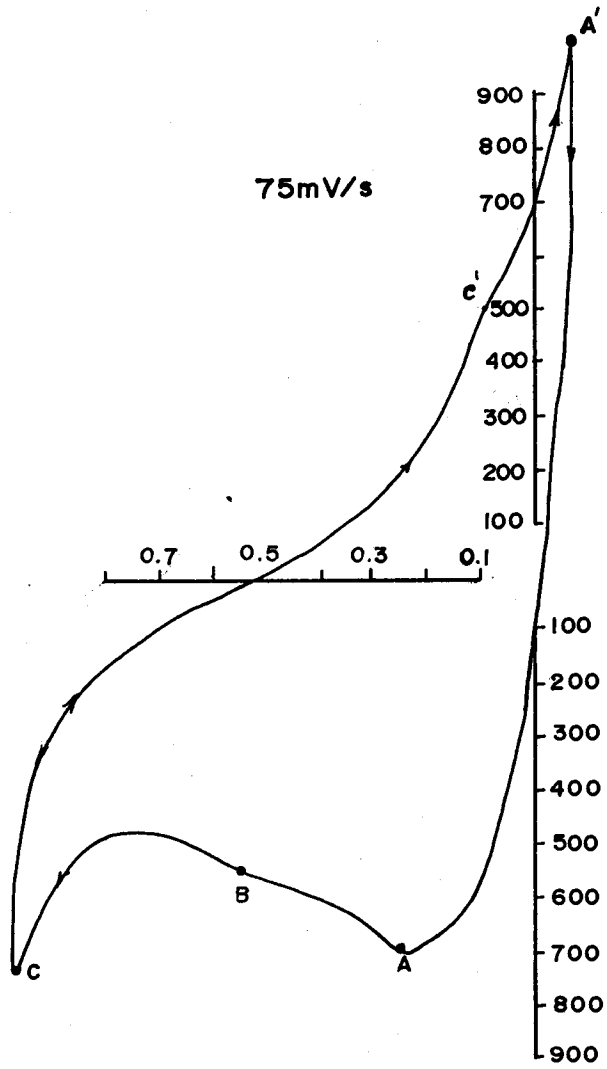


Fig 3. 21 Cyclic voltammograms of Pt(HY) catalyst at 60°C.



CONT. 3.21



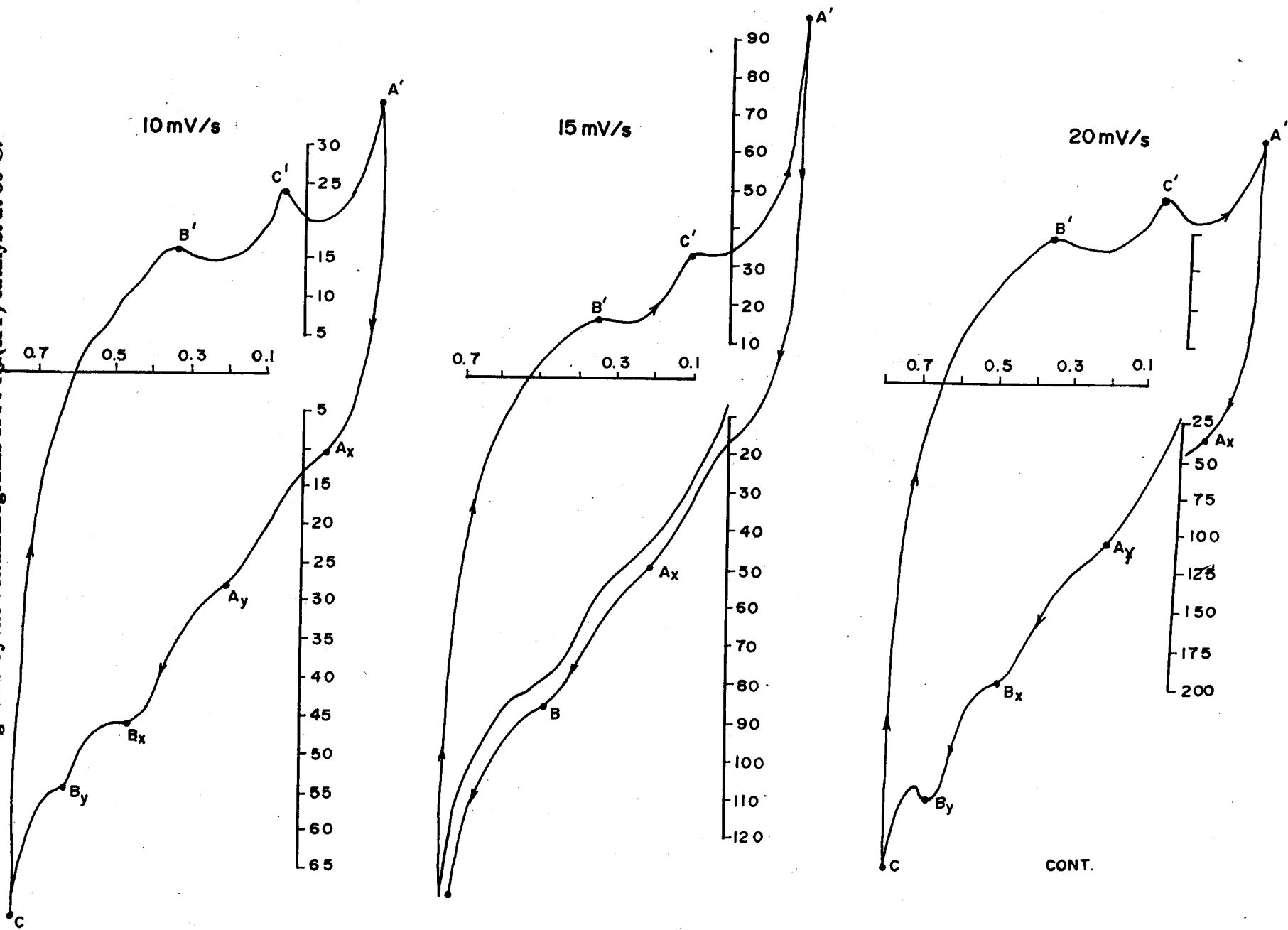
Recently Prabhuram and Manoharran [19] have investigated CV's of methanol oxidation at unsupported Pt electrode in 2.5 M H₂SO₄. They report hydrogen oxidation in the region 0.03 to 0.44 V and the onset potential for PtO layer formation at 0.84 V, while hydrogen adsorption begin in the range of 0.44V and finish at 0.03V during the reverse scan. Methanol oxidation of Pt-Sn alloy electrocatalysts has been reported by Arico et.al[20]. They attributed current increases during anodic sweep to methanol dehydrogenation between 0.05 to 0.1V at low sweep rates followed by oxidation of adsorbed methanolic residues in the region 0.4 to 0.6 V v/s SCE. They continued the anodic sweep up to the region where oxide layer grows. The reverse scan showed methanol oxidation at still positive potentials followed ^{by} cathodic reduction of the oxide layer.

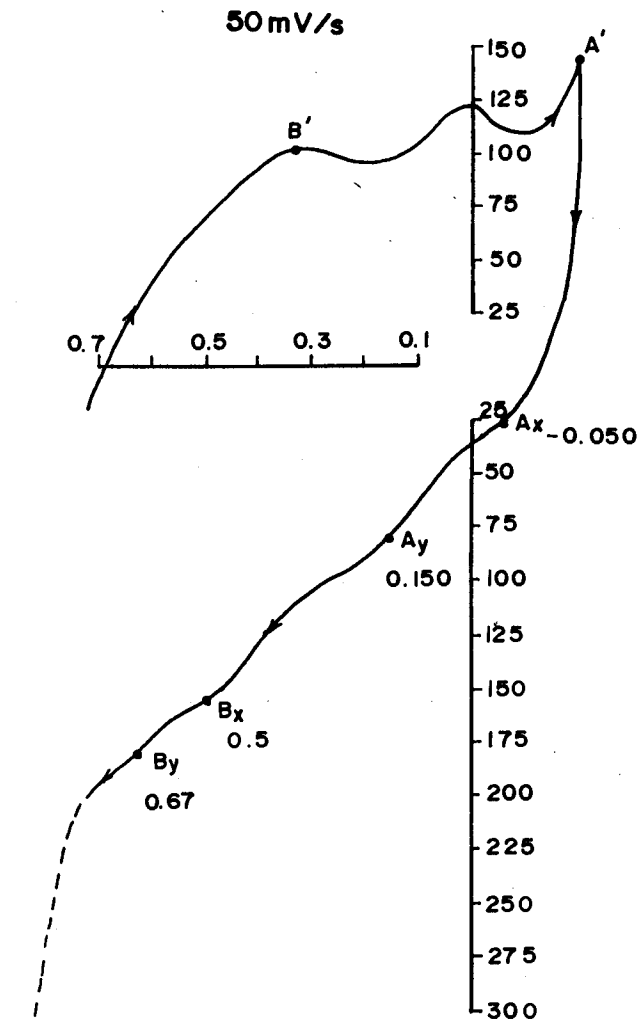
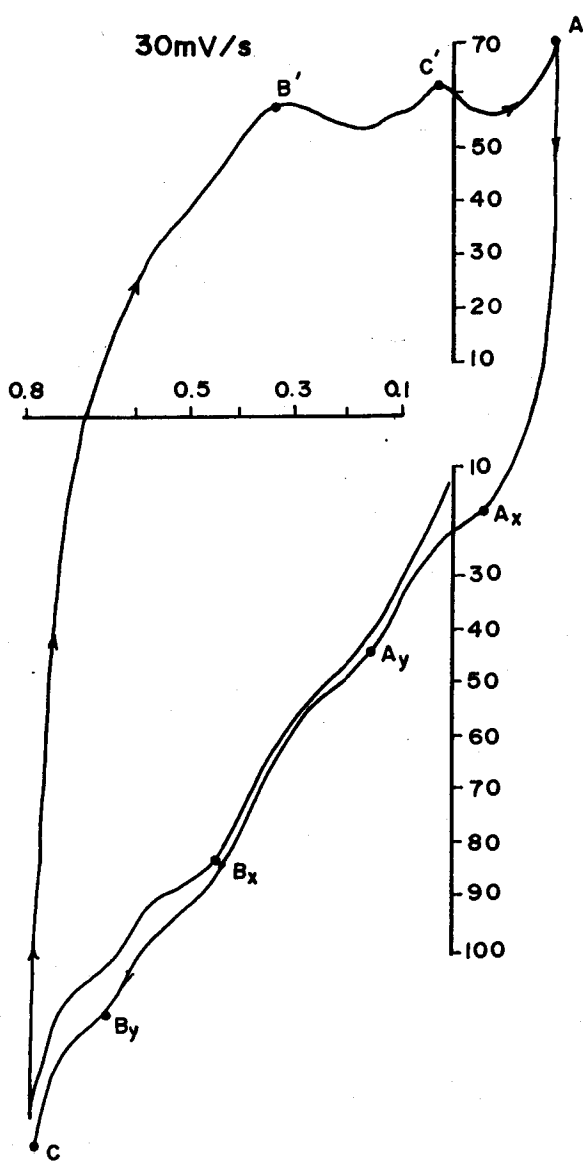
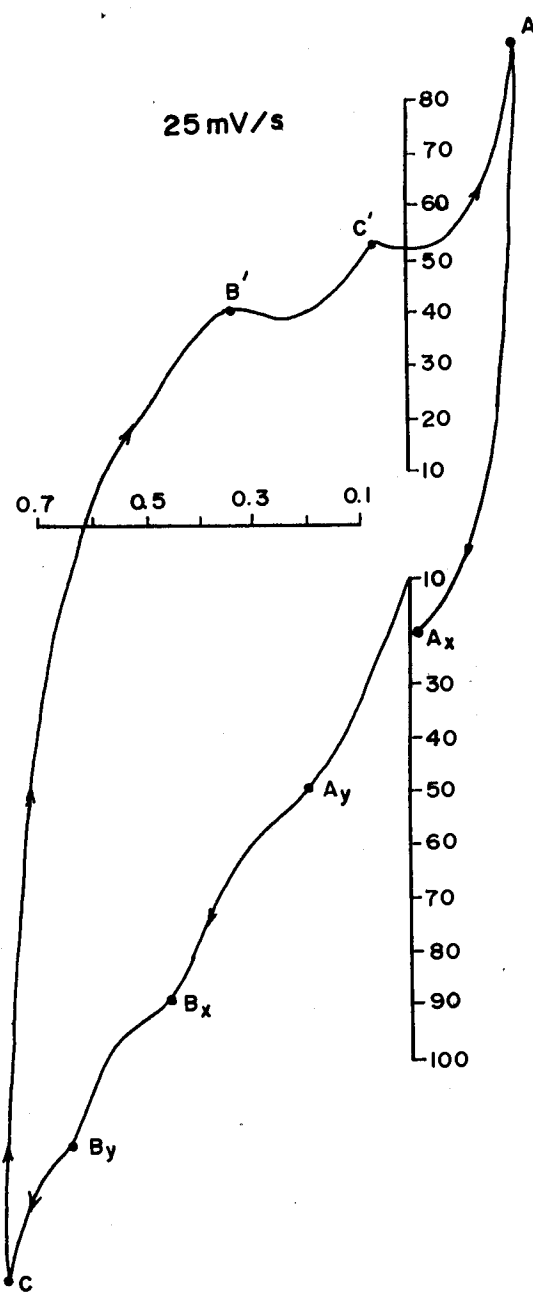
The results of present investigation on various catalysts are presented below.

3.4.1 HY catalyst:

The CV's of HY zeolite shown in fig 3.20 are smooth profiles with a clear anodic peak at around + 0.15V to + 0.2V due to oxidation of the adsorbed hydrogen on the catalyst surface. The forward scan is continued till the point C which corresponds to the growth of the oxide approx at 0.96 V. The rapidly rising portion in the cathodic region from approx 0.5V to approx - 0.15V is due to hydrogen adsorption due to point A. The formation of any oxide layer at point C did not appear significant at the scan rates 50mV/s and 100mV/s. However the CV profile 'C' taken ^{at} a slower scan rate of 20mV/s with amplification of the vertical current axis gave a better resolution of the anodic peaks. The growth of oxide layer at 'C' and corresponding reduction peak at C' was distinctly observed. Significantly one could discern the anodic peak at B approx at 0.7V v/s

Fig 3. 22 Cyclic voltammograms of Pt-Ru(HY) catalyst at 60°C.





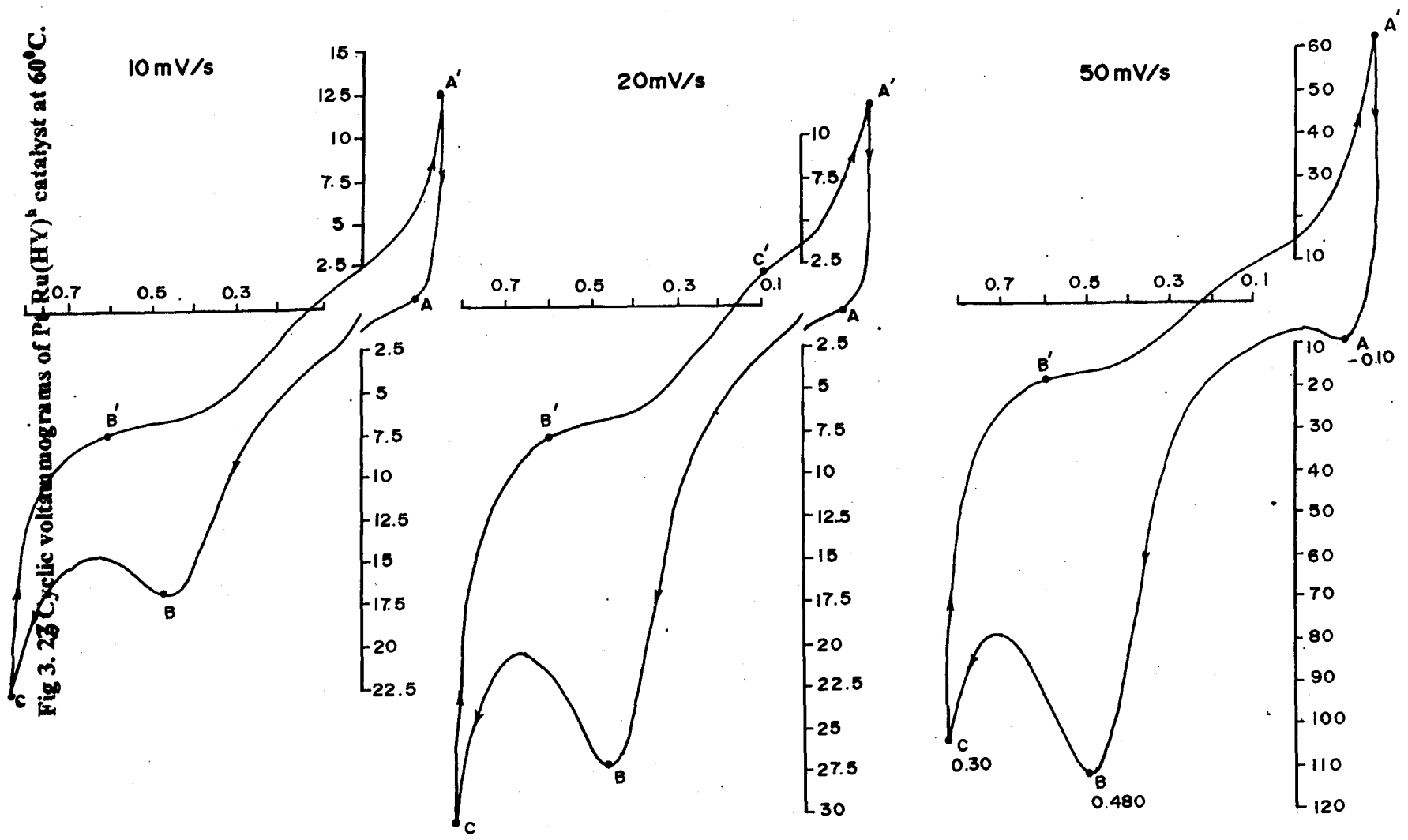
SCE which could correspond to some methanol oxidation. This ~~confirmed~~ that the zeolite (HY) have a small but significant electrocatalytic activity for methanol oxidation as was earlier observed in the half cell polarization studies Table 3.4

3.4.2 Pt(HY):

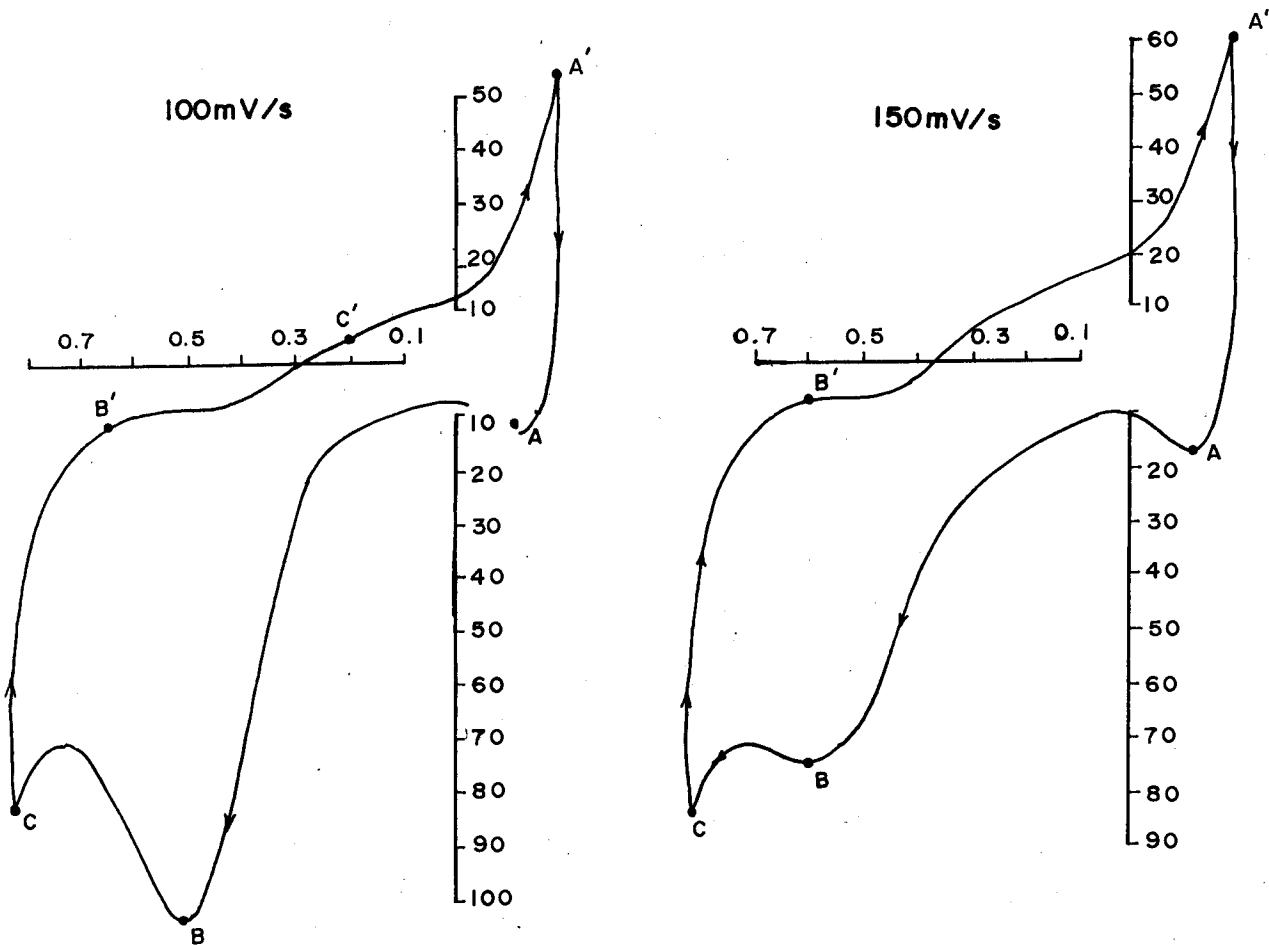
Fig 3.21 gives CV profiles of Pt(HY) catalysts taken in scan range 40mV/s to 100 mV/s. At all the scan rates, three anodic peaks at A, B and C are quite well pronounced as compared to the CV's corresponding to HY catalyst profiles. Particularly prominent is the oxide formation peak C and the corresponding oxide reduction peak at C'. Peak B which was not seen in HY is now seen as a shoulder or a slight depression in the mid anodic region around 0.550V while anodic and cathodic peaks C and C' respectively are attributed to formation/growth of oxide and its reduction. As discussed in the previous section, no complimentary peak B' corresponding to the anodic peak at B is discernible.

The peak at A which was seen at approximately 0.2V in the profile of HY is now seen distinctly grown in depth and centered at approx 0.25V. It appears that two kinds of processes are superimposed at A. While the peak in HY was attributed to oxidation of adsorbed hydrogen, in agreement with the finding reported by Prabhuram and Manoharran, it is now quite probable that the new additional effect observed by the deepening of the peak could be due to methanol dehydrogenation. In fact it is suggested [20] in their study of methanol oxidation on Pt/C catalysts in 0.032M Silicotungstic acid that methanol dehydrogenation occurs in the early part of anodic scan approx 0.05 to 0.1 $\frac{V}{s}$ SCE, and shifts positively in more concentrated solutions.

Fig 3. 23 Cyclic voltammograms of Pt-Ru(HY)^h catalyst at 60°C.



CONT.

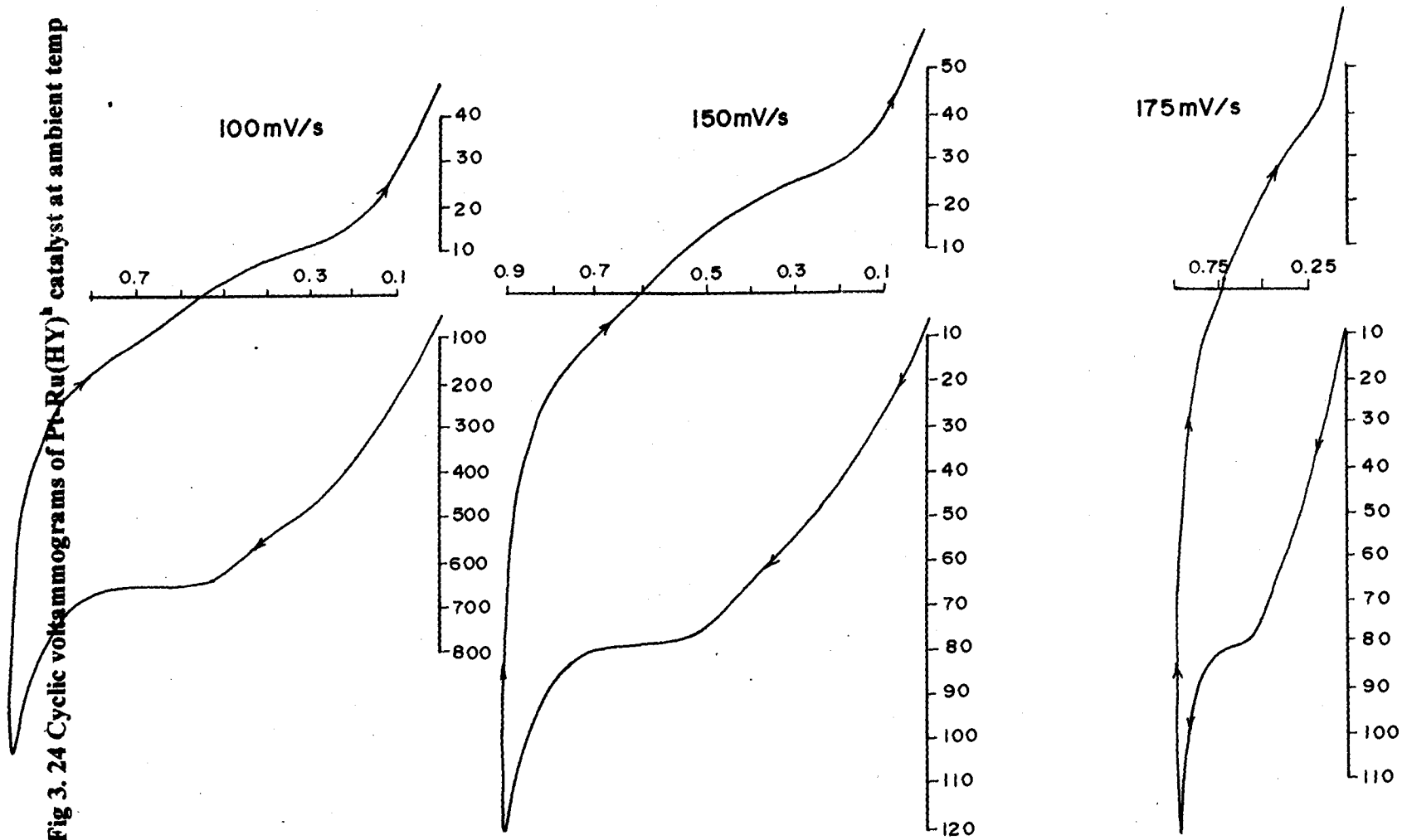


CONT. FIG. 3.23

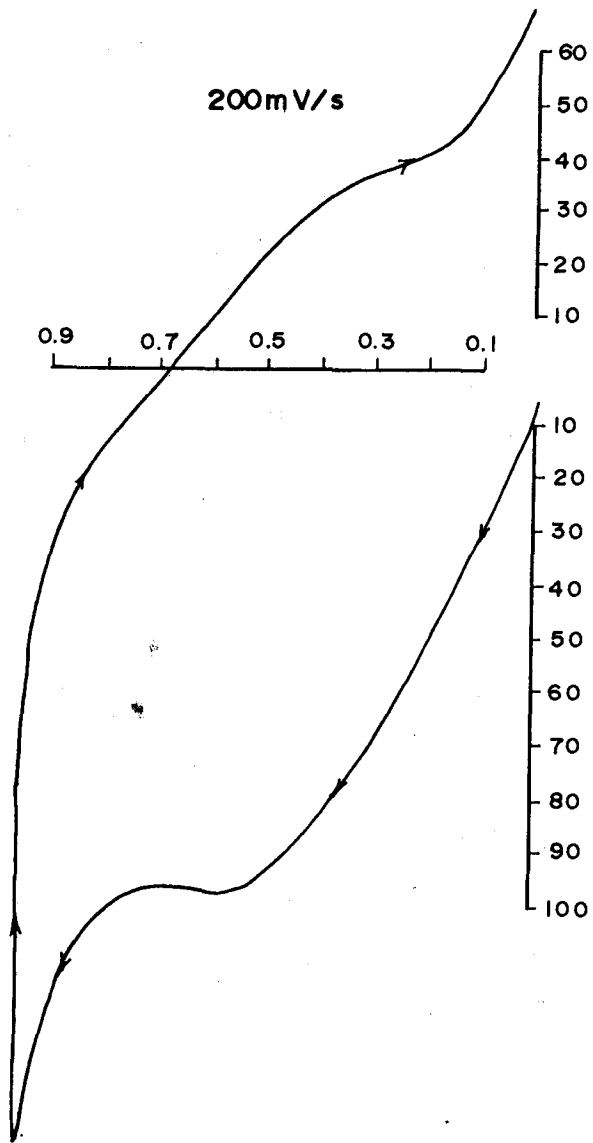
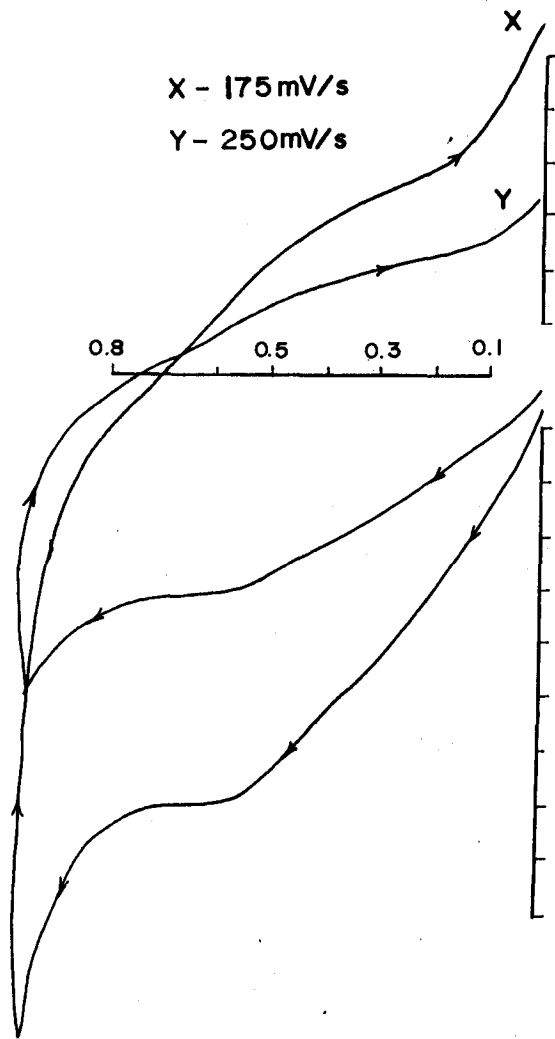
To study the process related to methanol oxidation peak in the anodic sweep, classical analysis of these CV's is done as suggested by [20]. Thus a linear relationship between I_p v/s $v^{1/2}$ is observed both for peaks A and B (Fig 3.25) suggests that the peak current is related to diffusion controlled process rather than to adsorption controlled process i.e. both methanol dehydrogenation as well as the subsequent oxidations could be diffusion controlled. However the curve C appears more to be asymptotic suggesting saturation coverage due to growth of the oxide layer.

In order to relate the anodic peak current to activity of the electrocatalyst a comparison is made between the current generated due to the peak A for the catalysts HY and Pt(HY) ; These currents observed were 95 and 630 microamperes respectively at 50mV/s sweep rate indicating that Pt (HY) is about 6.63 times more active than (HY) for anodic oxidation of methanol. As shown in section (C) it is extremely important to note that a comparison of the values of half cell polarization studies the catalysts HY and Pt (HY) showed current densities of 3 and 20 mA/cm² at an overpotential of 250 mV indicating that Pt(HY) is 6.66 times more active than HY. The almost identical values of relative activity obtained through two different approaches lead one to believe that the mechanism of formation of peak A is the rate determining step of methanol oxidation i.e. methanol dehydrogenation followed by hydrogen oxidation of the adsorbed hydrogen is the rate determining step. Thus an efficient catalyst could be the one which favours C-H bond breaking of methanol. That C-H bond scissoring could be the rate determining step has been earlier suggested by other workers[17]

Fig 3. 24 Cyclic voltammograms of Pt-Ru(HY)¹ catalyst at ambient temp



CONT.



3.4.3 Pt-Ru(HY)^b:

The CV profiles using this catalysts are presented in fig 3.22 scanned in the sweep range 10-50 mV/s. When the anodic scans are compared with that of Pt(HY) catalyst, it is seen that the peaks (A) and (B) which were composite in Pt(HY) have become distinct in Pt-Ru(HY) and for convenience designated as Ax and Ay and Bx and By. The peaks Ax and Ay could be accordingly attributed to hydrogen oxidation and methanol dehydrogenation respectively. Similarly peaks Bx and By is attributed to two stage oxidation of the methanolic residues while peak C represented the formation and growth of metal oxide layer. On the cathodic side, the peak C' is as before attributed to the reduction of the oxide layer; this reduction peak has become highly pronounced as compared to that which was observed in case of Pt (HY). Also a distinct peak B' observed at approx + 0.35V in the reverse scan could be due to reoxidation of methanol. Similar observation has been reported earlier [17] in case of Pt - Sn alloy catalyst.

It is further observed that the onset of all the anodic peaks in Pt-Ru (HY) CV^s has moved more towards the cathodic side, indicating greater activity of this catalyst in comparison to the Pt (HY) catalyst. Similar observation was earlier reported by Wasmus and Vielstich [28] with their studies on carbon supported catalysts. Also the anodic currents observed are much larger in the Pt-Ru(HY) catalysts.

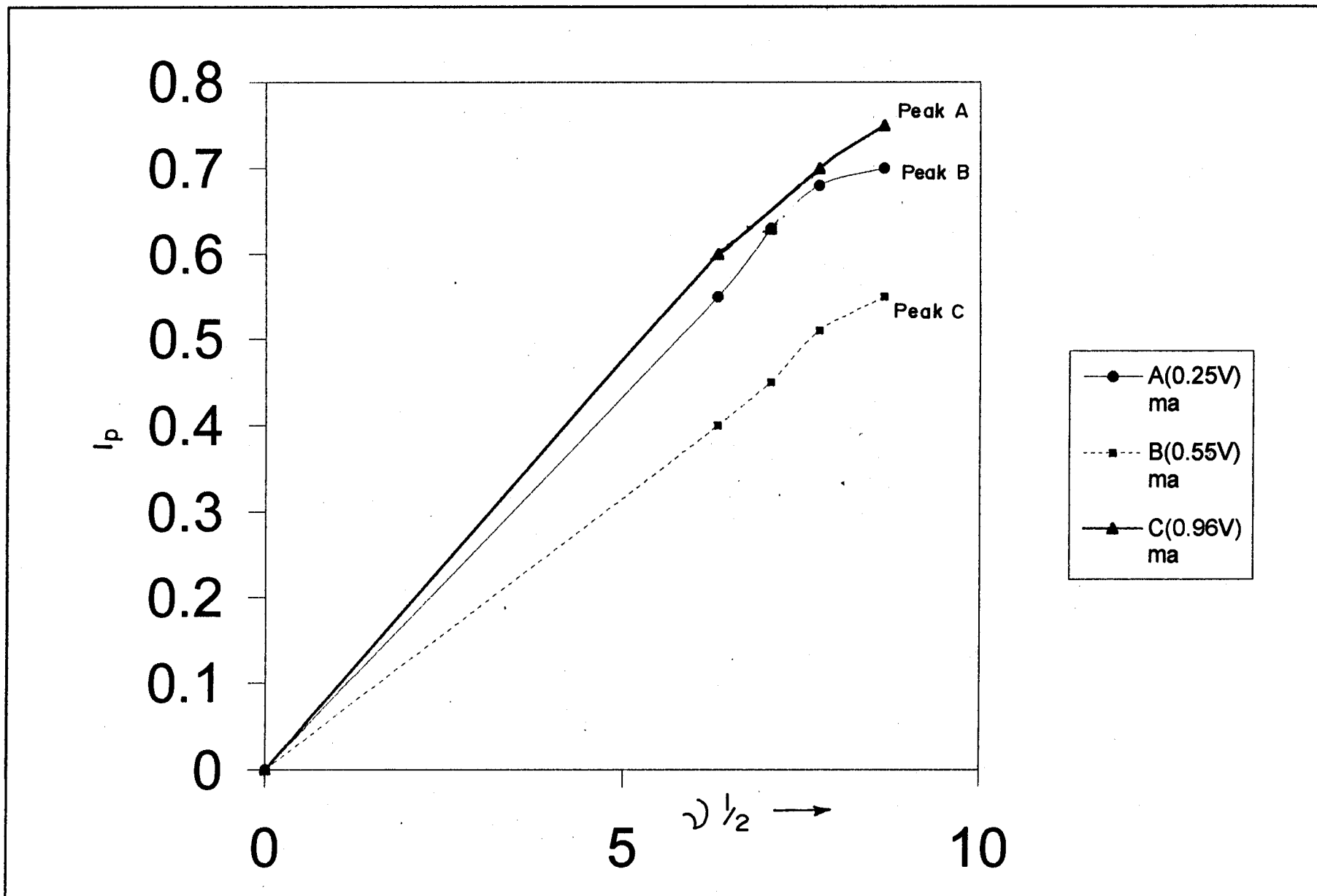


Fig. 3.25 Relation between I_p vs $t^{1/2}$

3.4.4 Pt -Ru(HY)^h :

Fig 3.23 gives the CV profile of the Pt - Ru (HY)^h catalyst. The distinctive feature of the catalyst is that its CV profiles are smooth and well pronounced. Further, while all the three peaks A, B and C are seen, the peak A is not evident in the initial forward scan but appears at the beginning of the second anodic scan quite analogous to the HY zeolite peak, which is attributed to the hydrogen oxidation/methanol dehydrogenation. Further this peak is well shifted cathodically at -0.12V, while in HY and Pt-(HY) catalysts it was observed in the forward scan at +0.2 to +0.25V; indicating facile oxidation of methanol on Pt-Ru(HY)^h catalyst, even better than Pt-Ru (HY)^b catalyst where this peak is observed at -0.05V. Moreover, the peak B (+0.48V) which correspond to subsequent oxidation of methanolic residues and peak 'C' of oxide formation are also observed on the less positive side of the anodic scan, confirming more facile oxidation of methanol on this catalyst. As an illustration, the peak currents and the corresponding potentials of the various catalysts at 50 mV/s. CV profiles are presented in the Table 3.5 below.

Catalyst	peak A		peak B		peak C	
	mA	V	mA	V	mA	V
HY	0.095	0.200	0.065	0.700	0.88	0.970
Pt (HY)	0.65	0.250	0.45	0.550	0.68	0.970
Pt-Ru (HY) ^b	25	-0.050	---	0.500	49.0	0.840
Pt-Ru (HY) ^h	5.0	-0.120	55	0.480	52.5	0.830

As before peaks B' and C' would correspond to methanol oxidation and oxide reduction in the reverse scan. Assuming in general that less positive peak potentials and higher anodic currents are reflective of methanol oxidation activity, it is clear from the table that the electrocatalytic activity would follow the order



The above activity trend is quite in agreement with the activity trend observed from the parameters of half cell polarization studies and Tafel plots as was discussed in previous section 3.3.c. Fig 3.24 gives CV profiles of the same catalyst at ambient temperature. It is observed that peaks are not well pronounced; peak A is not seen while peak B is faintly observed at more positive potentials (+0.550V instead of +0.48 V)^{than} seen for high temperature profiles. This confirmed that the catalytic activity increased with temperature.

Conclusion : Cyclic voltammetry could be used as a convenient technique for comparison of relative electrocatalytic activity of various catalysts, for methanol oxidation, vis a vis anodic reaction pathways.

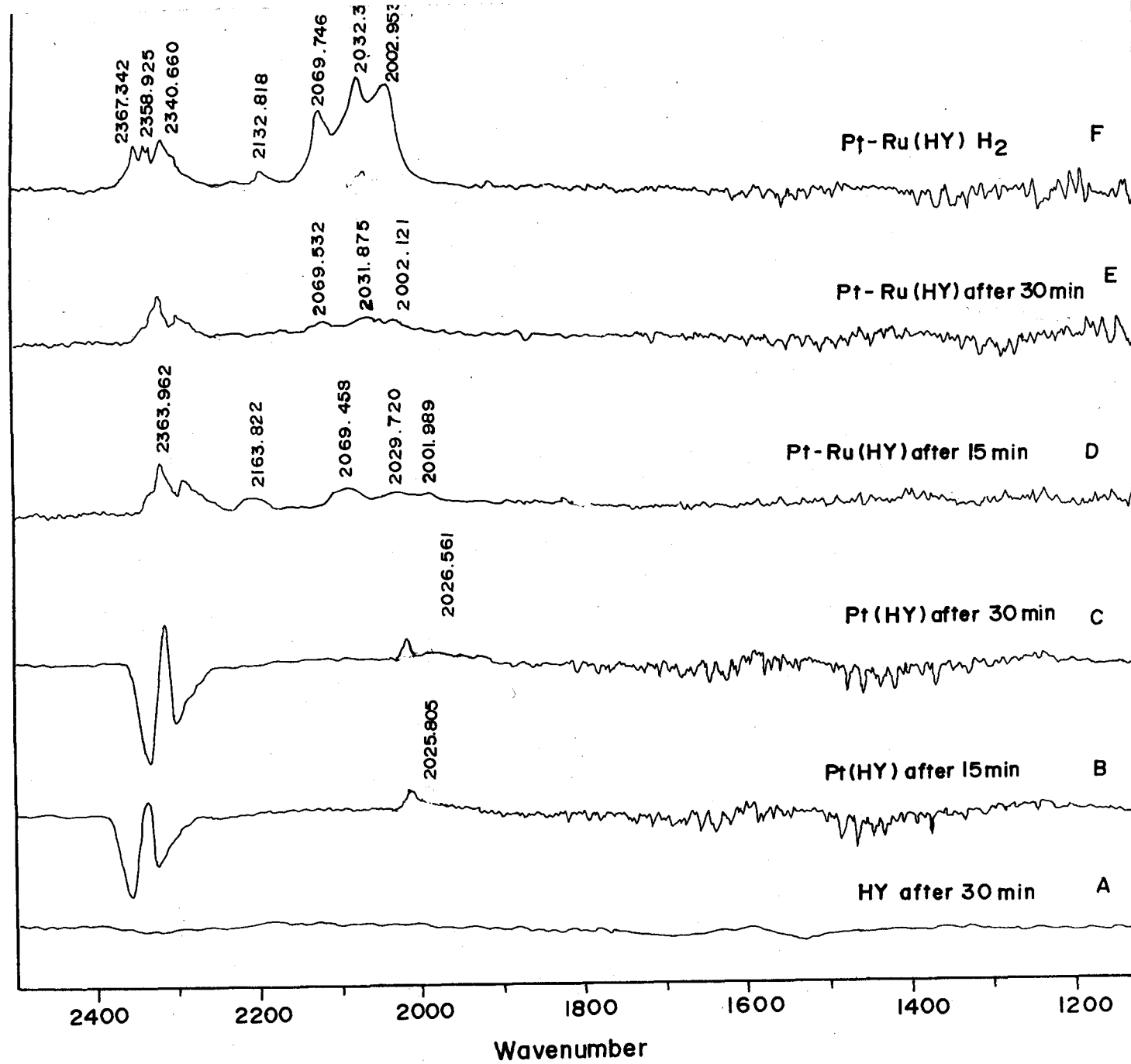
3.5 *in situ* FTIR studies:

In the continuing search for newer catalysts or improving the current catalyst composition, particularly Pt or platinum based alloy catalysts, it is desirable to understand the nature of the intermediates formed during decomposition of methanol. This section describes *in - situ ir* studies done on Pt (HY) and Pt-Ru (HY) catalysts.

3.5.1 CO adsorption studies:

As discussed earlier bridged or linear CO is one of the intermediates during methanol oxidation, forming CO₂. An effective catalyst therefore is the one which can readily decompose CO to CO₂. Hence *in situ ir* studies are carried out on the catalysts HY, Pt (HY) and Pt-Ru (HY), containing adsorbed CO. These spectra are presented in fig.3.26 They are subtraction spectra which highlight the effect of CO adsorption. It is seen that HY did not show any absorption due to CO even after exposure for 30 minutes. However, Pt (HY) catalyst showed CO absorption at 2026 cm⁻¹, which increased with time of exposure, from 15 minutes to 30 minutes. During this period the relative absorption intensity was increased 1.5 times. Also similar but enhanced effect was observed with Pt-Ru (HY) catalyst. The CO absorption bands were clearly seen. When comparison was made between CO absorption intensities in case of Pt (HY) and Pt- Ru (HY) catalysts, following 30 minutes exposure, it was seen that the later catalyst shows ~3 times more CO absorption than Pt-Ru (HY) catalyst. At the same time Pt-Ru showed a significant absorption at ~2364 cm⁻¹ indicating formation of large amount of CO₂ on this catalyst. Thus *ir* spectroscopy clearly confirms superiority of Pt-Ru alloy

Fig 3. 26 CO adsorption spectra on HY, Pt(HY) and Pt-Ru(HY)



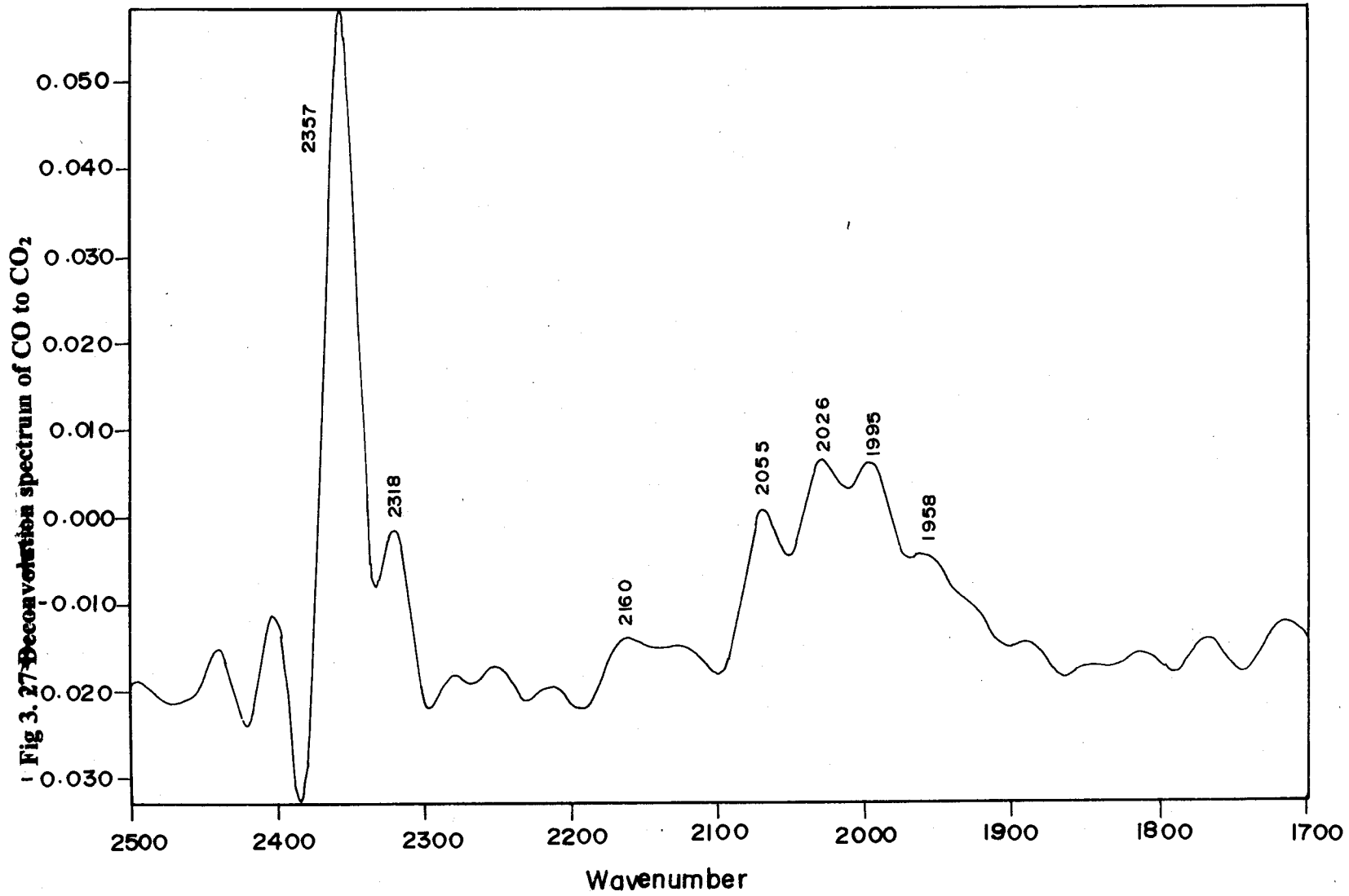


Fig 3.28 *ir* spectra of adsorbed methanol/O₂ on catalyst at various temperatures after evacuation.

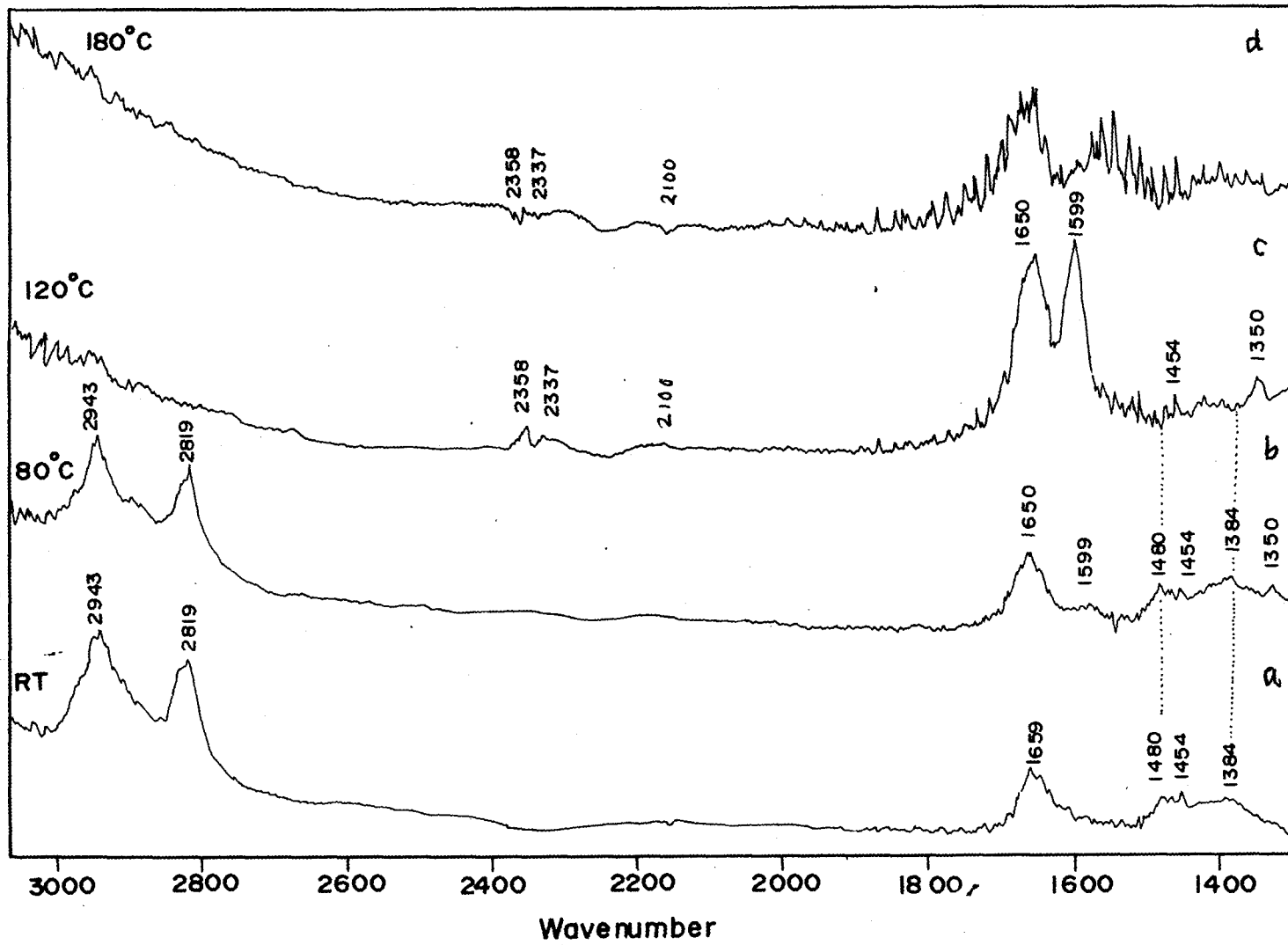
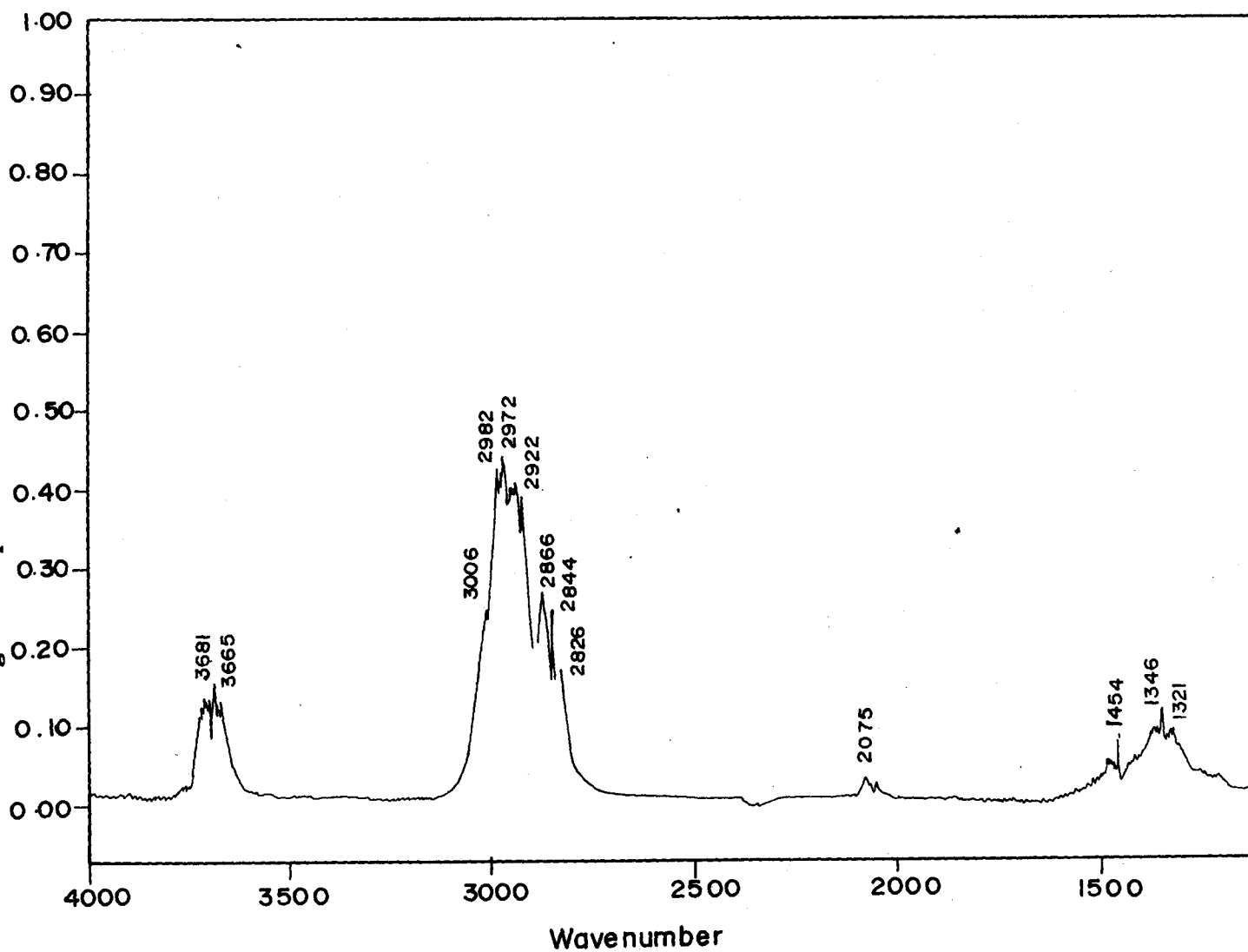


Fig 3.29 ir spectra of methanol

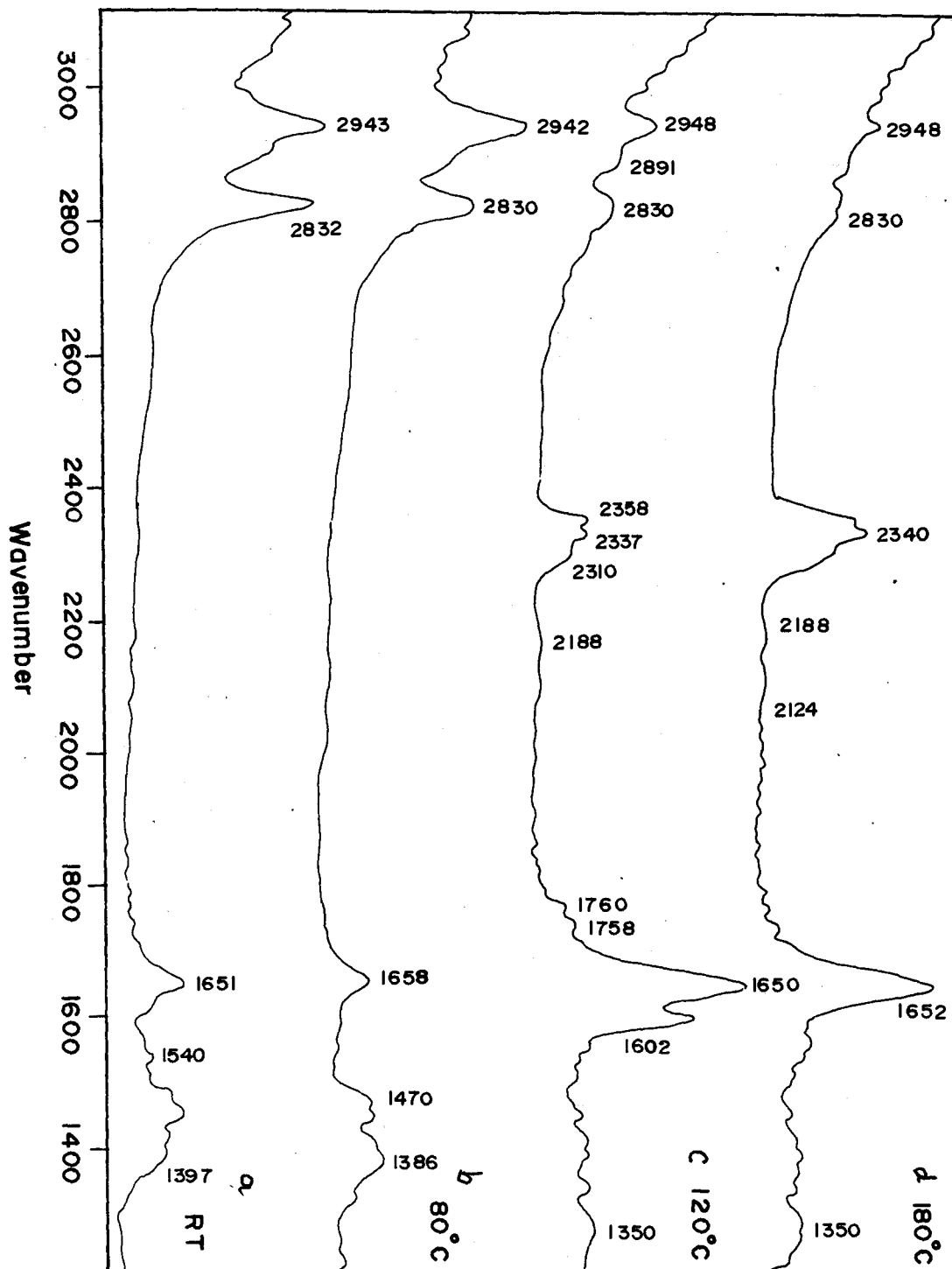


catalysts over pure Pt catalyst. Fig 3.26 (f) is a subtraction spectrum of CO adsorbed on Pt-Ru (HY) catalyst pretreated with hydrogen gas, done to ensure complete reduction of hydroxylated surface and activate the metal sites. The effect is immediately evident with much enhanced intensity of CO absorption as well as that of CO₂ formation. Fig.3.27 is a deconvolution spectrum of CO and CO₂ absorptions, characteristic of carbonyl cluster formation which occurs in zeolites [21].

3.5.2 Effect of CH₃OH/O₂ on Pt (HY):

CO adsorption studies as described above gave a measure of the ability of the catalysts to decompose CO to CO₂ in a model reaction. In actual methanol electrocatalysis, since methanol is a precursor to CO it is felt desirable to study in situ formation of CO species following methanol adsorption and subsequent oxidation of resulting CO to CO₂. It is with this view in mind, methanol adsorption / oxidation studies were carried out on Pt (HY) and Pt-Ru (HY) catalysts by using methanol oxygen feed in a 1: 1 molar ratio. The catalysts were exposed to the reactant mixture for 30 minutes, followed by evacuation at different temperatures. The *ir* spectra of adsorbed methanol over the Pt(HY) catalyst are presented in fig. 3.28 in the relevant mid *ir* region of 1300 cm⁻¹- 3000 cm⁻¹. For ready comparison, the absorptions in relation to corresponding assignments are presented in table 3.6 for Pt (HY) and Pt-Ru (HY) catalysts.

Fig 3.30 Subtraction spectra of CH₃OH /O₂ absorption on Pt(HY) after 30 minutes before evacuation



The ir spectrum of methanol alone is presented in Fig 3.29. It is seen that methanol has three distinct absorption regions:
 3600-3800 cm^{-1} : O---H vibrations of alcohol.
 2800-3100 cm^{-1} : C---H stretching vibrations.
 1200-1500 cm^{-1} : C---H deformation vibrations.

27 ^o C		80 ^o C		120 ^o C		* Band assignments.
Pt (HY)	Pt-Ru(HY)	Pt(HY)	Pt-Ru(HY)	Pt(HY)	Pt-Ru(HY)	
2943	2951	2943	2951	----	----	CH ₃ asymmetric stretching in CHO ⁻
2819	2842	2819	2842	----	----	CH ₃ symmetric stretching in CHO ⁻
1480	1480	1480	1480	----	----	C-H deformation vibrations of CH ₃
1384	1384	1384	1384	----	----	C-H deformation vibration of CH ₃
	1760	----	1720 1670	----	----	Bent CO ₂ molecule
1659	1648	1650	1648	1650	1648	Bidentate carbonates
1454	1425	1454	1425 1330	----	1425	Symmetric carbonates
----	----	1599	----	1599	----	Asymmetric OCO stretching in formate HCOO ⁻
----	----	1350	----	1350	----	Symmetric OCO stretching In formate HCOO ⁻
----	2352	----	2352	2351	2352	Formation of CO ₂
----	----	----	2330	2325	2336	Formation of CO ₂
----	----	----	----	2180	2025	Formation of CO

• Band assignments from [21-27]
 Table 3.6. Assignments of *ir* absorptions _{cm^{-1}} of Pt (HY) and Pt- Ru (HY) catalysts at various temperatures following methanol adsorption.

It is clear from Fig.3.28 that methanol adsorbed at ambient temperature, showed absorptions at 2943, 2819, 1480 and 1384 cm^{-1} which are characteristic of CH_3 stretching and deformation vibrations as also specified in Table 3.4. Peaks due to carbonates observed at 1659 cm^{-1} and 1454 cm^{-1} suggest that methanol oxidation could follow via carbonate intermediate. The peak at 1659 cm^{-1} is not attributed to hydroxyls or moisture as it grows in intensity at higher temperatures. Moreover carbonate peak around this value has been reported following methanol adsorption over alkali metal ion exchanged X zeolites [24].

However following evacuation at 80 $^{\circ}\text{C}$, two additional peaks began to appear at 1599 cm^{-1} and 1350 cm^{-1} , suggesting that at elevated temperatures electrocatalysis would involve simultaneous formation of formate intermediates also. Following further evacuation at 120 $^{\circ}\text{C}$, both the carbonate and formate peaks greatly increased in intensity fig 3.28(b) and 3.28(c), and the effect was also associated with complete disappearance of all the four methanol absorptions. Methanol gets apparently converted into the above intermediates simultaneously; the appearance of the intermediates was synonymous and not mutually exclusive. At the same time peaks due to formation of CO and CO_2 appeared at this temperature. When evacuation was carried out at 180 $^{\circ}\text{C}$, absorption of both the intermediates particularly that of formates decreased in intensity, as they decomposed further to CO or CO_2 . The intensity decrease was anticipated, as there was no further supply of methanol to the *in situ* catalyst.

It can thus be concluded that Pt (HY) catalyst decomposes methanol via simultaneous formation of carbonate / formate type intermediates. The spectra in fig 3.30 were recorded prior to evacuation, other conditions being same as in fig 3.28. It is evident that carbonate

peaks around 1650 cm^{-1} appear almost at same rate but the formate peak particularly at 120°C , appeared at significantly lower intensity probably indicative of its facile dissociation to give CO_2 , as large absorption of CO_2 is seen at this stage. However the carbonate peak intensity is almost same after and before evacuation. Therefore it appears that better electrocatalysis should follow via formate formation rather than carbonate and the catalyst composition should be such that it will prevent carbonate formation and or enhance its decomposition. Fig 3.31 give corresponding spectra of Pt (HY) catalyst when exposed to methanol alone without oxygen. The noticeable difference was that the formate peaks were not seen but a peak at 1574 cm^{-1} due to carboxylate appeared instead of 1599 cm^{-1} while the carbonate peaks continued to be prominent at $\sim 1650\text{ cm}^{-1}$ at all the temperatures studied even though they were also reduced in intensities. Thus one may conclude that methanol decomposition to CO_2 follows carbonate / formate pathway in presence of oxygen and carbonate / carboxylate pathway in absence of oxygen. It is known from previous studies that Pt_2CO obtained from deprotonation of methanol, is a precursor for the carboxylate type intermediate. In the light of the observations made in the present studies *vis a vis* the existing concepts, the mechanism for methanol decomposition on Pt catalyst may be summarized as follows:

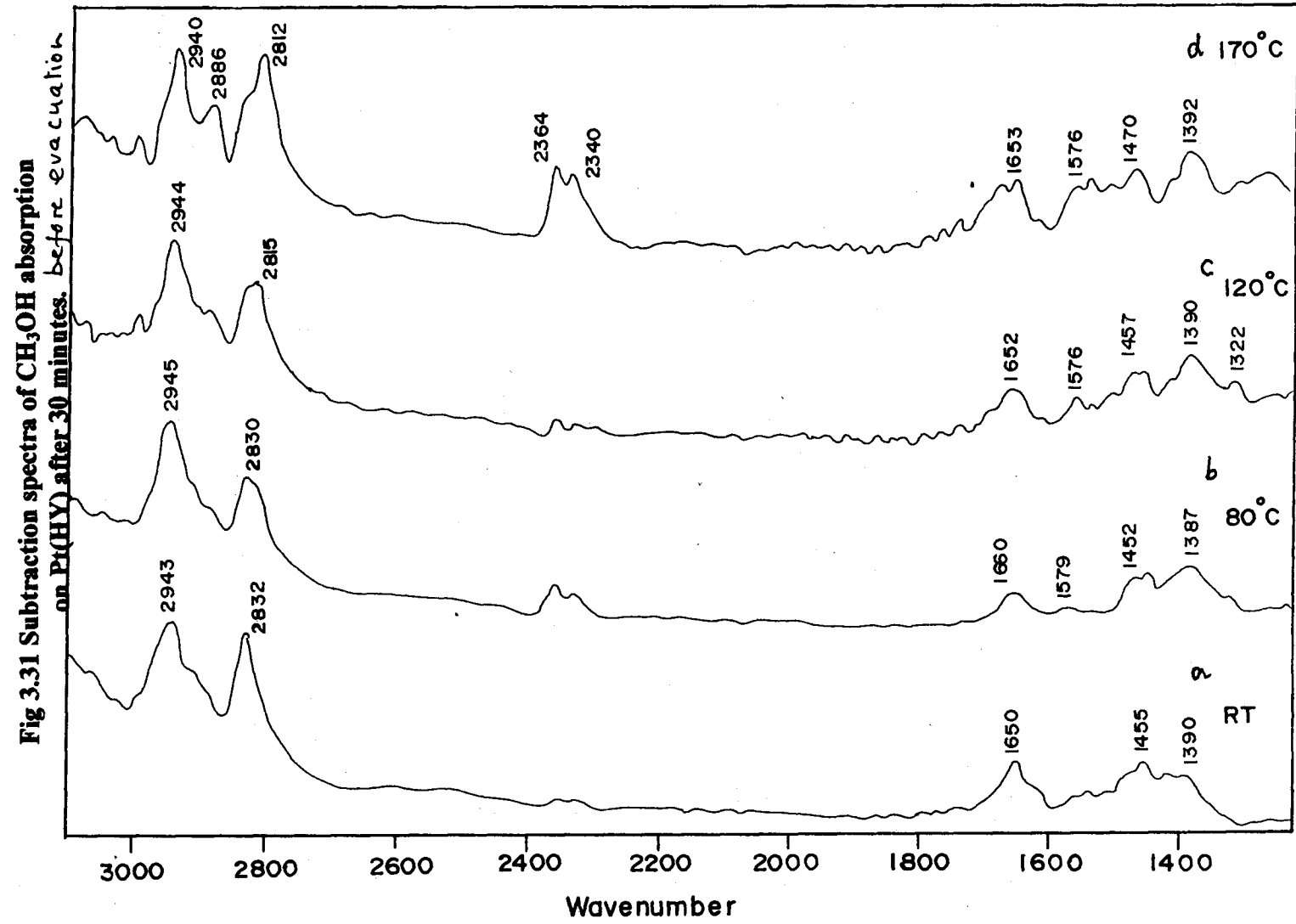


Fig 3.32 CH₃OH/O₂ absorption spectra on Pt(HY) at various temperatures after evacuation.

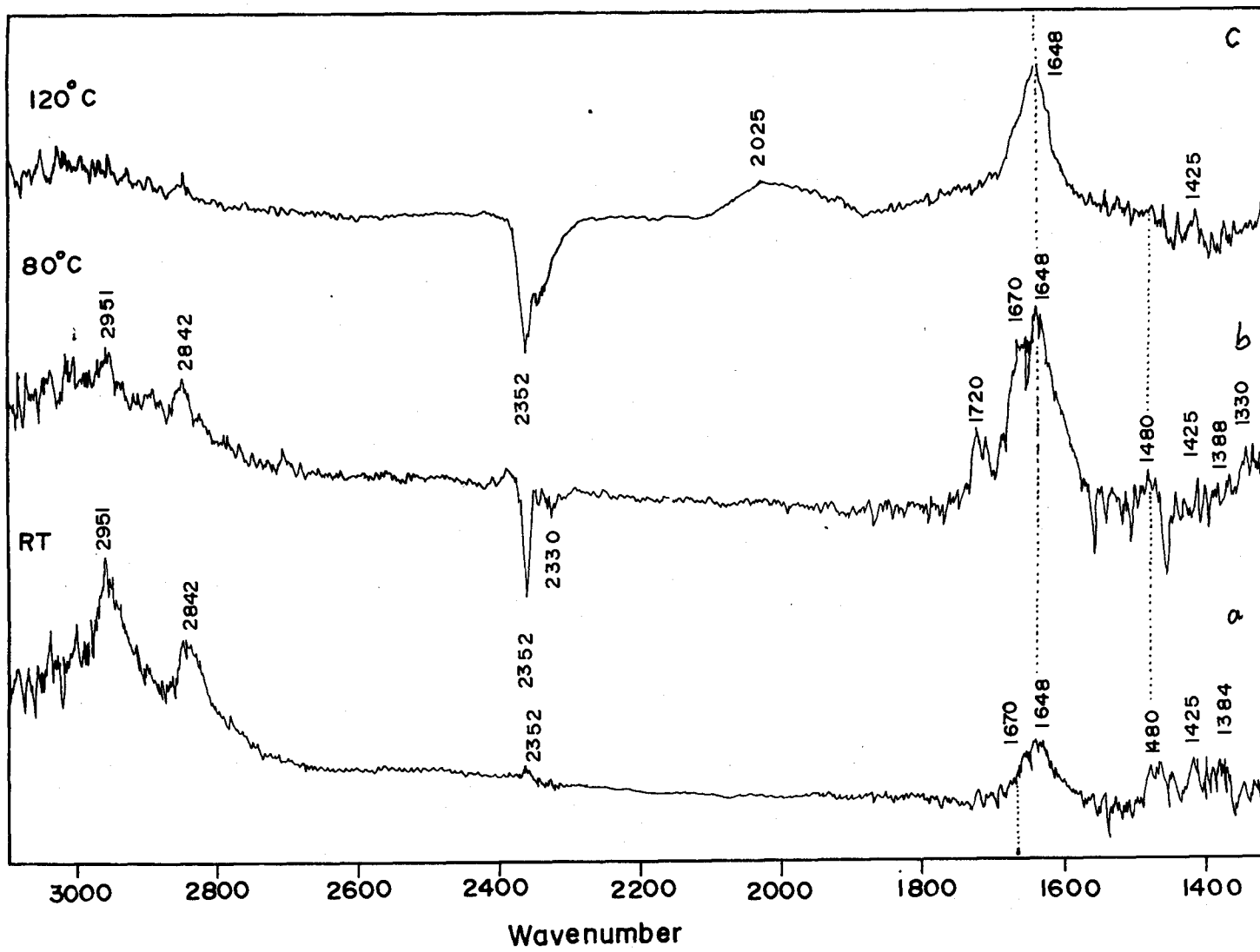
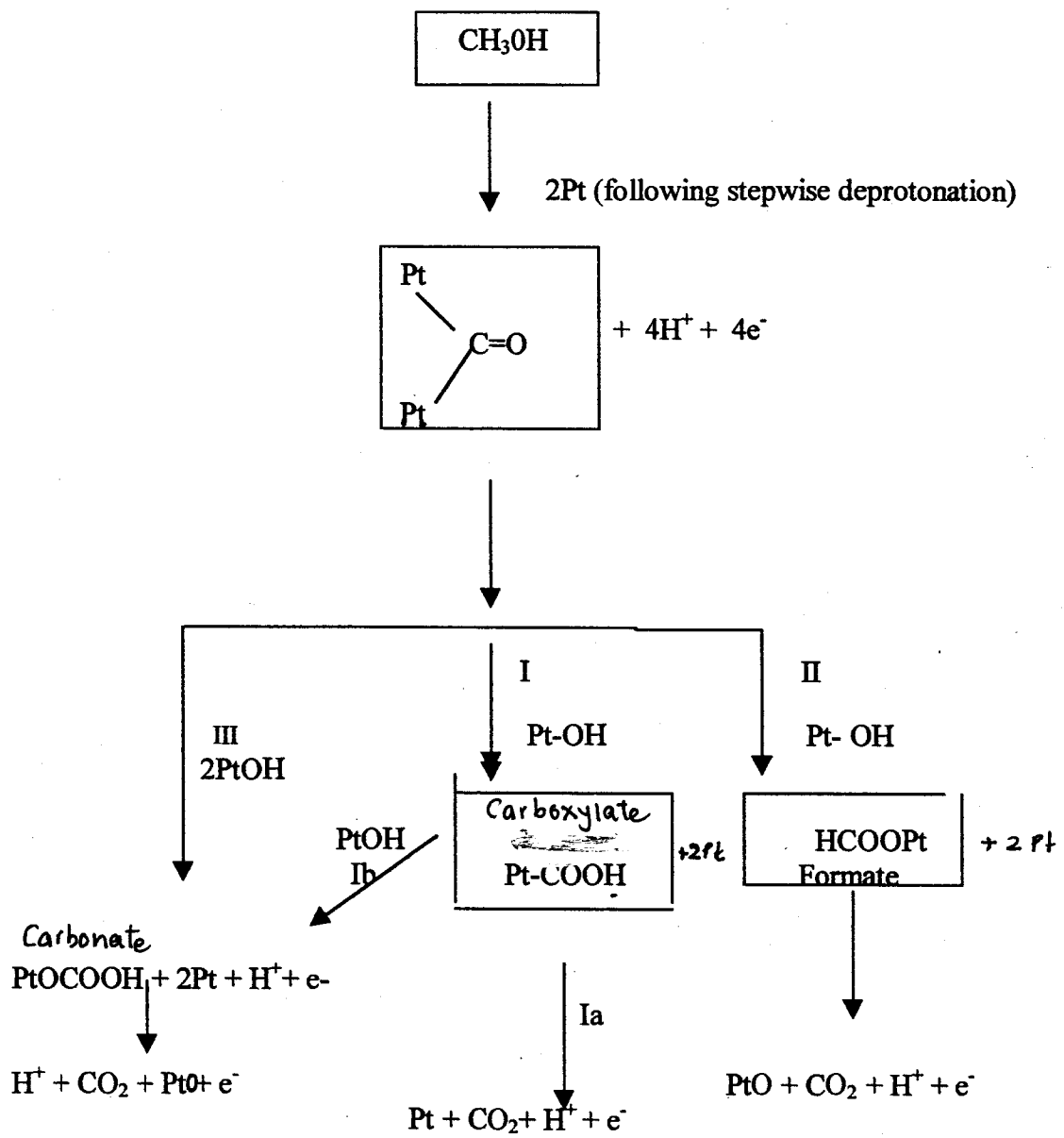


Fig. 3.32

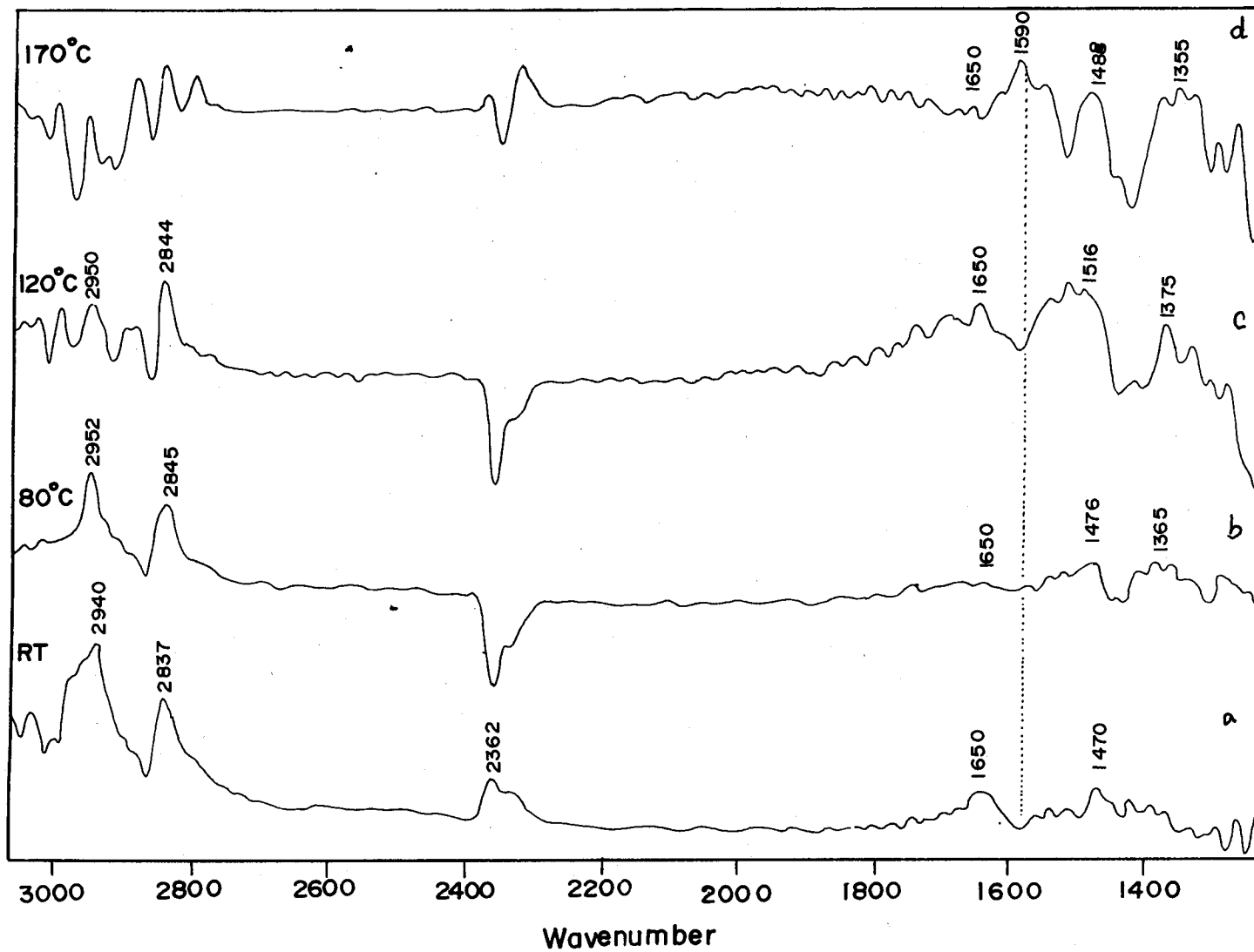


Also the spectra at 120⁰ C & 180⁰ C, fig 3.28 c & d, show small but broad absorption due to CO formation between 2100 cm⁻¹ to 2250 cm⁻¹ and also peaks due to CO₂ formation are seen at 2337cm⁻¹ and 2358 cm⁻¹; further these peaks are better evident in the spectra taken prior to evacuation (fig. 3.30 c & d). Since CO or CO₂ formation appears at or beyond 120⁰ C, one may conclude that platinum electrocatalyst would presumably show optimum efficiency for methanol oxidation, when operated around 120⁰ C.

3.5.3 Effect of CH₃OH /O₂ on Pt -Ru (HY):

The room temperature *ir* spectrum (fig. 3.32) following methanol adsorption on the Pt-Ru (HY) catalyst is similar to that with Pt (HY) catalyst. The band assignments corresponding to various absorptions are also shown in table 3.6. However the spectrum following evacuation at 80⁰C is markedly different. Thus the formate bands at 1599 cm⁻¹ and 1350 cm⁻¹ seen in Pt (HY) catalysts are conspicuous by their absence. Also additional peaks at 1720 cm⁻¹ and 1330 cm⁻¹ appeared. These were attributed to bent CO₂ molecules lying on the surface with its carbon attached to the surface. At this point there is simultaneous appearance of bands at 2330 cm⁻¹ and 1352 cm⁻¹ corresponding to CO₂ absorption; CO₂ being desorbed following evacuation. The carbonate absorption is greatly enhanced with simultaneous diminishing of methanol absorption. CO₂ formation was not significant at 80⁰ C on Pt (HY), but showed intense CO₂ bands on Pt -Ru (HY) at this temperature. This re-emphasizes higher efficiency of the Pt -Ru over Pt catalyst for methanol decomposition. Still enhanced effect (more intense CO₂ absorption) was seen following evacuation (120⁰C).

Fig 3.33 ir spectra of CH₃OH/O₂ absorption on Pt(HY) at various temperatures after 30 minutes



Further no formate peaks were observed on Pt-Ru (HY) catalyst unlike the case with Pt (HY) catalyst suggesting different methanol decomposition pathways on the two catalysts. This observations suggest that Pt-Ru (HY) catalyst decomposes methanol to CO₂ through intermediate formation of carbonate and CO.

Since carbonate phase also persists substantially without decomposition, even at higher temperature, it seems to be one of the factors responsible for poor catalyst efficiency. This conclusion is well brought ^{out} when spectra fig 3.31 and 3.33 are compared. These spectra of Pt (HY) and Pt-Ru (HY) respectively were taken following exposure to methanol alone without oxygen and prior to evacuation. Comparing absorption at 1650 cm⁻¹, it is seen that carbonate phase (even though much less intense peaks than seen when catalyst was treated with CH₃OH & O₂) appeared at all the temperatures studied. It is much more prominent in Pt (HY) spectra than in Pt-Ru (HY) while the formate peak (1590 cm⁻¹) appeared only at high temperature (170^oC) in Pt-Ru(HY) and absent in Pt (HY). Significantly, CO₂ formation appeared at all temperatures on Pt-Ru(HY), catalyst once again re-emphasizing high efficiency of Pt-Ru(HY) catalyst to decompose methanol even in absence of oxygen.

Compare figs. 3.28 and 3.32. It is seen that the carbonate band ~1650 cm⁻¹ which was smooth in Pt (HY), tend to show multiple splitting in Pt-Ru (HY) both at room temperature and 80^o C, more prominently at 80^o C. This could be due to lower stability of the carbonate showing tendency to dissociate into CO₂ via intermediate CO formation. This hypothesis appears to be justified when one looks at the spectrum 'c' at 120^o C. The carbonate band has greatly decreased in intensity with simultaneous appearance of a clear broad band due to C---O stretch of

carbonyls in the region 1880-2100 cm^{-1} and is known to be associated with the formation and growth of $(\text{CO})_x$ clusters [21]. The $(\text{CO})_x$ clusters get constrained due to entrapment in zeolite cages and have a facile tendency to dissociate into CO_2 . In fact an intense band due to CO_2 formation is simultaneously seen at $\sim 2352 \text{ cm}^{-1}$.

3.5.4 Conclusions:

- 1) Pt-Ru (HY) adsorbs at least three times more CO than Pt (HY) catalyst confirming higher catalytic efficiency of the former.
- 2) The decomposition of methanol on Pt (HY) catalyst occurs via carbonate/ formate pathway in presence of oxygen and carbonate/ carboxylate pathway in absence of oxygen.
- 3) Considering decomposition of the intermediates into CO or CO_2 , it appears that optimum efficiency of the Pt (HY) catalyst occurs $\sim 120^\circ\text{C}$.
- 4) CO_2 formation on Pt-Ru (HY) catalyst occurs even at room temperature, thus re-emphasizing its higher catalytic efficiency.
- 5) The carbonate intermediate is unstable on the Pt-Ru (HY) catalyst and shows facile tendency to dissociate into CO_2 through intermediate formation of $(\text{CO})_x$ clusters formed in zeolite cages.

REFERENCES :

1. A. S. Arico, H. Kim, A. K. Shukla, M. K. Ravikumar, V. Antonucci, N. Giordino, *Electrochim Acta*, 39 (1994) 691.
2. A. Hamnett, B. J. Kennedy, S. A. weeks, J. B. Goodenough, *J. Appl. Electrochem.*, 25 (1995) 333.
3. J. B. Fernandes, B. D. Dessai, V. N. Kamat Dalal, *J. Power Sources*, 15 (1995) 209
4. J. B. Fernandes, B. D. Dessai, V. N. Kamat Dalal, *J. Power Sources*, 16 (1985) 1
5. P. Ruetschi, R. Gionoholi, *J. Electrochem Soc.*, 135(11) 2663.
6. J. B. Fernandes, B. D. Dessai, V. N. Kamat Dalal, *J. Appl. Chem.*, 15(1985) 351
7. J.W. Li, G. Calzaferri, *J. Electroanal Chem.*, 377(1994) 163.
8. P. V. Samant, S. B. Kakodkar, S. Naik, and J. B. Fernandes, *Recent trends in catalysis* edited by V. Murugesan, B. Arbindo, M. Palamchamy(Eds)(1999)230.
9. L. Persaud, A. Bard, A. Champion M. A. Fox, T. E. Mallouk, S. E. Webber, 26 (1887) 3825.
10. N. Markovic, H. A. Gasteiger, P. N. Ross, Jr, X. Jiang, I. Villegas, *Electrochim Acte*, 40(1995) 91.
11. H. A. Gasteiger, N. Markovic, P. N. Ross, Jr, E.J Crain, *J. Phy Chem.*, 98 (1994) 617.
12. B. S. Shete, V. S. Kamble, and V. B. Kartha, *J. Phy Chem.*, 102 (1988) 581.
13. N. M. Gupta, *Bull Chem Soc., India*, 8 (6) (1999) 2.
14. A. M. Ferrari, K. M. Neyman, T. Belling, M. Mayer and N. Rosch, *J. Phy Chem.*, 103 (1996) 239.
15. Z. Wei, H. Guo, *J. Power Sources* 58 (1996) 239.
16. A. Hamnett and B. J. Kennedy, *Electrochim Acta*, Vol 33 (1988) 1623.
17. L. D. Burke, M. B.C. Roche, W. A. O'Leary, *J. Appl. Electrochem.* 18(1988)781
18. I. Iwasita and W. Vielstich, *J. Electroanal.chem.* 250(1988)452
19. J. Prabhuram and R. Manoharran, *J. Power Sources* 74(1998) 54.
20. A. S. Arico, N. Giordino, *Electrochim Acta*, 39 (1994) 691.
21. N. M. Gupta, *Bull Catal. Soc. India*, 8 (6) Nov, 1998.
22. M. L. Hair, *Infrared spectroscopy in Surface Chemistry*, " Marcel Dekker, New York, N. Y, 1967 p204.
23. L. M. Sver, M. A. Kovner and E.P. Krainer " *Vibration spectra of Polyatomic Molecules*" Nauka, Moscow, 1990.
24. M. L. Unland *J. Phy Chem.*, 82 (1978) 580.
25. S. Matsushita and T. Nakata, *J. Chem. Phy.*, 30 (1962) 665.
26. V. S. Kamble, N. M. Gupta, V. B. Kartha and R. M. Iyer, *J. Chem soc. Faraday Trans.* 189 (1993) 1143.
27. B. S. Shete, V. S. Kamble, N. M. Gupta, V. B. Kartha, *J. Phy, Chem.*, 102 (1998) 581.
28. S. Wasumus, W. Vielstich, *J. Appl. Electrochem*, 23 (1993) 220.

CHAPTER 4

VAPOUR PHASE DIRECT METHANOL FUEL CELL.

VAPOUR PHASE METHANOL OXIDATION FUELCELL

This Chapter is divided into following sections:

4.1 Introduction.

4.2 Cell Design and Construction.

4.3 Fabrication of Electrode.

4.4 Results and Discussion.

4.1 Introduction:

The PEM cells show great promise in portable, automotive and stationary applications because of their high power density and adaptability of different system requirements [1-2]. It uses methanol in the form of vapour/ liquid to generate electricity. The DMFC based upon solid polymer electrolyte has advantage of no liquid acidic or alkaline electrolyte [3]. The adaptation of SPE technology for DMFC has two advantages: (1) Operating temperature can be raised, which improves efficiency. (2) The other important advantage is that by using methanol vapour, access to electrode is improved by increasing current density [4]. The schematic diagram of DMFC with solid polymer electrolyte is shown in fig 4.1 and is similar to that adopted elsewhere. [5].

Inspite of tremendous international efforts and high theoretical efficiency DMFC has not yet reached the optimum performance of the conventional combustion engine. Two key issues that need to be addressed, if DMFC's are to be commercialized are 1. The sluggish kinetics of methanol oxidation 2. Cathode performance degradation resulting from methanol cross over [6-7].

Improvement in performance can be identified by evaluating the polarization curves of a fuel cell. Fig. 4.2 gives a typical fuel cell polarisation curve[8].

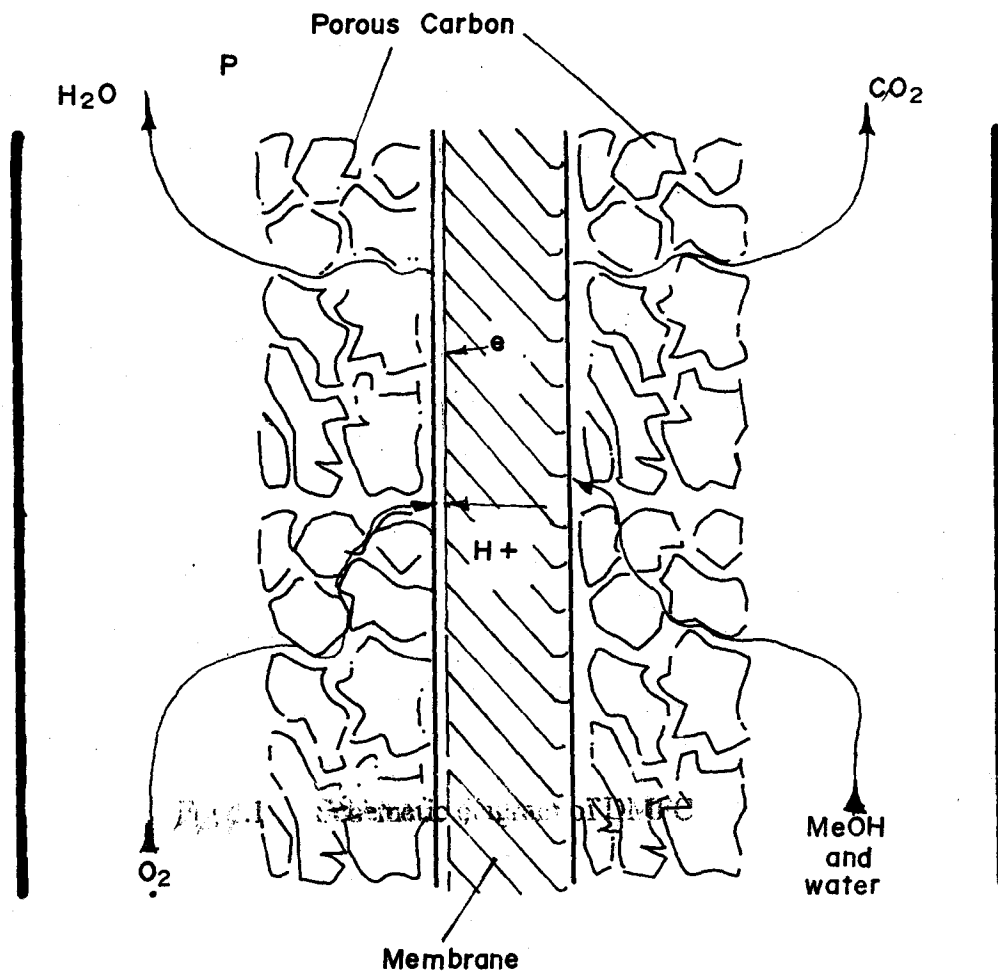


Fig 4.1 Schematic diagram of DMFC

Fig 4.1

The curve is divided into three regions.

(1). The sharp voltage drop of first region is associated with the activation resistance r_{act} is attributed to the type of catalyst and catalyst surface area in contact with electrolyte- electrode interface.

(2). The gradual drop in the voltage of second region known as ohmic region, the voltage loss is attributed to the electronic, ionic and contact resistance of the components such as electrode, membrane and current collecting components. Lowering this resistance will raise the polarization curve and reduce the slope of the curve resulting in higher power densities close to heat engine efficiencies.

(3) The sharp voltage drop of the third region is due to voltage loss associated with mass transport resistance. It is attributed to concentration polarisation which occurs as a result of depletion of the reactant at the reaction interface. This voltage loss region associated with mass transport has not been fully overcome. Attempt has been to minimize the loss by raising the gas pressure and gas stoichiometric flow rate.

By introducing liquid water directly into the anode and allowing it to contact the anode membrane interface provide benefit of higher membrane hydration and therefore higher conductivity [8].

Among the various membrane electrode assemblies [MEA], attention has particularly been focussed on Nafion membrane, since it has higher ionic conductivity, mechanical, thermal and chemical stability along with considerable engineering advantages [9-10]. Key to cell construction is the MEA, which is the heart of fuel cell system.

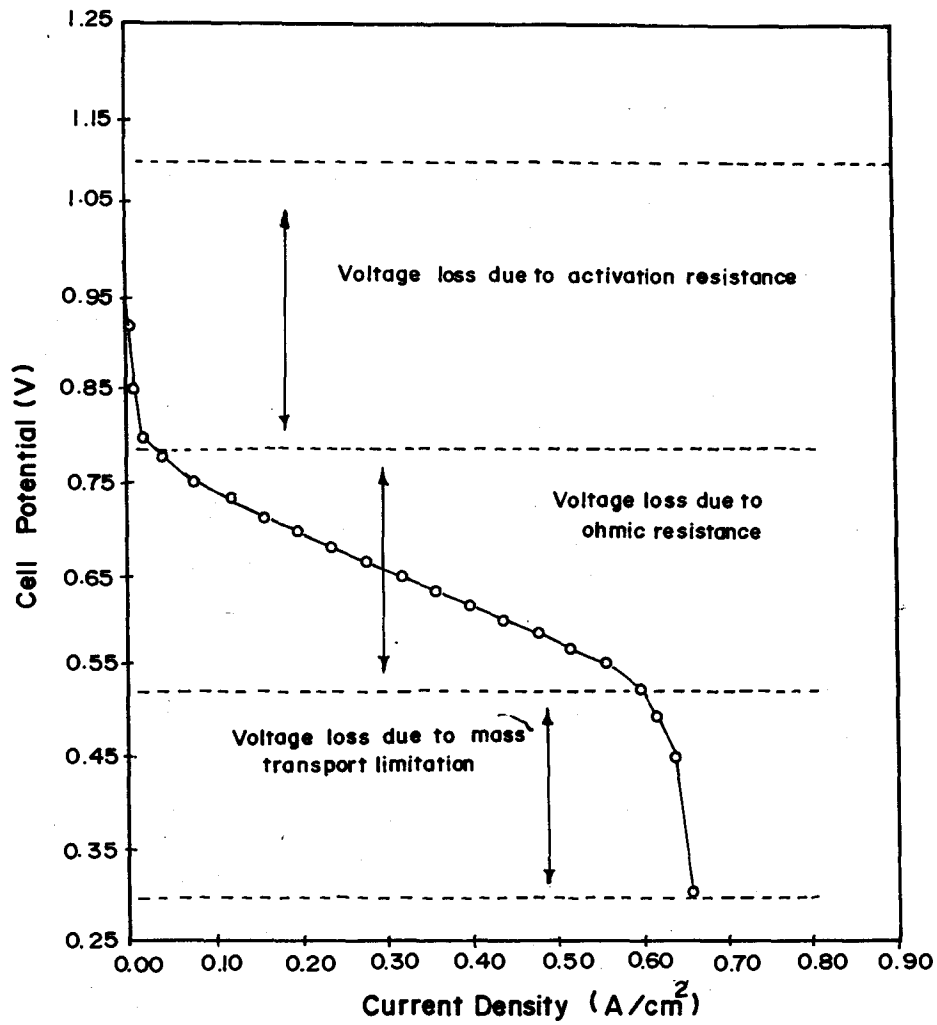


Fig4.2 Typical polarization curve of a PEM cell

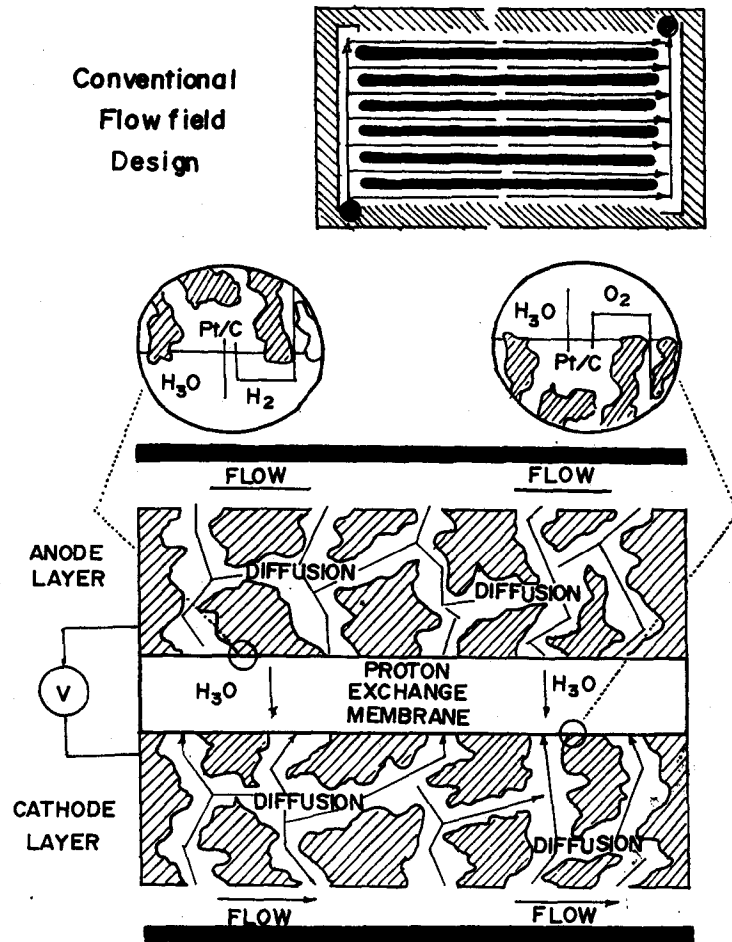


Fig4.3 Gas transport inside a MEA using a conventional flow field design.

During construction of the cell following guidelines are to be followed

1. Cell must be constructed from low corrosion material e.g. Stainless steel.
2. Cell material should be thermally conducting to allow efficient heat transfer.
3. Bulky design should be avoided.
4. Complex designing and machining must be avoided.

The MEA with number of subsystems is capable of sustaining necessary optimum performance. Outside the electrode housing there should be 1. fuel injection system 2. An oxidant system with distinct approaches like use of ambient air and use of air at elevated pressure.

In vapour feed fuel cell system, mass transport and electrode kinetics is enhanced resulting in significant increase in cell performance [11-13].

4.2 Cell Design and construction:

The designed specification of the cell used for the vapour phase experiment is shown in fig 4.4.

Graphite plates were used for machining flow channels since it is soft, offers more rigid support for the electrode and also a good current collector. The flow channels as shown in fig 4.5 (a) and (b) were cut directly into each graphite block to a depth of 1mm as per the envisaged design for cathode and anode.

Each graphite plate has two bore holes in one of its narrow sides into which fuel and oxidant system can be introduced. The bore holes emerge at right angles out through the front face of the block at opposite corners of the flow channel pattern. A open channel area of 2 cm^2 flow pattern was machined on a graphite block 4 cm^2 in area. Small hole on the side of graphite was also made to introduce the thermocouple.

The cell was heated using integrated heating pads, having temperature controller across it, for heating up to temperature 150°C . A copper plate was embedded in each graphite blocks which acts as a current collector to make connection with external load.

PTFE sheet (5 cm^2) was inserted as an insulator to prevent external heating. The two PTFE gaskets were cut into a hole of area of 3 cm^2 , so as not to cover the flow channels of graphite plates. The PTFE gasket along with teflon tape serves as gas seal.

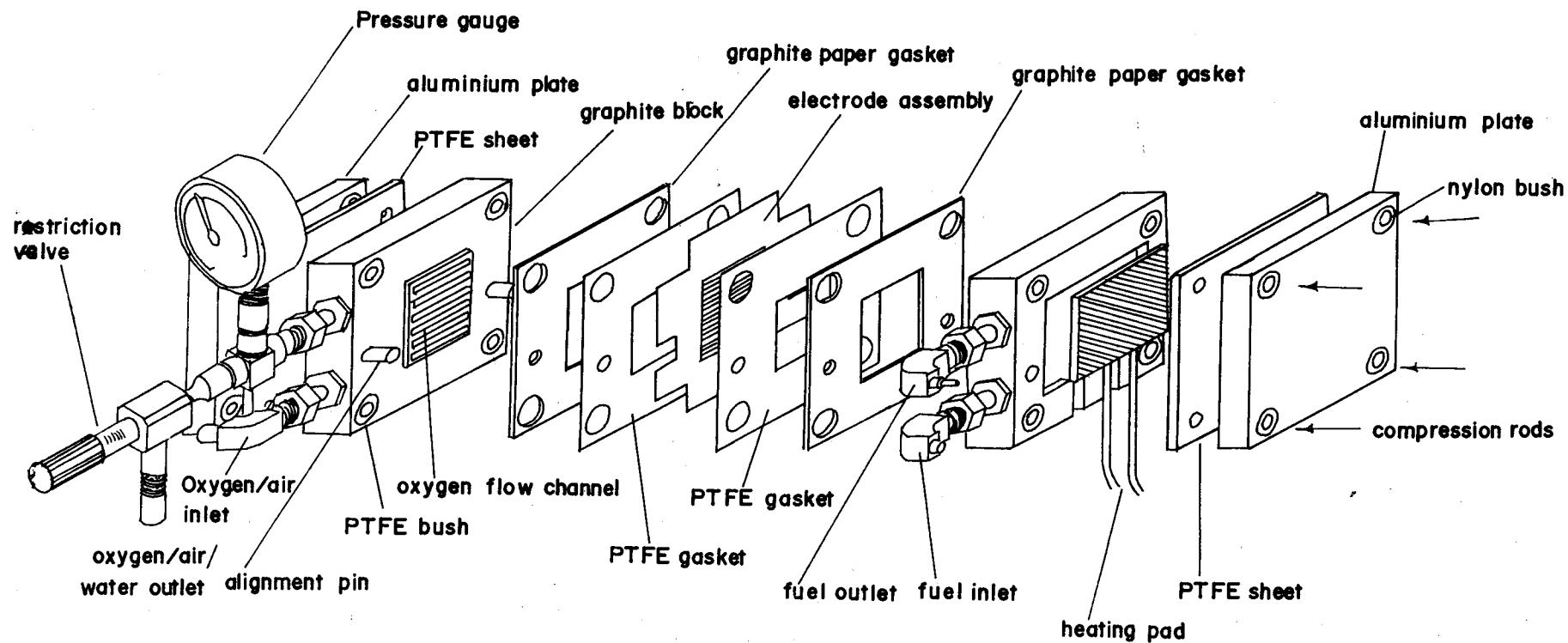


Fig.4.4 Design specification of the cell used for vapour phase DMFC

Adopted from : M. Hogarth et. al., J. Power sources 69 (1997) 125

All the components along with the membrane electrode were assembled between two Aluminium plates (6cm^2) and held tightly using stainless steel compression rods from each corner of the Aluminium plate. This cell can withstand pressure up to 5 bars without any leakage.

Both fuel and oxidant were supplied from the side portion of the cell. This configuration of the cell was successful in preventing drying at the cathode and any excess of water could be transported through a manifold into the reservoir.

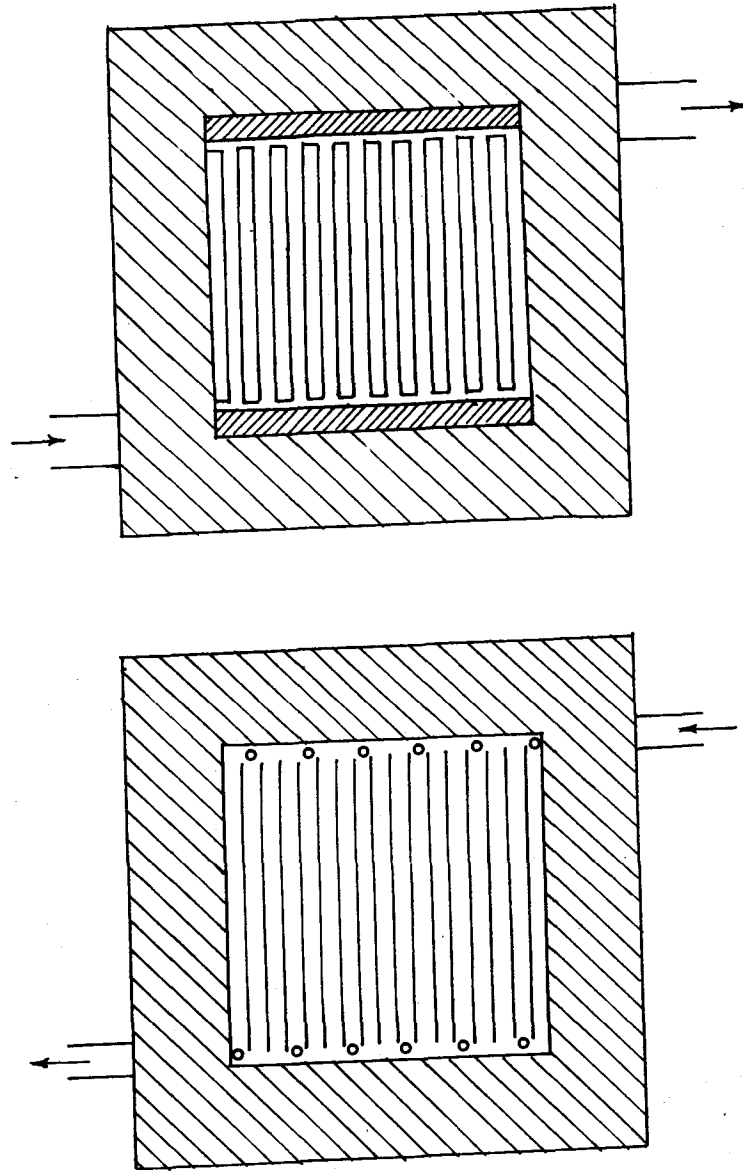


Fig. 4.5

Fig4.5 Flow pattern of channels on cathode and anode.

4.3 Electrode Fabrication :

The encapsulated electrode assembly was developed using following techniques wherein porous carbon electrodes were bound with nafion and did not contain PTFE. The electrodes obtained by this method were very thin and highly loaded which helped in reducing ohmic loss and increase in catalyst utilization.

The anode layers were prepared using following steps

1. A toray carbon paper of geometric area 16 cm^2 was first soaked in PTFE emulsion for 30 seconds and dried in an oven at 110°C and further sintered at 350°C for 45 minutes. This treatment offers mechanical strength to toray carbon paper.
2. A small quantity of PTFE emulsion along with cyclohexanol and water were mixed manually with weighed quantity of Vulcan XC 72 carbon for 30 minutes to obtain a putty like material.
3. The above carbon / PTFE paste was then spread uniformly using brush repeatedly on a carbon paper to obtain a carbon loading of $0.4 \text{ mg} / \text{cm}^2$.
4. Appropriate quantity of catalyst, nafion solution and teflonised carbon along with 2-3 drops of water were mixed thoroughly for 90 minutes.
5. Uncatalysed carbon paper was held tightly with cellophane tape on a graphite window of geometric area 9 cm^2 . Catalyst / nafion ink like paste was then applied uniformly over carbon paper.
6. Above the carbon paper loaded with catalyst, was placed a stainless steel plate and covered with nonstick paper, which was then cold pressed at $700 \text{ Kg} / \text{cm}^2$ for 10 minutes and then cut into $2.8 \times 2.8 \text{ cm}^2$ area. Similar procedure was followed for the fabrication of anode.

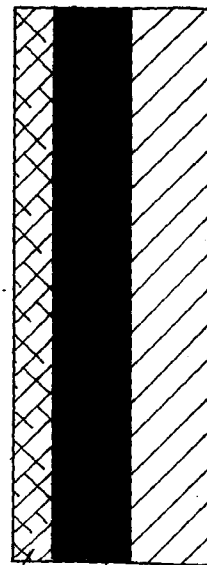
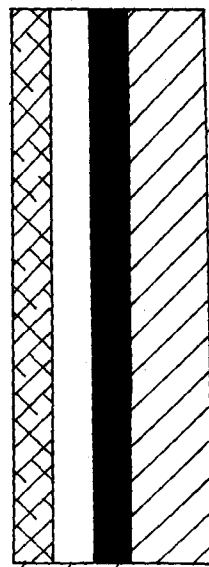
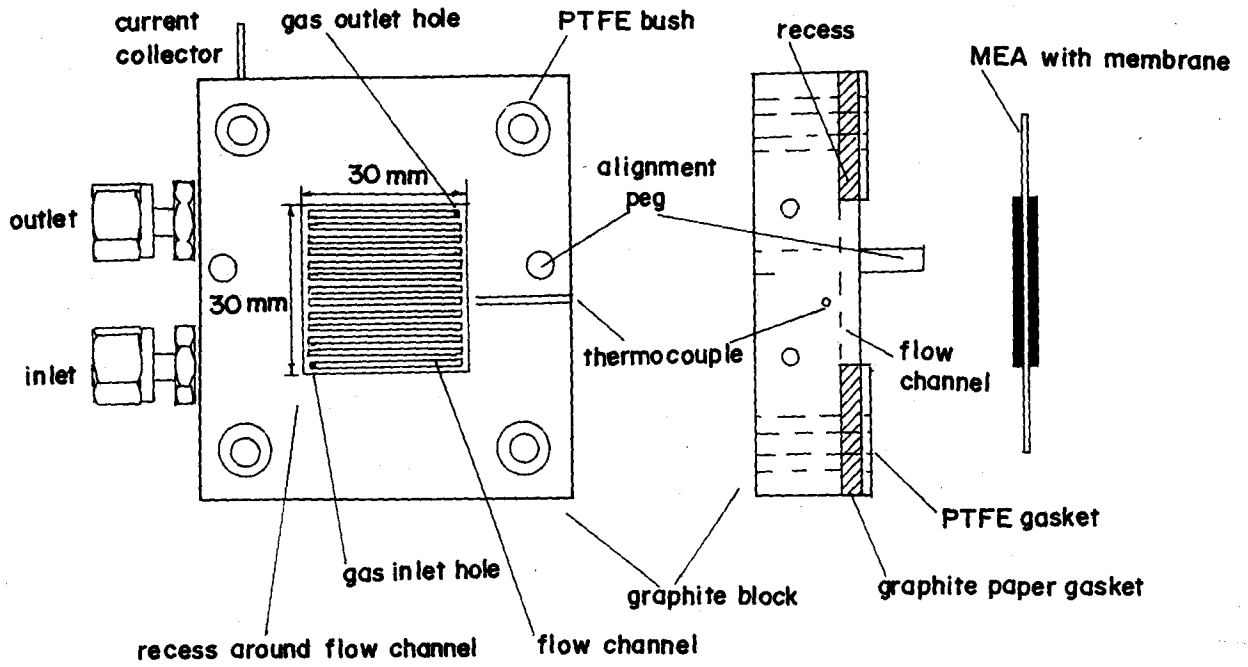


Fig4.6 Comparison between composite electrode and standard catalyst layer electrode.

uncatalysed carbon layer
carbon paper
(a) Composite electrode

catalyst layer
carbon paper
(b) Standard electrode

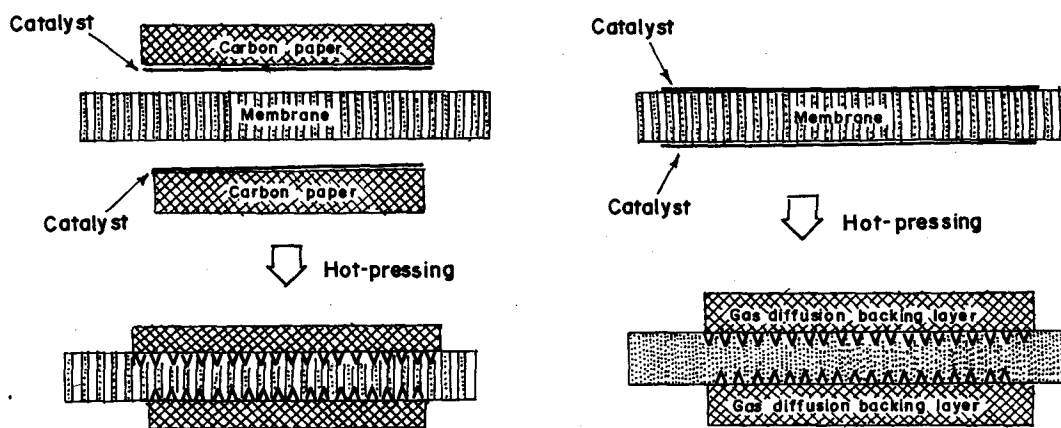


Fig. 4.7

Fig 4.7 Schematic diagram illustrating a conventional MEA and thin film MEA.

Nafion encapsulated electrode is obtained using following method. Prior to use of nafion membrane, it requires to obtain the fully hydrated membrane.

Following steps were followed for cleaning and hydrating the nafion membrane.

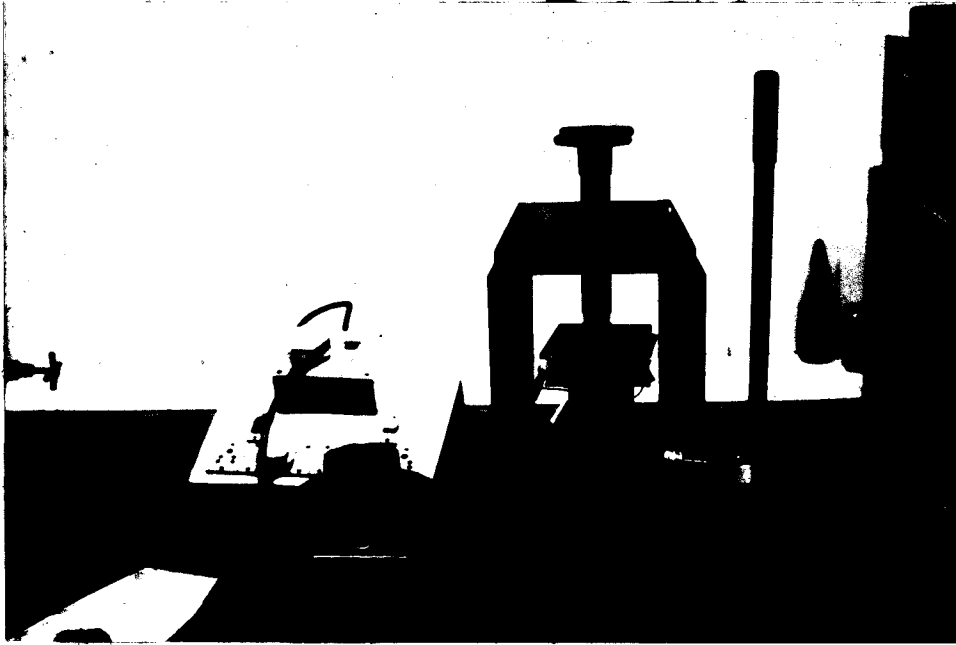
1. Boil the membrane in (1:1) HNO_3 for 30 minutes.
2. wash with distilled water (5 times) and soak it in H_2O_2 [6% w/v] for 90 minutes and again wash with distilled water five times.
3. It is then further boiled in 1M H_2SO_4 for 1 hour.
4. finally membrane is washed with double distilled water plentifully and then kept for soaking in distilled water .

The nafion membrane thus obtained will be clean and highly hydrated.

Both the electrodes were given 2-3 brush coats of nafion solution and allowed to dry in air for 10 minutes before being assembled with nafion membrane. A window of $2.8 \times 2.8 \text{ cm}^2$ area was made using Whattmann paper and placed on stainless steel plate. The cathode was then carefully inserted on it. The hydrated nafion was then carefully placed on it and held tightly. The anode composite was immediately and appropriately placed on it and then covered with another stainless steel plate. The assembly was then heated at 130°C and subsequently pressure of 350 kg/ cm^2 was applied for 3 minutes. The assembly was then immediately immersed in cold water and membrane electrode thus obtained was soaked for 2 hours in distilled water. Comparison between the composite electrode and standard electrode configuration is shown in fig 4.6. Fig 4.7 shows schematic diagram illustrating a conventional MEA and thin film MEA.



Assembly of die for making pellet



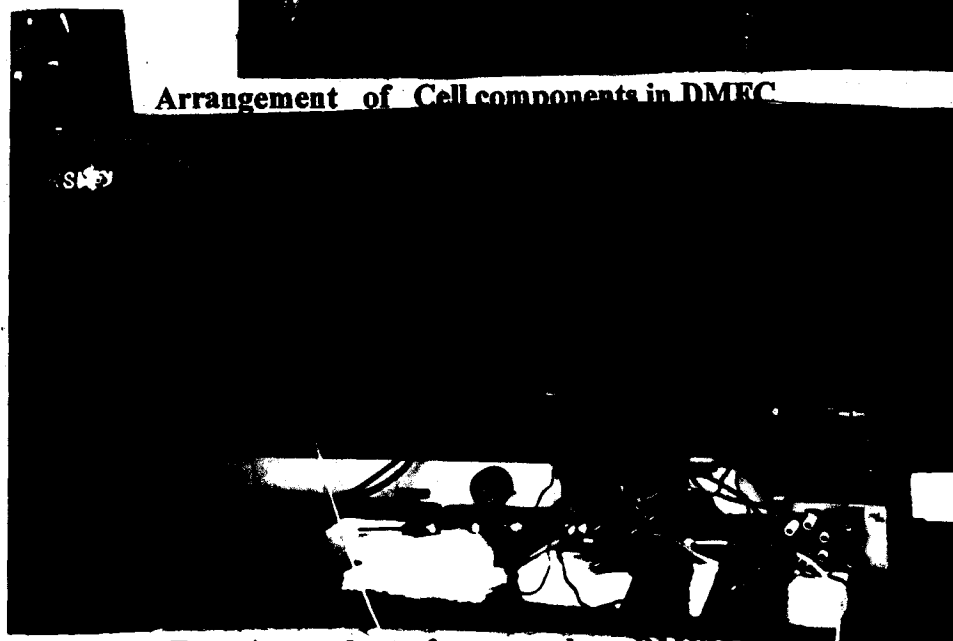
Assembly for giving heat treatment to pellet



Pattern of flow channel on graphite block



Arrangement of Cell components in DMFC



Experimental set of vapour phase DMFC

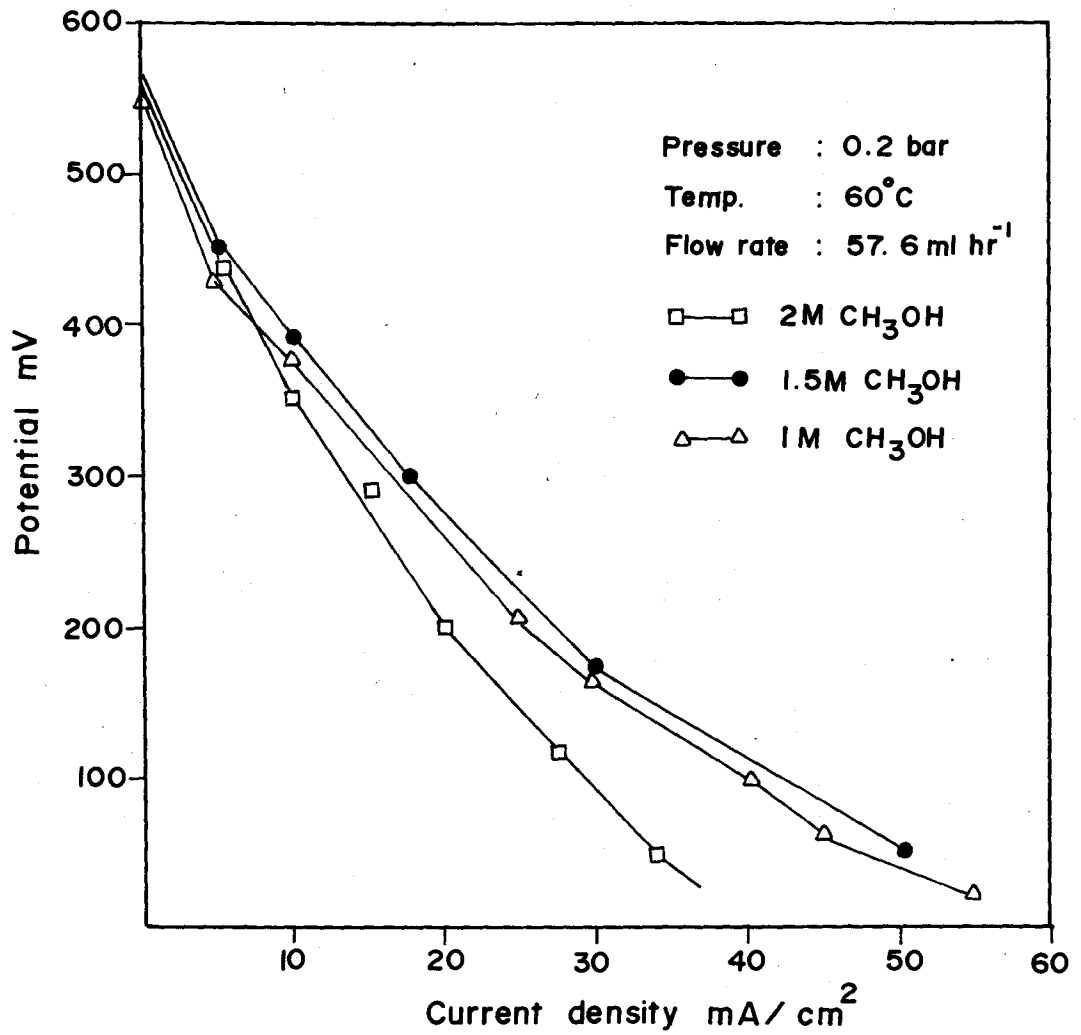
4.4 Results and Discussion:

The performance of a fuel cell is generally understood from slopes of potential current curves of the type shown in fig 4.2 or corresponding power density achievable. However for a given fuel cell set up, the observed power output is influenced by several parameters such as

- i) Operating temperature, which affect electrocatalytic activity – generally better activity at higher temperature. Generally fuel cells are designed to operate from ambient temperature to $\sim 120^{\circ}\text{C}$ high temperature limits will be restricted by membrane stability.
- ii) Level of membrane hydration and hence proton conduction across the membrane
- iii) Pressure differentials across the membrane influenced by methanol flow rate at anode and air or oxygen pressure at the cathode.

At the present time, the fuel cell voltage output is believed to be considerably affected by methanol crossover from anode to cathode with subsequent poisoning of the cathode electrocatalyst. Till such time, methanol non-permeable membranes are discovered, one has to work out optimum conditions for the fuel cell operation, with the lasting polymeric membranes such as Nafion 110, despite this inherent limitation of significant methanol permeability after the appropriate choice of electrocatalyst.

The electrocatalyst used in the present investigation is Pt-Ru (HY) for the anode, shown to be most active ~~as anode~~ catalyst among the various types tested as reported in section 3.3. The cathode electrocatalyst used was Pt/C.



• Fig. 4.8 V-I Plots of PEM fuel cell as a function of methanol concentration

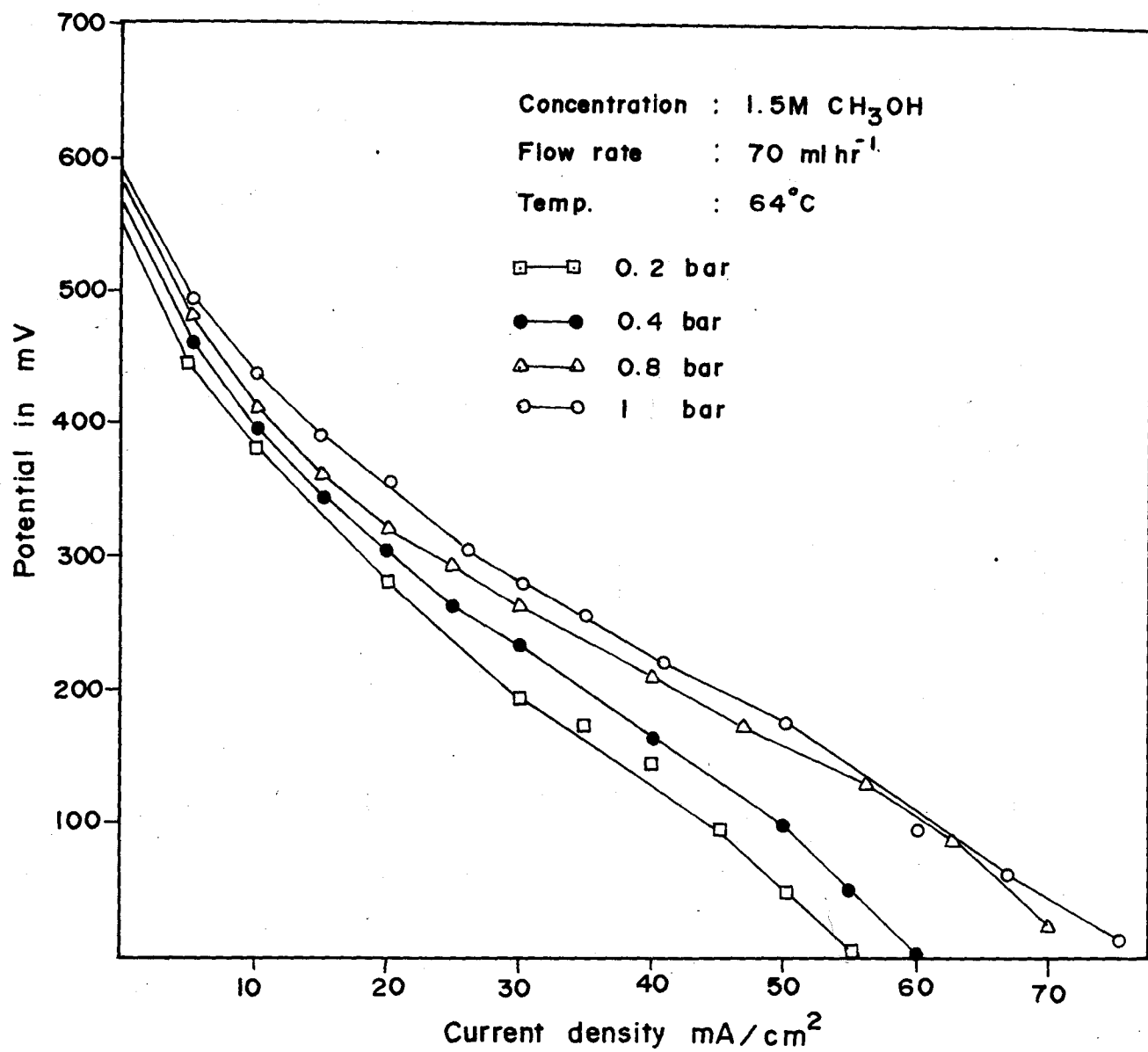


Fig. 4.9 V-I Plots of PEM fuel cell as a function of Oxygen pressure

The effect of various operating parameters are presented in fig 4.8 - 4.12. The results may generally be interpreted in terms of electrocatalyst performance and the effect of methanol crossover.

A mathematical model structure is given in fig 4.13. A mathematical model for methanol diffusion flux [3,5], is given by the relation

$J = 1 / (a + b \Delta p)$, derived on the basis of following assumptions are made.

1. Due to high thermal conductivities of the graphite and aluminum cell components, the cell temperature is assumed to be constant and uniform.

1. Transport along the flow channels can be described by plug flow.
2. The pressure is uniform within each compartment - any pressure drop occurs across membrane.
3. Due to thinness of the diffusion region of the electrodes, transport in this region is not considered.
4. Due to high electronic conductivity of the carbon substrate and the graphite flow beds, no voltage drop is considered to occur through the thickness of the electrode, or along the flow channel.
5. Due to amount of water in the anode flow channel, the membrane is considered to be fully hydrated.
6. The concentration of the reactant is taken as the weighted average of the inlet and outlet concentrations.
7. Electrode kinetics can be described by the Tafel equation.
8. The overpotential caused by methanol crossover is directly proportional to the concentration of methanol at the cathode. [3]

$$a = [1 / DC_1] + [1 / kC_1]$$

$$b = K / kC_1D$$

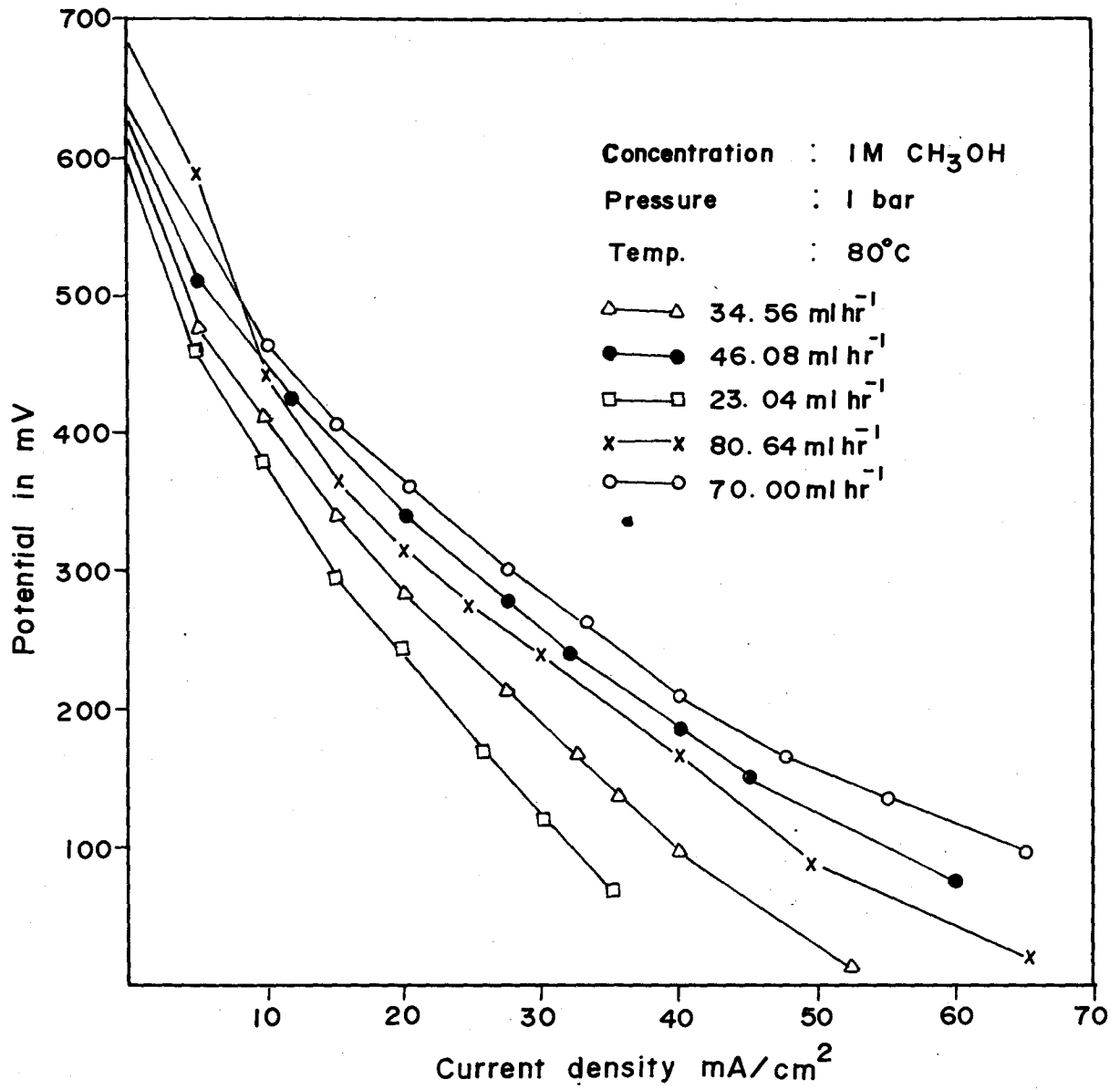


Fig. 4.10 V-I Curves of PEM Fuel cell as a function of methanol flow rate

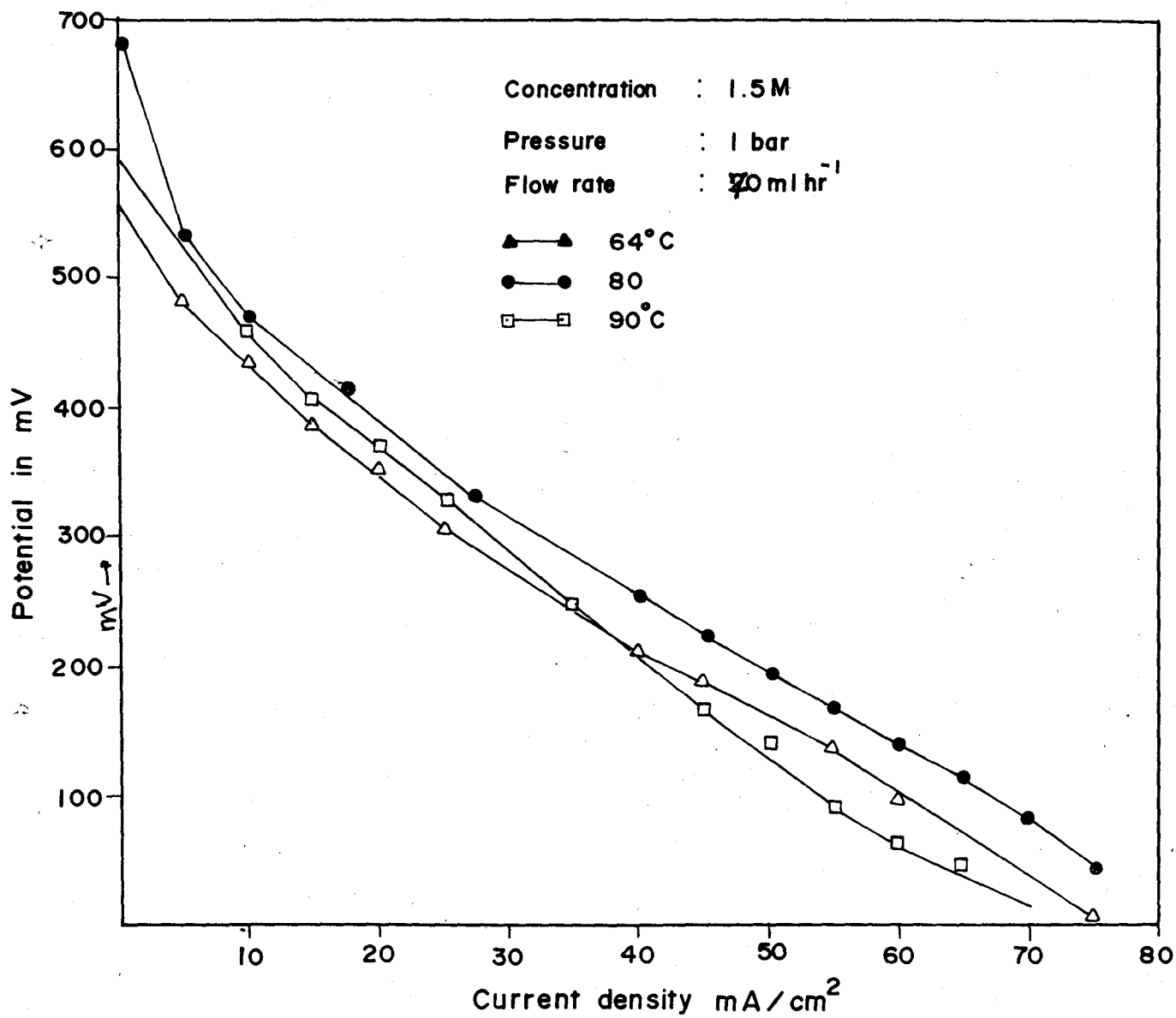


Fig. 4.11 V-I Plots for PEM fuel cell as a function of Temperature

where D = effective diffusion coefficient of the membrane (cm^2s^{-1})

C_1 = concentration at feed-membrane interface (mmol cm^{-3})

K = Constant related to effective hydraulic permeability (cm^2s^{-1} atm^{-1})

k = rate of permeate removal (cm s^{-1})

Table 4.1 and 4.2 below give the flux or permeability of methanol across the nafion membrane and conductivity of nafion membrane at various temperatures. Mathematical calculations are done as reported in [5,15].

Table 4.1 gives the permeation rates corresponding to various methanol concentrations

Methanol Concentration (mmol cm^{-3})	Permeation rate ($\text{mmol cm}^{-2}\text{s}^{-1}$)
1.76×10^4	0.1743
2.64×10^4	0.2624
3.25×10^4	0.3490

Table 4.2 shows variation of conductivity of nafion with temperature

Temperature	K	K	D
337	1.44×10^{-6}	3.17×10^{-5}	1.504×10^{-5}
353	3.82×10^{-4}	13.82×10^{-4}	2.280×10^{-5}
363	7.808×10^{-4}	7.808×10^{-3}	2.255×10^{-5}

C_1	a	b	j	cond. of nafion
1.76×10^4	5.58	0.17	0.172	0.1142
1.76×10^4	2.53	0.0672	0.385	0.1465
1.76×10^4	2.78	0.0438	0.471	0.1552

It is seen from fig 4.8, that better performance is obtained at 1.5 molar concentration of methanol as compared to 1M (less sloping curves are indicative of better performance). However at still higher concentration of 2 M instead of a further improvement, the voltage dropped rapidly, probably due to higher methanol diffusion flux across the membrane due to increased pressure differential that resulted. That the methanol flux actually increases with concentration is evident from the theoretical data shown in table 4.11

Increase in oxygen gas pressure is expected to reduce the pressure differential and hence minimize the methanol crossover thereby causing enhanced performance. At the same time higher pressure would cause enhanced O_2 reduction rate by more efficient utilization of the active catalyst surface area. It is thus evident from fig 4.9 that increasingly higher currents are obtained when oxygen pressure at the cathode was increased from 0.2 bar to 1 bar while concentration of methanol was kept unchanged on 1.5 M. CH_3OH .

Also as seen from fig 4.8, the slope of the V-I curve at 1.5 M methanol concentration (O_2 pressure 0.2 bar) is 9 volt amp^{-1} in the current range of 15-40 $mAcm^{-1}$ which is higher than the corresponding V-I curves of fig 4.9 (slopes 0.2 volt amp^{-1}) under the same condition; the better performance in the latter case could therefore be attributed to higher flow rate of methanol used, (increased of flow rate of from 50 $ml\ hr^{-1}$ to 70 $ml\ hr^{-1}$) which could have resulted due to greater methanol adsorption on the anode catalyst.

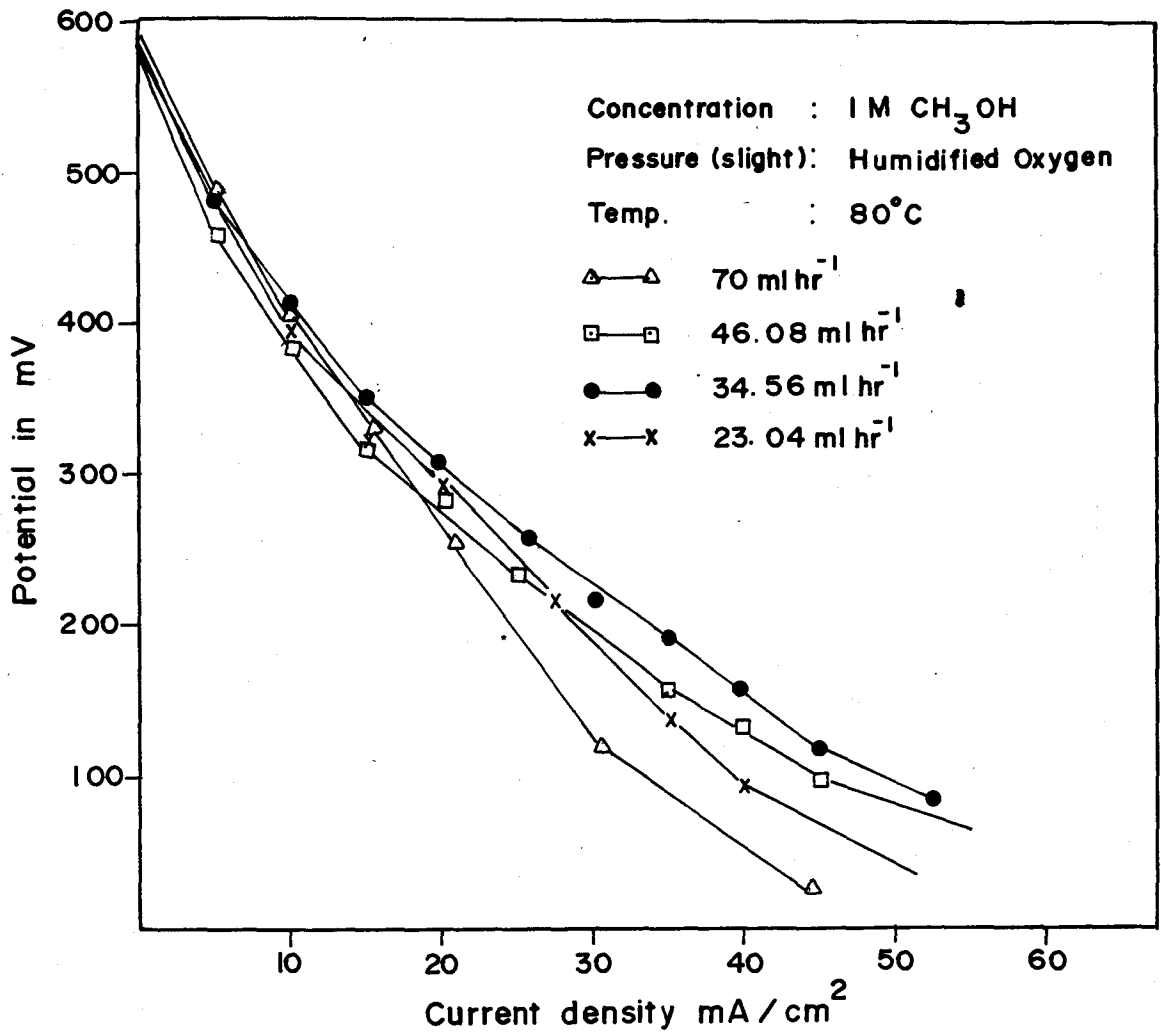


Fig. 4.12 V-I Plots for PEM fuel cell with humidified Oxygen as a function of flow rate

The cell output gradually increases with flow rate. This is seen from the polarization curves of fig 4.10. The methanol flow rates were increased from 23 ml hr⁻¹ to 80 ml hr⁻¹ at a fixed methanol concentration of 1 M. Best results were obtained at 70 ml hr⁻¹, which appeared to be the optimum value as further increase in flow rate e.g. 80 ml hr⁻¹, the performance dropped significantly. This is believed to be due to increased methanol cross over to the cathode region, when the flow rate increases beyond or certain value.

Fig 4.11 describes the effect of cell temperature on its performance. It can be seen that there is higher current output as temperature is increased from 64°C to 80°C e.g. at cell potential of 250 mV, the current increased from 35 mA to 40 mA with a relatively low activation energy of 6 kJ mol⁻¹, assuming Arrhenius first order rate law is obeyed; this is in agreement with a well known fact that electrocatalysis increased at a higher temperature. Similarly at the cell voltage of 500 mV at the initial V-I region controlled by activation resistance at the electrolyte surface, activation energy was needed 23 kJ / mol to produce current increase with rise in temperature.

Further at 500 mV, Ren et [14] reported that current output of 170 mA cm⁻² and 452 mA cm⁻² by operating a fuel cell at high power density at high temperatures of 80 °C and 130 °C. Also assuming Arrhenius first order rate equation, the above data shows similar activation energies ~ 27 kJ mol⁻¹, a slightly higher value, than observed in this work which is ~ 23 kJ mol⁻¹

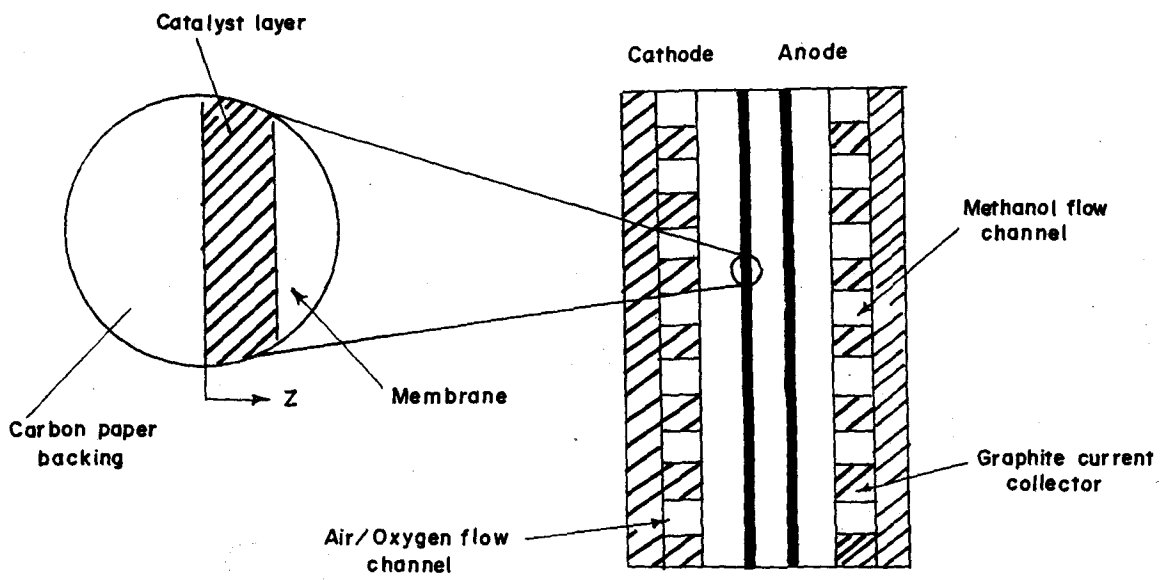


Fig 4.13 Model structure of methanol fuel cell.

Fig. 4.13

It may however be noted from fig 4.11 that at 90 °C, higher power output is shown only in the initial region of the V-I profile. This is attributed to the lower activation resistance of the catalyst for methanol oxidation. Subsequently, however the V-I profile at 90 °C falls below that of 80 °C inspite of higher methanol flux and conductivity of nafion as evident from table 4.1 and 4.2 . The drop in potential this middle region, as mentioned earlier, is due to ohmic voltage loss. The higher voltage loss for the 90 °C profile could be due to decreased ionic conductance of the membrane, probably due to its inadequate hydration at higher temperature, in absence of a special liquid water injection arrangement in the cell design used for the present work. Special arrangement to introduce liquid water in anode compartment are recommended in advanced fuel cell designs to facilitate higher membrane hydration and therefore higher conductance [8].

Fig 4.12 depicts polarization curves obtained by using ~~per~~humidified oxygen gas by bubbling the gas through saturated KCl solution. This necessitated the passage of gas at very low pressure (<0.1 bar). The plots were obtained at various flow rates. Since the oxygen gas pressures were low, the current outputs decreased relatively faster as evident by inspection of the later half of the curves. This is due to higher rate of methanol crossover at such low cathode pressures. Nevertheless, it is worth noting that in the first half of these plots, the cell potential are quite high and the values are comparable to those obtained when the oxygen gas pressure is 1 bar (fig 4.10). As an instance compare the values at some convenient reference point such as at 15 mA (flow rate 23 ml hr-) with respect to the curves of fig 4.10 and 4.12 .The cell potentials were

325 mV and 290 mV respectively at <0.1bar (humidified oxygen) and 1 bar unhumidified oxygen. These higher voltages are obtained with humidified oxygen gas even with much less pressures.

These results therefore underline the great importance of humidification of the both anode and cathode compartments which contribute to higher protonic conductivity of the membranes and hence lower voltage losses, as current is drawn out of the fuel cells.



References:

1. J. Stumper, Stephen A Campbell, D. Wilkinson, M. Johnson
Electrochim Acta vol 43, No 24 (1998)3773.
2. A. Kuver, W. J. Power Sources 74 (1998)211.
3. K. Scott, W. Taama, J. Appl. Electrochem.. 28 (1998) 289.
4. A. Hamnett, Catalysis Today 38 (1997)445.
5. K. Scott, W. Taama, J. Cruickshank, J. Power Sources 65 (1997)159.
6. R. Ramkumar, S. Dheendayalan, R. Pattbiram, J. Power Sources, 69
(1997) 75.
7. Li Lue, Long Pu, R. Vishwanathan, Q. Fan, R. Liu, E.S. Smotkin
Electrochim Acta, vol 43, No 24, (1998)3657.
8. David L. Wood III, Jung S. Yi, Trung V. Nguyen, Electrochim Acta,
Vol 43, No24, 1998(3795
9. K. Kordesch, G. Simader, Fuel Cell and their application VCH
Weinheim, 1996.
10. T. Okada, G. Xie, O. Gorsyth, S. Kjelstrup, N. Nakamura and T.
Arimura, Electrochim Acta, Vol43, No24, (1998)3741.
11. A. K. Shukla, P.A. Christensen, A. J. Dickinson, A. Hamnett, J.
Power Sources, 76(1998) 54.
12. A. Shukla. M. Hogarth, P. Christensen, A. Hamnett, J. Power Sources,
69 (1997) 5413.
13. A. Shukla, M. Hogarth, P. Christensen, A. Hamnett, J. Power
Sources, 69 (1997) 113.
14. X. Ren, M. S. Wilson and S. Gottesfield, J. Electrochem. Soc., 143
(1), 1996, L 12
15. J. Cruickshank, K. Scott, J. Power Sources, 70 (1998) 40.

ACHIEVEMENTS

1. Y zeolites are investigated for the first time as active supports for methanol oxidation catalysts in fuel cells.
2. Pt-Ru (HY) is found to have enhanced electrocatalytic activity as compared to conventional carbon supported catalysts.
3. The present investigation is successful in achieving a catalyst with lower catalysts loading, cost and obtaining catalyst of higher stability.
4. An improved mechanism for methanol oxidation is suggested on the basis of cyclic voltammetry and *insitu* FTIR studies.

►Future Directions:

- 1. Substitute materials like Ni-Ru, Mn-Ni oxides combined with Y zeolites or other porous or shape selective supports are expected to give higher electrocatalytic activity for methanol oxidation through which it should be possible to achieve catalysts with lower cost.**
- 2. More detailed structural characterization of the catalyst support is required to understand anode reaction pathways.**
- 3. A comprehensive theoretical model for a priori prediction of current-potential profiles is yet to be emerged.**
- 4. A tough future challenge is to develop polymer electrolyte membrane having**
 - i) high stability.**
 - ii) high tendency of hydration.**
 - iii) low or negligible permeability for methanol.**
 - iv) low production cost.**